GEM TECHNICAL REPORT
2014-07 V1.0.0

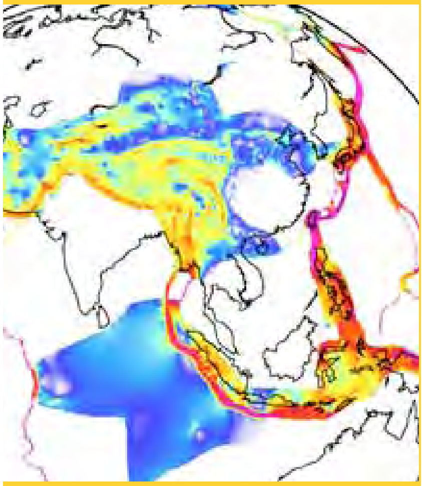

GEOLOGICAL, EARTHQUAKE AND GEOPHYSICAL DATA

Global geodetic strain rate model

Kreemer, C., E. Klein, Z-K Shen, M. Wang, L. Estey, S. Wier, F. Boler

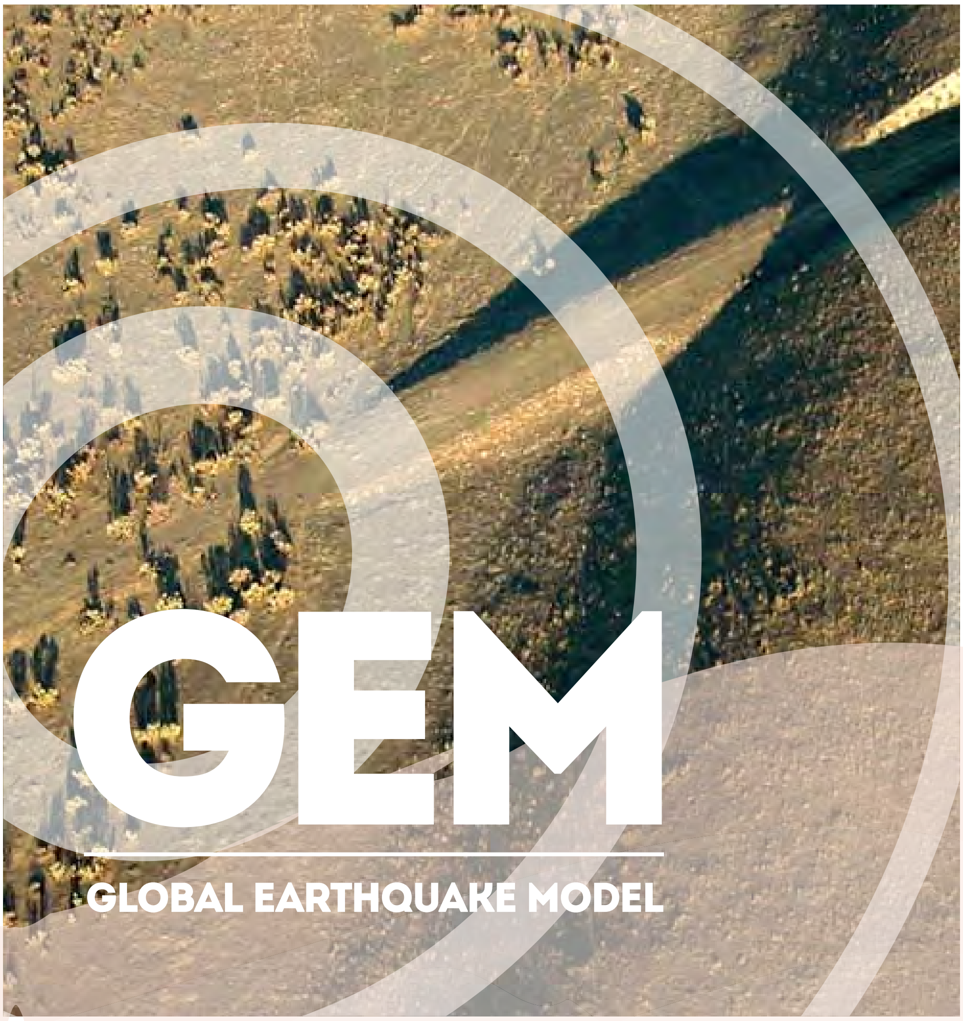

Global geodetic strain rate model

GEM Technical Report 2014-07

Version: 1.0.0

Date: March 2014

Author(s)*: Corné Kreemer, Elliot Klein, Zheng-Kang Shen, Min Wang, Lou Estey, Stuart Wier, Frances Boler

(*) Authors' affiliations:

Corné Kreemer, Nevada Bureau of Mines and Geology, University of Nevada, Reno, USA

Elliot Klein, Nevada Bureau of Mines and Geology, University of Nevada, Reno, USA

Zheng-Kang Shen, Department of Earth and Space Sciences, UCLA, USA and China Earthquake Administration, Beijing, China

Min Wang, China Earthquake Administration, Beijing, China

Lou Estey, UNAVCO, Boulder, CO-USA

Stuart Wier, UNAVCO, Boulder, CO-USA

Frances Boler, UNAVCO, Boulder, CO-USA

Rights and permissions

Citation advice

Kreemer, C., G. E. Klein, Z.-K. Shen, M. Wang, L. Estey, S. Wier, F. Boler (2014), Global Geodetic Strain Rate Model, GEM Technical Report 2014-07 V1.0.0, 129 pp., GEM Foundation, Pavia, Italy, doi: 10.13117/GEM.GEGD.TR2014.07.

Photo credits

http://www.globalquakemodel.org/

Note on this release

This report details the data, model assumptions, and results for GSRM v.2.0. Since the writing of this report, a new version of GSRM (v.2.1) has been created and is now being released. Below are the details of how GSRM v.2.1 differs from v.2.0:

+ The UNR analysis produced 6739 velocities, all but 34 of those are used in the strain rate analysis.

+ We included 233 studies, from which 15,772 velocities were taken, and all but 62 were used in the strain rate analysis.

+ This makes a total of 22,415 velocities, at 18,336 locations, used in the analysis.

+ 17,567 data points are in the deforming zones, 4848 on rigid plates.

+ There are a total of 145,086 deforming grid cells. This increase is due to the inclusion of the Tyrrhenian Sea in the deforming zones.

+ The width of the zone along the creeping portion of the San Andreas Fault in which we exclude data was extended from 5 to 22 km. This explains the total of 96 excluded velocities, mentioned in the first two points above.

+ The definition of the motion of the Indian plate was changed to that using data from after (instead of prior) the 2004 Sumatra earthquake. This change minimizes any strain incompatibilities along the edges of the plate.

+ The a priori strain rate value for the Colorado Plateau area is now set to 3×10^{-9}/yr.

+ In the new model all grid cells use an a priori strain rate value taken from the result of an initial damped inversion, not just the cells that are constrained by GPS

ACKNOWLEDGEMENTS

We greatly appreciate the help of G. Blewitt, who processed all the RINEX data used in this project and produced the GPS time-series.

The GPS analysis would not have been possible without the efforts of the International GNSS Service and all GPS network investigators for network maintenance and for, together with the data archives, making data freely available. In particular, we thank the following networks/archives: AFREF; Alabama Department of Transportation (DOT) CORS network, U.S.; Albuquerque Real Time GNSS Network, U.S.; Arpa Piemonte, Italy; Asia Pacific Crustal Monitoring System; AZGPS, U.S.; BANIAN, New Caledonia; BARD, U.S.; Bureau of Meteorology, Australia; Canary GNSS Centre; CDDIS, U.S.; CORS-NGS, U.S.; Danish GPS Center; DPGA-TUDELFT, The Netherlands; EarthScope Plate Boundary Observatory, U.S.,; ERVA Instituto Geográfico Valencia, Spain; EUREF; FLEPOS, Belgium; FREDNET, Italy; GEODAF, Italy; Geodetic Observatory Pecny, Czech Republic; GeoNet, New Zealand; Geosciences Australia; Gobierno de la Rioja, Spain; GREF-BKG; GPSCOPE-INSU; HEMUNET, Bulgaria; Idaho National Laboratory, U.S.; Indiana DOT CORS network, U.S.; Institut Teknologi Bandung, Indonesia; Instituto Geográfico Nacional, Spain; Instituto Geográfico Nacional, Tommy Guardia, Panama; Instituto Geográfico Português, Portugal; Instituto Technologico Agrario, Castilla y León, Spain; Institut Cartogràfic de Catalunya, Spain; Iowa DOT CORS network, U.S.; KARA, U.S.; Laboratorio di Topografia, Università degli Studi di Perugia, Italy; LATPOS, Latvia; Leica Kazachstan; Leica SmartnetUSA, U.S. and Canada; Lower Colorado River Authority, U.S.; MAGNA-ECO, Colombia; Maine DOT CORS network, U.S.; Mesa county, Colorado, U.S.; Missouri DOT CORS network, U.S.; Minnesota DOT CORS network, U.S.; Natural Resources Canada; NEGAR, California Institute of Technology, U.S.; MAGNET/NEARNET, University of Nevada, Reno, U.S.; NOANET, Greece; Norwegian Mapping Authority; OLGGPS, Austria; Pacific Geoscience Centre, Canada; Pacific GPS Facility, Hawaii, U.S.; Panamá Canal Authority, Panama; PANGA, U.S.; Provincia di Milano, Italy; RAMSAC, Argentina; RBMC Brasil; Red Andaluza de Poscionamiento, Spain; Red de Estaciones de Referencia GNSS de Euskadi, Spain; Red Extremeña de Posicionamiento, Spain; Red de Geodesia Activa de Navarra, Spain; Regione Autonoma Friuli Venezia Giulia, Italy; Regione Campania, Italy; Regione Emilia Romagna, Italy; Regione Liguria, Italy; Región de Murcia, Spain; REMOS, Venezuela; RENAG, France; Réseau GNSS Permanent, France; Rete GPS Veneto, Italy; RING-INGV, Italy; SCIGN, U.S.; Seiler Instrument Company, U.S.; SONEL, France; SOPAC, U.S.; South Carolina DOT CORS network, U.S.; STPOS Bolzano, Italy; SUGAR-NTU, Singapore; Survey of Israel; TAZNET, Arizona, U.S.; Texas DOT CORS network, U.S.; TGRef, Romania; TRIGNET, South Africa; UNAVCO, U.S.; Universidad de Cantabria; Universidad Politécnica de Madrid, Spain; University of Western Ontario, Canada; Washoe County, Nevada, U.S; and West Virginia DOT CORS network, U.S.

We also thank all Principal Investigators for making data available from the following NSF-funded networks or regions: Africa Array, Andes (CAP), Antarctica (PoleNet), Bhutan, Calabria, CocoNET, Costa Rica, El Salvador, Eritrea, Ethiopia, Greenland (PoleNet), Hawaii, Iceland, Mediterranean, Mexico, Mid-America (GAMA), New Zealand (SAGE). Pamir Mountains, Puerto Rico, Rio Grande Rift, SUOMI-NET, Tanzania, and Uganda

We thank these Institutions/networks which provided raw RINEX data that are otherwise not available publicly/anonymously: British Columbia Active Control System, Canada; British Isles continuous GNSS Facility (BIGF), U.K.; Central-Asian Institute for Applied Geosciences (CAIAG), Kirghistan; GEONET, GSI, Japan; Instituto Nacional de Estadística y Geografía (INEGI), Mexico; Jeddah Municipality, Saudia Arabia; Las Vegas Valley Water Authority, Nevada, USA; Leica SmartNet, Australia; Leica SmartNet (ITALPOS), Italy; Linz AG, Austria; LITPOS, Lithuania; Low-Latitude Ionospheric Sensor Network (LISN); Provincia Autonoma di Trento, Italy; REGNA, Servicio Geográfico Militar, Uruguay; TURNGPS, Utah, USA; and WALCORS, Belgium.

We thank these individuals who provided unpublished GPS velocity results: J. Bogusz, J. Dawson, A. Holland, H. Mora, M. Steckler, and C. Subarya.

We furthermore thank all investigators who contributed additional information to help us include their published results. We particularly thank N. Teferle for making the results of *Almuselmani et al.* [2008] available, and M. Sato for sharing results that were, at the time, not yet published.

We finally thank the Jet Propulsion Laboratory for the GIPSY-OASIS II software and for clock and orbit parameters.

ABSTRACT

This is the final report produced in the context of the GEM Strain Rate Project, one of the global components of the GEM Foundation. The project was charged to analyse and synthesize all available geodetic data in order to create a global data set of geodetic velocities that can be used to model plate motions and strain rates in plate boundary zones. To this end, we estimated 6533 velocities from position time-series that we derived from the analysis of RINEX data that was either freely available or made available to us specifically for this project. All but 15 of these velocities were used in the modelling. In a separate analysis, we also re-analysed all RINEX data in China and effectively added 1143 velocities to the data set. Finally, we added 13,318 velocities from 216 studies in the published literature (or from personal communications) to achieve a grand total of 20,979 velocities at 17,491 unique locations used in the modelling. Of all velocities, 16,325 are in plate boundary zones (as defined by us) and the remaining 4654 velocities are for points on, predefined, rigid tectonic plates or blocks. We created a global mesh that has 144,827 deforming cells of 0.2° (latitudinal) by 0.25° (longitudinal) dimension covering the plate boundary zones, with the remaining cells covering 50 rigid plates and blocks. For 36 of these plates, we estimated the rigid-body rotation from our data set, and the rotations of the remaining plates are taken from the literature. The rigid-body rotations are used as boundary conditions in the strain rate calculations. The strain rate field is modelled using the Haines and Holt method, which uses splines to obtain an interpolated velocity gradient tensor field, from which strain rates, vorticity rates, and expected velocities are derived. We also estimated model uncertainties, specific for this high-resolution mesh, which indicates that there still are many areas with large strain rate uncertainties where the data spacing is often much larger than the cell dimensions. Nevertheless, the model and data input are a tremendous improvement to the previous global strain rate model from 2004. All results are transferred to GEM and are also archived and displayed by a dedicated server hosted by UNAVCO (gsrm2.unavco.org), one of the project's partners. In addition, we created a kmz-layer of contour's of the second invariant of the model strain rates, and we created an online tool that would allow a user to upload his own velocities and plot them with the velocities in the GEM dataset in 53 different reference frames.

Keywords

strain rate, geodetic velocities, GPS, plate boundaries

TABLE OF CONTENTS

LIST OF FIGURES

Page

LIST OF TABLES

Page

1 Introduction

In 2009, the GEM foundation solicited proposals to create a geodetic strain rate model. The project presented here successfully proposed to update the Global Strain Rate Model (GSRM) v.1.2 of 2004 [*Kreemer et al.*, 2000, 2003; *Holt et al.*, 2005]. The new model, named GEM Strain Rate Model (GSRM v.2), is a large improvement on its predecessor, mostly because of the enormous increase in data. The data increase is large enough that the new model is almost exclusively based on the geodetic data alone, whereas the older model used faulting information and earthquake focal mechanisms as additional constraints. The data increase is due to two reasons: 1) we benefited from the proliferation of continuous GPS (CGPS) stations around the world and analysed all available raw data ourselves to obtain a unique consistent set of horizontal velocities, and 2) a large number of studies with geodetic velocities have been published since 2004.

2 GPS Data Analysis

The GPS analysis consisted of two components: 1) Analysis of all raw GPS data available to the University of Nevada, Reno (UNR) (section 2.1), and 2) Analysis of all raw GPS data in China (section 2.2). The two resulting velocity fields are combined by transforming the Chinese velocity field into the global solutions by inverting for, and applying, a translation rate and rotation rate that would minimize velocity differences at 36 collocated stations (i.e., IGS stations). We only maintain the UNR velocities for the collocated stations. The combined velocity field will be referred to as the “core solution”.

2.1 Analysis of Global Data

The analysis of all available GPS data (i.e., daily RINEX files) from around the world is performed at the University of Nevada, Reno. Most data come from public ftp/http sites, but some come from archives for which we have been given specific access (see Acknowledgements). Most data come from GPS stations that are operating continuously (CGPS), but we also analyse data for stations for which data are recorded intermittently but at a stable monument (e.g., MAGNET in Nevada, USA [*Blewitt et al.*, 2009; *Hammond et al.*, 2011], CBN network, Canada [*Henton et al.*, 2006], and Jura, France [*Walpersdorf et al.*, 2006]). Furthermore, some data come from CGPS stations for which only data for a few days per year are available (e.g., APRGP [*Dawson et al.*, 2004]).

We use GIPSY-OASIS II software for the data analysis package from the Jet Propulsion Laboratory (JPL) as well as JPL’s final fiducial-free GPS orbit products. Station coordinates were estimated every 24 hours by applying the Precise Point Positioning method to ionospheric-free carrier phase and pseudorange data [*Zumberge et al.*, 1997]. Data initially at the 15 or 30 second data intervals were automatically edited using the TurboEdit algorithm, and carrier phase data were decimated and pseudorange carrier-smoothed to obtain the ionosphere-free combinations of carrier phase and pseudorange every 5 minutes [*Blewitt*, 1990]. The observable model includes 1) ocean tidal loading and companion tides [*Scherneck*, 1991] using the FES2004 ocean tidal model [*Lyard et al.*, 2006], 2) estimation of wet zenith troposphere and two gradient parameters every 5 minutes as a random walk process [*Bar-Sever et al.*, 1998] using the Global Mapping Function (GMF) [*Boehm et al.*, 2006], 3) antenna calibrations for ground receivers and satellite transmitters [*Schmid et al.*, 2007], and 4) estimation of station clocks as a white-noise process. Finally, ambiguity resolution was applied to double differences of the estimated one-way bias parameters [*Blewitt*, 1989], using the wide lane and phase bias (WLPB) method, which phase-connects individual stations to IGS stations in common view [*Bertiger et al.*, 2010] Resolving ambiguities significantly reduces the scatter in the East component time-series. Satellite orbit and clock parameters were provided by JPL, who determine them in a global fiducial-free analysis using a subset of the available IGS core stations as tracking sites. The fiducial-free daily GPS solutions are aligned to IGS08 [*Rebischung et al.*, 2012] by applying a daily 7-parameter Helmert transformation (3 rotations, 3 translations and a scale component) obtained from JPL [*Bertiger et al.*, 2010]. IGS08 is a frame that is derived from ITRF2008 and consists of 232 globally distributed IGS stations. The data processing system includes quality control, such as iterative outlier detection of the input observations, and rejecting output coordinates if the data fail to meet certain criteria such as number of unresolved cycle slips, fraction of the day spanned by the data, and formal errors.

We consider all data between January 01, 1996, and July 01, 2013, but only derive velocities from time-series that are at least 2.5 years long, so as to best account for seasonal cycles [*Blewitt and Lavallée*, 2002]. In some cases, time-series for (near) collocated stations are concatenated to extend their length and/or to derive a single velocity for two stations that operated consecutively. Because we are interested in capturing the "secular", or interseismic, velocity, we exclude parts of the time-series that show significant transient motion. These transients are often due to postseismic deformation or slow-slip events (where the excluded part of the time-series is replaced with an offset). In the extreme, the exclusion could be for periods >10 years, sometimes at stations as far as several thousands kilometres from the largest earthquakes [*Baek et al.*, 2012; *Tregoning et al.*, 2013]. We model the time-series as an offset + trend (i.e., velocity) + annual cycle + semi-annual cycle + offsets. Offsets could come from equipment changes, earthquakes, or unknown reasons discovered in the analysis. Some stations only have intermittent data limiting our ability to model the seasonal terms, which could bias the velocity estimate. We therefore obtain the model parameters in a damped inversion, which ensures that the amplitude of the seasonal cycles remains small in those cases where data are only available for short periods year(s) apart. The velocities uncertainties are not adopted from this inversion, because it is well-known that those are too small due to the time-correlation of the errors. Instead we use the CATS software to calculate velocity uncertainties under the assumption that the error model consists of flicker-noise plus white-noise. We then multiplied the standard deviations with a factor of 2.0 so that the reduced chi-squared for fitting rigid-body rotations to velocities on stable plates is closer to 1.0.

Stations for which the time-series indicated rapid subsidence, unexplained transients, or for which the velocities were significantly different than nearby stations, were excluded. We also excluded any station near volcanic activity.

For the strain rate modelling we removed 15 velocities for stations within 5 km of the creeping section of the San Andreas Fault . The reason for this that the velocity profile across this fault is a step-function, which causes artefacts in the model, i.e., the spline function that we fit to the data will contain "overshoots" [*Kreemer et al.*, 2012]. Removal of the data points close to the fault allows us to model the step-function as close as possible without creating "overshoots".

2.2 Analysis of Chinese Data

We have processed GPS data to obtain a most updated velocity field in China. These data are not available outside China. The dataset includes mainly the campaign-mode field observations from the Crustal Motion Observation Network of China (CMONOC) sites in China, surveyed in 1999, 2001, 2004, 2007, 2009, and 2011, plus data from some other regional projects. Regional data are processed daily, and the solutions are subsequently combined with global daily solutions to tie the final solutions to the global ITRF2008 reference frame. Secular velocities, co-seismic offsets, and post-seismic logarithmic relaxations are incorporated in modelling GPS position changes. The final solution includes 1154 regional station velocities whose horizontal uncertainties are 1.5 mm/yr or less.

To produce this set of solution we have overcome numerous obstacles, such as properly modelling the antenna phase centre offset of the TOPCON antennas, removing biases introduced by using different geophysical models and satellite phase centre models employed by different GAMIT versions, and adequately modelling of the co-seismic and post-seismic displacements of the 2008 M7.9 Wenchuan earthquake, as well as some other large earthquakes occurred during the 1999-2011 period.

The handling of the data errors mostly follows Shen et al. [2011]. Gaussian errors are assumed for the GPS phase data during data processing to obtain the daily solutions. A priori uncertainty of 10 mm is assigned for the phase data, which are subsequently reweighted by a function associated with the observation elevation angle. Because GPS data are known to be correlated in time, a random-walk error model is assumed in time series modelling, with a set of constant perturbations of 1.0, 1.0, and 2.0 mm^2/yr assigned for the variances of east, north, and up components of station positions, respectively. We also inspect the station position time series for outliers, and remove a few extreme outlier points and downweight a few others.

The resulting velocity field is shown in Figure 2.1

Because of Chinese regulations, station coordinates of the final results are given with only two decimal places, as opposed to three decimal places for the station coordinates of all other data analysed.

This velocity solution replaces previously published results [*Shen et al.*, 2000, 2001, 2005; *Wang et al.*, 2001; *Zhang et al.*, 2004; *Gan et al.*, 2007].

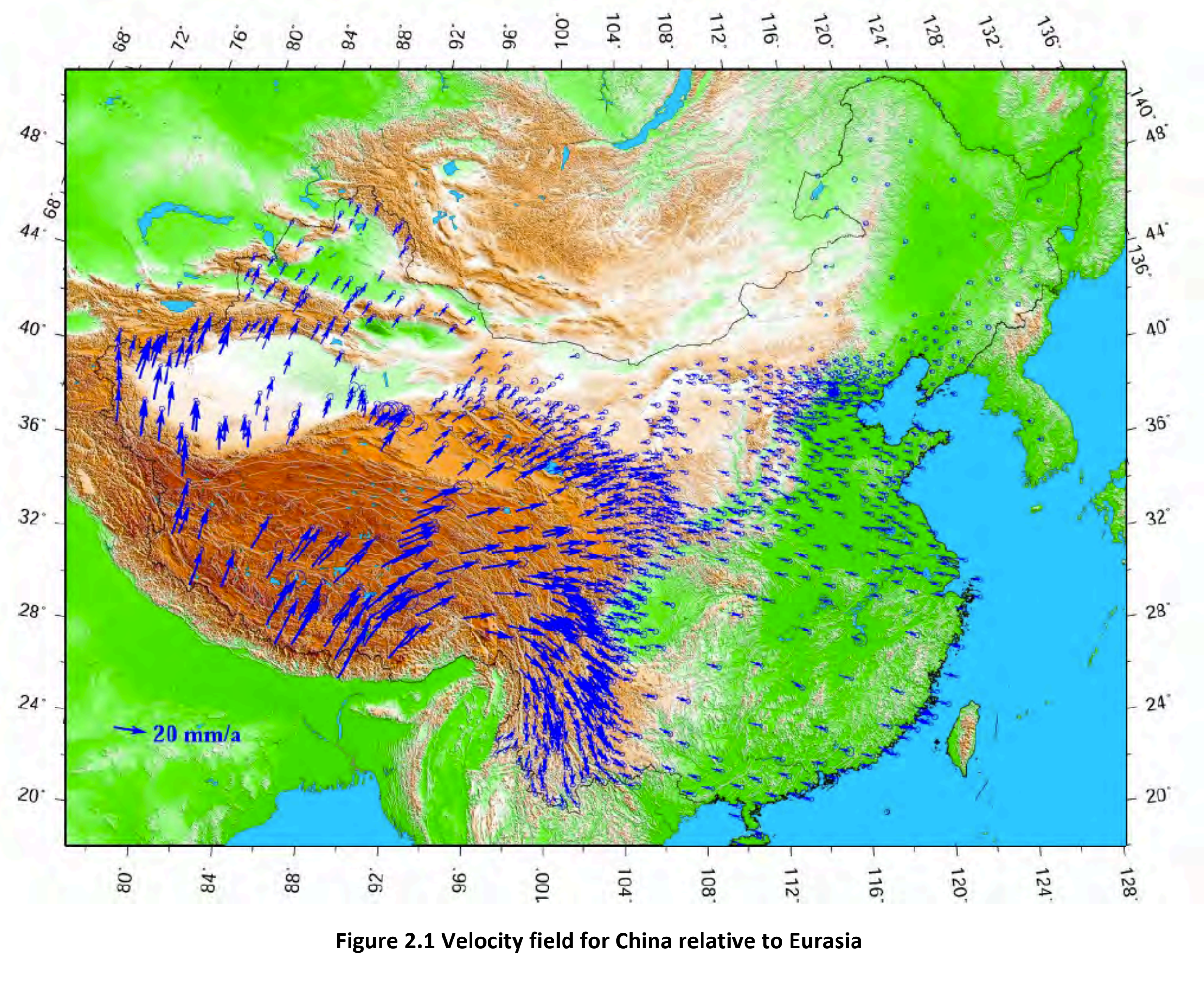

Figure 2.1 Velocity field for China relative to Eurasia

3 Synthesis of Published Velocities

The majority of geodetic velocities are derived from campaign-style measurements and are typically published in the literature. In other cases, publications report velocities for CGPS stations for which data is not publicly available. A very small minority of publications also report velocities derived from non-GPS techniques, such as DORIS [*Bettinelli et al.*, 2006; *Saria et al.*, 2013], VLBI [*Shen et al.*, 2011], or trilateration [*Shen et al.*, 2011; *Weber et al.*, 2011]. For several studies did researchers supply us with additional information such as station coordinates or velocities at nearby IGS sites. Six investigators sent us unpublished results (see Acknowledgements). All 210 publications from which data were used are listed in Appendix A. (For comparison, the previous model used data from 86 studies). For the first time, we included a handful of velocity estimates from submarine markers, off shore Peru [*Gagnon et al.*, 2005; used through the compilation *Chlieh et al.*, 2011] and Japan [*Tadokoro et al.*, 2012; *Sato et al.*, 2013].

In the synthesis, we included several studies focused exclusively on intraplate areas even though we do not solve for the strain rates there. The reason for this is that these studies could provide useful data in the future, when strain rates in plate interior will be modelled, and it would be sensible to already have them in the velocity compilation. We considered studies that put constraints on either the strain rates due to Glacial Isostatic Adjustment (GIA) [*Mazzotti et al.*, 2005; *Lidberg et al.*, 2010; *Kierulf et al.*, 2013] or on a known seismically active intraplate area such as the Carpathian Mountains [*van der Hoeven et al.*, 2005].

Where strain rates due to GIA interferes with tectonic strain rates, such as in southeast Alaska, we include GPS velocities that have been corrected for GIA by the original studies [*Elliott et al.*, 2010, 2013].

We applied the following criteria to decide whether data should be included:

1. studies were excluded when the velocity field was entirely based on publicly available data from (semi-)CGPS stations already analysed for the core solution [some examples since 2004 are: Prawirodirdjo and Bock, 2004; Wdowinski et al., 2004; Wernicke et al., 2004; Walpersdorf et al., 2006; Calais et al., 2006a; Hill and Blewitt, 2006; Kogan and Steblov, 2008; Teferle et al., 2009; Argus et al., 2010; Kreemer et al., 2010a, 2010b; Hammond et al., 2011; Asensio et al., 2012; ten Brink and López-Venegas, 2012; Berglund et al., 2012; de Lis Mancilla et al., 2013; Ganas et al., 2013].
2. if study a clearly superseded study b, then only results from study a were used. When in doubt both were included;
3. clear outlier velocities were removed, including those affected by volcanic deformation;
4. results reflecting postseismic deformation were not included;
5. velocities derived from <2.5 year (or sometimes just <2 year) time-series were excluded;
6. any station that was also excluded from the core solution;
7. velocities for 21 stations near the creeping portion of the San Andreas Fault (see section 2.1), but only after all data are combined (see below).

Next, we performed one large inversion in which we solve for, and apply, a translation rate and rotation rate that transform that would transform all results into the IGS08 reference frame of our core solution. The model parameters are obtained by minimizing velocity differences at collocated sites (within ~1km, short enough to avoid combining stations on opposite sides of the creeping section of the San Andreas Fault). We do this analysis for all studies simultaneously, because study *a* may, for example, not have any collocated sites with the core solution, but has them with study *b*, which does have collocated sites with the core solution. Any velocity for a site collocated with the core solution will be removed, under the assumption that the velocity of the core solution is superior (e.g., it is typically derived from longer time-series and we checked offsets ourselves). At least three collocated sites are needed to solve for a translation and rotation rate. If only two collocated sites are present, we only solve for a rotation rate. To avoid solving for a large translation rate when the geographic footprint is small (in which case there may be a trade-off between translation and rotation rate), we down-weight the translation rate parameters in the inversion. In the few cases where study *a* mostly supersedes study *b*, but some velocities from study *b* are not in study *a*, we first translate study *b* onto study *a* before we perform the global transformation. In those cases we do not duplicate the velocities at the collocated sites. Fifteen studies could not directly be transformed, because they had less than two data points collocated with the other studies [*Duquesnoy et al.*, 1994; *Antonelis et al.*, 1999; *Genrich et al.*, 2000; *Bacolcol et al.*, 2005; *Medak and Pribicevic*, 2006; *Rodriguez*, 2007; *Matson*, 2007; *Mullick et al.*, 2009; *Meng et al.*, 2009; *Ashurkov et al.*, 2011; *Tadokoro et al.*, 2012; *Miranda et al.*, 2012; *Sato et al.*, 2013; *Tserolas et al.*, 2013; *Mendes et al.*, 2013], where we should note that only part of velocities presented by *Genrich et al.* [2000] could not be transformed and also that the results in *Rodriquez* [2007] seemed partly in difference reference frames. Six of these studies were presented in an ITRF-flavor reference frame, and we assumed that those were similar to our IGS08 frame. In addition, 2 studies were relative to a stable plate, and we fixed those velocities relative to the respective plates in our model. This leaves six studies which were then rotated into the model reference frame (i.e., Pacific) as part of modelling the velocity gradient tensor field while minimizing misfits between observed and model velocities. Although *Mullick et al.* [2009] was presented in an ITRF and plate-fixed fame, and has velocities at regional IGS stations, we solved for the transformation parameters in the strain rate model, because of notable problems with the velocity field if transformed or adopted as described above.

The procedure described above is an improvement on that followed in the previous GSRM when the transformation (i.e., rotation) of each study was determined in the modelling of the strain rates. The new approach is superior in that (except for the few exceptions mentioned above) the data is independent of the model.

In the end, we included 13,318 velocities from the literature. Together with the core solution, there are 20,979 velocity data at 17,491 unique locations available for the modelling. The sites are shown in Figure 3.1 For comparison, the previous model used 5170 velocities.

We show in Appendix A the GPS velocity field for many, well-covered, areas.

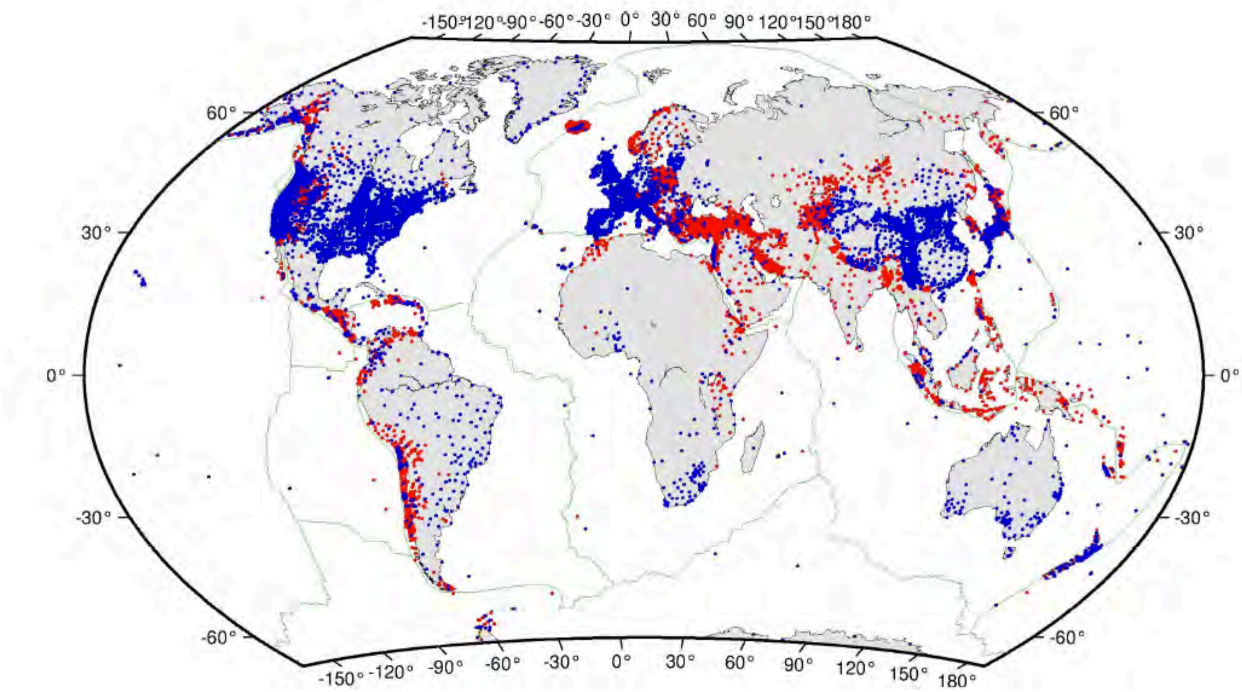

Figure 3.1 Locations for all 7661 GPS velocities for which we derived and used velocities (blue) and all 13,318 velocities we synthesized from the literature (red)

4 Strain Rate Modelling

4.1 Mesh Definition

We completely redefined the mesh for the modelling compared to what was used for the previous model. We consider the whole globe between 87.5°S and 87.5°N, which includes all data points, and the mesh is continuous in longitudinal direction. Individual grid cells are 0.2° (latitudinal) by 0.25° (longitudinal) in dimension. For comparison, the cells in the previous model were 0.5° by 0.6°. To determine which cells should be allowed to deform (i.e., cover the plate boundaries) and which not (i.e., move with a rigid plate), we started with the plate definitions of the PB2002 model of *Bird* [2003]. For each node of the mesh it was determined if it was within the polygon of a plate (and which plate) or not. As a result, for plate boundary zones that are defined by a single "line", such as oceanic ridge-transform systems, the boundary consist of a single grid cell, which four corner nodes are typically divided over two plates. The definition of the diffuse zones in PB2002 was augmented by the boundary definitions of *Chamot-Rooke and Rabaute* [2006]. We made numerous adjustments to these definitions, mostly guided by the information from the GPS data. In total, the model contains 144,827 deforming cells, compared to 22,310 cells in the previous model. The deforming cells are shown in Figure 4.1 Of the total 20,979 velocities, 16,325 are inside the deforming cells (Figure 4.2).

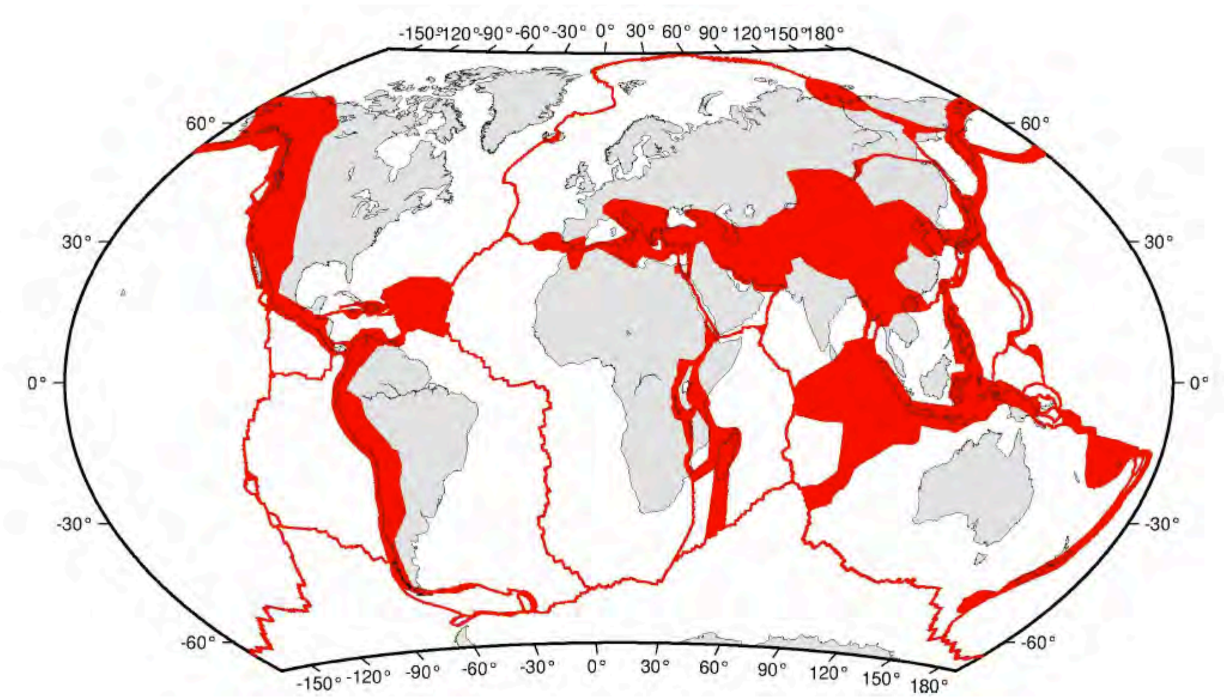

Figure 4.1 Red areas comprise the deforming grid cells, each 0.2° (latitudinal) by 0.25° (longitudinal) in dimension

A number of blocks defined in PB2002 were allowed to deform in our model, typically in areas of diffuse deformation such as Southeast Asia or the Andes. The rationale for this is that these blocks are typically in areas of large and complex deformation. If the blocks are covered by GPS stations, their velocities do often not reflect long-term motion because of elastic strain build-up along its margin (e.g., the Altiplano block) or, if they have no GPS coverage, the motion defined in PB2002 may not be compatible with nearby GPS data, causing spurious strain rates along the blocks' edges. This is not to say that no rigid blocks exist in continental back-arcs [*Brooks et al.*, 2003; *Wallace et al.*, 2004; *Chlieh et al.*, 2011; *McCaffrey et al.*, 2013], but that it is not possible to properly model the surface deformation (i.e., rigid block motion with localized high strain rates along its edges) without correcting/modelling for elastic strain accumulation.

Our model contains 50 rigid plates and blocks, compared to the 25 plates assumed in the previous model. We added a number of blocks that were not in PB2002. All these additional blocks have been shown to exist in the literature and, with two exceptions (Capricorn and Lwandle), we were able to constrain their rigid-body rotations by the GPS data (see Section 4.2). The new blocks are listed below with references arguing for their existence:

- Bering [*e.g., Mackey et al.*, 1997; *Cross and Freymueller*, 2008]
- Baja California [*e.g., Umhoefer and Dorsey*, 1997; *Plattner et al.*, 2007]
- Capricorn [*e.g., Royer and Gordon*, 1997; *Conder and Forsyth*, 2001]
- Danakil [*McClusky et al.*, 2010]
- Gônave [*e.g., Mann et al.*, 1995; *Benford et al.*, 2012]
- Lwandle [*e.g., Hartnady*, 2002; *Horner-Johnson et al.*, 2007]
- Puerto Rico [e.g., *McCann*, 1985; *Jansma et al.*, 2000; *Manaker et al.*, 2008]
- Rovuma [e.g., *Hartnady*, 2002; *Calais et al.*, 2006b]
- Sakishima [*Nishimura et al.*, 2004]
- Satunam [*Nishimura et al.*, 2004]
- Sinai [*e.g., Salamon et al.*, 2003; *Mahmoud et al.*, 2005]
- Victoria [e.g., *Hartnady*, 2002; *Calais et al.*, 2006b]

The Sakishima and Satunam blocks are sub-blocks of PB2002's Okinawa block and named here for the first time. In our model the Okinawa block is limited to only the central portion of the block defined in PB2002, with Sakishima to its south and Satunam to its north.

The Bering, Capricorn, Lwandle are part of the MORVEL plate motion model [*DeMets et al.*, 2010], although MORVEL did not have a rotation rate for Bering, which we estimated from the GPS data.

Compared to the previous strain rate model, other new plates and blocks in the model are (from PB2002): Aegean Sea, Burma, Easter, Galapagos, Juan Fernandez, Mariana, Niuafo`ou, North Bismarck, Okinawa, Panama, Shetland, Sandwich, Solomon Sea, South Bismarck, Tonga, Woodlark

For some of these blocks (Aegean Sea, Mariana, Okinawa, Panama, Shetland, South Bismarck, Tonga, Woodlark) we were able to estimate the rigid-body rotation from the GPS data (see section 4.2) and thus replace the rotation given by PB2002.

Two plates that existed in the previous model are now part of a deforming zone. One is the Anatolia micro-plate, which also exists in PB2002. While it has long been considered as a rigid micro-plate [*McKenzie*, 1970; *McClusky et al.*, 2000], it is now evident from a new dense GPS network that there is significant internal deformation within Anatolia [*Aktuğ et al.*, 2013]. The other plate is Tarim. While it may indeed be a rigid micro-plate [*Avouac et al.*, 1993; *Shen et al.*, 2001; *Meade*, 2007; *Zhang and Gan*, 2008], there is now significant GPS coverage to constrain the Tarim area as having low strain rates within the greater India-

Eurasia subduction zone. Following the same argument, we do not consider, for example, a central Iranian block [*Jackson and McKenzie*, 1984; *Vernant et al.*, 2004], a rigid Sierra Nevada-Great Valley block in the western United States [*Argus and Gordon*, 1991; *Dixon et al.*, 2000; *McCaffrey*, 2005], or an Adria and/or Apulia block(s) between Italy and the Balkans [e.g., *Anderson and Jackson*, 1987; *Ward*, 1994; *Battaglia et al.*, 2004; *D'Agostino et al.*, 2008].

Polygon coordinates of all 50 plates/blocks are available upon request.

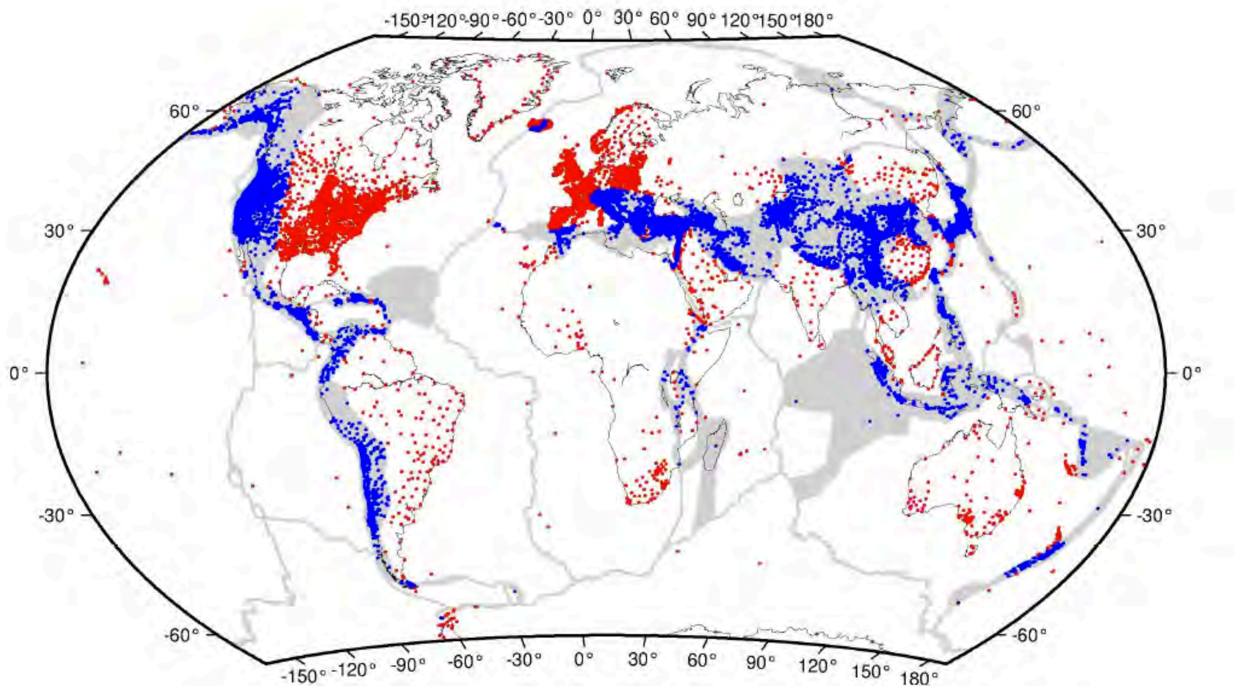

Figure 4.2 Deforming zones (in grey), locations of data points inside deforming grid (blue circles) and location on rigid plates (red circles). 16,326 velocities are used inside the deforming areas.

4.2 Rigid Body Rotations

In Table 4.1 we list the angular velocities (in terms of the corresponding Euler pole and rotation rate) for all assumed rigid plates and blocks included in the model. They are listed relative to the Pacific plate, which is the model's reference plate. Of the 50 plates, 36 angular velocities were estimated from the GPS velocities by this project, 6 were taken from PB2002 [*Bird*, 2003] and 8 were taken from MORVEL [*DeMets et al.*, 2010].

Appendix C lists the IGS08-velocities used to constrain the plate motions, their residuals, and the study from which the velocity was taken.

Table 4.1 Euler pole location and rate, relative to Pacific, for all rigid plates/blocks in model. All results are derived by us, except * is from Bird [2003] and # is from DeMets et al. [2010]

Latitude (ºN)	Longitude (ºE)	Rate (º Myr^{-1})	Plate Abbreviation	Plate Name
59.14	-73.32	0.942	AF	Africa
63.16	-79.68	0.944	AM	Amur
64.09	-83.73	0.882	AN	Antarctica
60.52	-45.39	1.112	AR	Arabia
73.68	-37.71	0.808	AS	Aegean Sea
60.56	3.64	1.082	AU	Australia
37.75	-8.22	0.037	BC	Baja California
34.78	-63.17	0.665	BG	Bering Sea
8.89	-75.51	2.667	BU	Burma*
56.03	-81.68	0.928	CA	Caribbean
10.13	-45.57	0.309	CL	Caroline#
42.20	-112.80	1.676	CO	Cocos#
62.30	-10.10	1.139	CP	Capricorn#
33.05	29.51	2.864	DA	Danakil
28.30	66.40	11.400	EA	Easter*
61.38	-78.85	0.927	EU	Eurasia
9.40	79.69	5.275	GP	Galapagos*
47.07	-78.99	1.070	GV	Gônave
61.34	-39.20	1.133	IN	India
-0.60	37.80	0.625	JF	Juande Fuca#
35.91	70.17	22.520	JZ	Juan Fernandez*
60.00	-66.90	0.932	LW	Lwandle#
28.24	147.84	2.143	MA	Mariana
49.29	-76.04	0.791	NA	North America
-0.66	144.60	0.743	NB	North Bismarck

Latitude (ºN)	Longitude (ºE)	Rate (º Myr^{-1})	Plate Abbreviation	Plate Name
6.87	-168.87	3.255	NI	Niuafo`ou*
57.23	-88.59	1.252	NZ	Nazca
53.64	-76.91	0.831	OK	Okhotsk
62.40	163.77	1.561	ON	Okinawa
0.00	0.00	0.000	PA	Pacific
33.47	-82.09	1.743	PM	Panama
47.33	-76.68	1.135	PR	Puerto Rico
-3.96	-41.88	0.864	PS	Philippine Sea
25.70	-104.80	4.966	RI	Rivera#
59.74	-70.66	0.930	RO	Rovuma
55.14	-83.42	0.684	SA	South America
11.49	-33.95	6.996	SB	South Bismarck
57.80	-78.00	0.755	SC	Scotia#
62.92	-39.75	1.094	SI	Sinai
32.73	129.75	7.031	SK	Sakishima
78.23	149.12	2.240	SL	Shetland
58.85	-79.53	0.983	SO	Somalia
19.53	135.02	1.478	SS	Solomon Sea*
48.65	139.00	3.053	ST	Satunam
59.20	-79.26	1.004	SU	Sunda
-3.80	-42.40	1.444	SW	Sandwich#
29.42	2.23	9.229	TO	Tonga
57.96	-84.86	0.973	VI	Victoria
17.69	134.28	1.763	WL	Woodlark
65.16	-83.04	0.991	YA	Yangtze

We chose to not use every GPS velocity on each rigid plate to estimate the angular velocities. Typically we would only use the best-behaved, longest running stations from our own analysis. In some cases, there were insufficient stations from our own analysis (or a sufficient number was not well distributed across the plate) to estimate the angular velocity. In those cases we also used velocities from the literature synthesis. In general, we would omit stations near plate boundaries, as those may be affected by elastic strain accumulation. A more detailed discussion is warranted for a subset of the plates:

1. Baja California

We estimate an Euler pole for Baja California relative to the Pacific plate at almost 90 away from the block, suggesting a pure translational nature of its motion. The predicted motion relative to the Pacific plate is ~4 mm yr^{-1} to N40ºW. A GPS station near Cabo San Lázaro [*Plattner et al.*, 2007], moves at ~2 mm yr^{-1} to the southeast, suggesting that the boundary between the Pacific plate and the Baja California block is likely accommodated across a broad zone along the western margin of the Baja Peninsula.

2. Caribbean

We estimate the angular velocity for the Caribbean plate by using our velocity estimates for San Andres Island and Grenada and the additional estimate for Aves Island from *Weber et al.* [2001]. Most studies have considered station CRO1 on Saint Croix, U.S. Virgin Islands, to be part of the Caribbean plate [e.g., *Sella et al.*, 2002; *Prawirodirdjo and Bock*, 2004; *Altamimi et al.*, 2012]. In our analysis, CRO1 and nearby station VIKH move to the SSW at 0.4-1.3 mm yr^{-1} relative to the Caribbean plate, possibly suggesting that the Muertos Trough is active as far east as south of the U.S. Virgin Islands [*McCann*, 1985].

3. Eurasia

The station coverage for the Eurasian plate is highly biased towards western Europe. To estimate the angular velocity, we used our velocity estimates from ten long-running CGPS sites that are roughly equally distributed across the plate. We excluded stations in Scandinavia, where velocities are affected by GIA [*Lidberg et al.*, 2010; *Kierulf et al.*, 2013]. The areas in the far-field from the former Fennoscandian ice-sheet may be moving towards the ice-sheet, but by picking areas equally covered over the plate, that affect should be averaged (see discussion North American plate below).

4. India

We observe a change (i.e., speed-up) in the east velocity of the long-running station at Bangalore (IISC) at the time of the 26 December, 2004, Mw=9.15, Sumatra earthquake. Even though this station is >2000km from the epicentre, it is likely that this velocity change is due to visco-elastic postseismic relaxation. Similar results are seen in stations in SE Australia after the 23 December, 2004, Mw=8.1, Macquarie Ridge earthquake [*Tregoning et al.*, 2013] and in Korea after the March 11, 2011, Mw=9.0 Tohoku-Oki event [*Baek et al.*, 2012]. However, we do not see a velocity change for the CGPS station in Hyderabad, 500 km north of Bangalore. We restricted the data for Bangalore to be before the 2004 earthquake. Many of the studies that we added in this area have velocities based on data (partially) from after the 2004 earthquake. This could have some effects in the strain rate estimates along the boundaries of the rigid plate. However, it is not really possible to avoid this subtle effect, unless we only consider studies based on data from before the event. Most studies present velocities based on similar time-span, which is most important in inferring reliable strain rates within the footprints of those studies.

5. Mariana

For the Mariana plate we used our CGPS velocity on Mariana Island (CNM0, formed by concatenating the time-series of CNMI and CNMR) and three additional velocities from *Kato et al.* [2003] along the central Mariana Islands. Like *Kato et al.* [2003], we don't correct for any possible elastic strain accumulation along the Marianas trench. We find a significant N-to-S increase in the back-arc spreading rate, but overall 3-8 mm yr^{-1} slower than predicted by *Kato et al.* [2003].

6. Nazca

It has been shown that significant deformation near Easter Island affects the GPS station there [*Kendrick et al.*, 2003] (ISP0, formed by concatenating the time-series of EISL and ISPA). We therefore add to the single CGPS station on the Galapagos Islands (GLP0, formed by concatenating the time-series of GALA and GLPS), the two velocities on San Felix and Robinson Crusoe Islands originally presented by *Kendrick et al.* [2003], but taken from *Wang et al.* [2007]. ISP0 moves 2.8 mm yr^{-1}. towards S52ºE relative to our definition of stable Nazca.

7. North America

Most previous studies of the motion of the North American plate only considered stations south of the former ice-sheet [e.g., *Sella et al.*, 2007; *Argus et al.*, 2010; *Altamimi et al.*, 2012]. However, the predictions from the latest GIA models predict a far-field motion towards the former ice-sheet [*Peltier and Drummond*, 2008]. If we were only to choose GPS stations south of the ice-sheet to estimate the plate's angular velocity, the assumed rigid-body motion of the northern part of the plate will be biased. We therefore chose 10 long-running stations that covered the entire plate roughly uniformly. Unfortunately, this still causes a small problem; we find artificial elevated strain rates along the eastern edge of the Pacific-north America plate boundary in the western U.S., because of the northerly oriented velocities (1-1.5 mm yr^{-1}) of the numerous stations in the eastern end of the boundary (due to GIA) relative to the (artificially) fixed plate interior. For future models, to avoid this artefact, all of the North American plate should be allowed to deform. Then, the strain rates due to GIA would be correctly found around the former ice-sheet.

8. Okhotsk

It is difficult to estimate an angular velocity for the Okhotsk plate, because GPS can only be found along its margins, where velocities may be affected by elastic loading (for which we do not account). Nevertheless, we are fairly confident about our results, which predicts (relative to Amur plate) ~8 mm yr^{-1} WSW directed shortening across the island of Sakhalin and ~2 mm yr^{-1} NE directed motion relative to North America across the Chersky Range. Both results are, at least in direction, consistent with regional focal mechanisms, with the motion across the Chersky Range being partitioned between E-W directed left-lateral strike-slip and N-S shortening [e.g., *Cook et al.*, 1986; *Riegel et al.*, 1993].

9. Pacific

Our definition of a stable Pacific plate includes the first global use of velocities at two stations (Kiritimati (KRTM), Kiribati Islands, and Gambie Island (GAMB), French Polynesia) for which data were collected by the Asia Pacific Crustal Monitoring System [*Harada*, 2000; *Munekane and Fukuzaki*, 2006], which allows for a better geometric spread of stable stations. Although the station on Guadalupe Island (GUAX), southwest of Baja California, would provide an important geometric constrain in the rotation estimation, the suggestion of thermal contraction in the young oceanic lithosphere precludes us from using it [*Kumar and Gordon*, 2009; *Kreemer et al.*, 2010c]. Indeed, GUAX moves at ~1.2 mm yr^{-1} towards S27ºE.

10. Philippine Sea

There are a couple of islands with GPS stations on this oceanic plate. The data from station G140 on Okino Torishima (also called Parece Vela) near the centre of the Philippine Sea plate is noisy and are not used. To avoid a geometric bias, we used only one of the two velocities on the Daito Islands, namely on Kita Daito (J746), and combine it with the velocity for Koro, Palau Islands (PAL0, concatenated from PAL1 and PALA). In this definition G140 moves ~0.8 mm yr^{-1} towards the NNE.

11. Scotia

There are a few GPS sites located on the very western side of the plate, but this provides a very poor geometry to estimate the angular velocity. We therefore adopted the rotation from MORVEL [*DeMets et al.*, 2010].

12. Shetland

We combined data for various studies (table 4.2) to present the first angular velocity estimate for the small Shetland block, which is almost entirely surrounded by the Antarctic plate. The pole of rotation of the block relative to Antarctica is near Gibbs Island. The result predicts northward directed shortening across the South Shetland Trench, from 6 mm yr^{-1} in the east to 12 mm yr^{-1} in the west, and a maximum of 9 mm yr^{-1} NNE directed extension across the Bransfield Rift System near Deception Island.

13. Tonga

As for the Mariana block, we assume that the three velocities we use to estimate the angular velocity of the Tonga block are not affected by elastic loading along the subduction interface.

4.3 Strain Rate Model

We used the method of Haines and Holt [*e.g., Haines and Holt*, 1993; *Holt et al.*, 2000; *Beavan and Haines*, 2001] to model the strain rate field. This method uses bi-cubic splines to obtain a continuous velocity gradient tensor field in the plate boundary zones. The rigid-body rotations listed above are applied as *a priori* boundary conditions, relative to the Pacific plate, which is the reference plate in the model.

4.3.1 Methodology

To model the strain rate field as a continuous model, we explicitly assume that the crustal thickness over which the strain rates apply is relatively small compared to the horizontal dimension. We actually model the velocity gradient tensor field, which comprises both strain rates and vorticity. For this, we relate the velocity gradient tensor field to a three-dimensional rotation rate vector $\dot{W}$ (which intercepts the Earth's centre and surface). A continuous velocity field $v(\hat{x})$ can then be written as:

$$v(\hat{x}) = R[\dot{W}(\hat{x}) \times \hat{x}] \quad (1)$$

where R is the Earth's radius, and $\hat{x}$ is a 3-dimensional unit vector for any point on the Earth's surface with latitude θ and longitude φ:

$$\hat{x} = (cos\theta cos\varphi, cos\theta sin\varphi, sin\theta) \quad (2)$$

If $\dot{W}$ is constant over a given area, then (1) gives the well-known formulation for a rigid body rotation. In fact, we define a rigid block/plate by enforcing $\dot{W}$ to be constant (i.e., its spatial derivatives are zero) for part of the grid. For the new GSRM, $\dot{W}$ is set *a priori* for each plate/block, using the results in Table 4.1.

The horizontal strain rates on a sphere can be written using the spatial derivatives of $\dot{W}$:

$$\dot{\varepsilon}_{\varphi\varphi} = \frac{\hat{\Theta}}{cos\theta}\frac{\partial\widehat{W}}{\partial\varphi} \tag{3}$$

$$\dot{\varepsilon}_{\theta\theta} = -\hat{\Phi}\frac{\partial\widehat{W}}{\partial\theta} \tag{4}$$

$$\dot{\varepsilon}_{\varphi\theta} = \frac{1}{2}\left(\hat{\Theta}\frac{\partial\dot{W}}{\partial\theta} - \frac{\hat{\Phi}}{cos\theta}\frac{\partial\dot{W}}{\partial\varphi}\right) \tag{5}$$

where $\hat{\Theta}$ and $\hat{\Phi}$ are the unit vectors in the North and East directions, respectively. In these definitions the contribution of any gradient in vertical velocities is omitted, because it is small.

The rotation rate about a local vertical axis (i.e., vorticity) can be written as:

$$\dot{\omega_r} = \hat{x}\cdot\dot{W} - \frac{1}{2}\left(\frac{\hat{\Phi}}{cos\theta}\frac{\partial\dot{W}}{\partial\varphi} + \hat{\Theta}\frac{\partial\dot{W}}{\partial\theta}\right) \tag{6}$$

The rotation vector function ($\dot{W}$) is expanded spatially using bi-cubic Bessel functions.

The objective function that is minimized in the inversion is:

$$\sum\nolimits_1^N\left(\dot{\varepsilon}_{ij}^{fit} - \dot{\varepsilon}_{ij}^{obs}\right)\left(\dot{\varepsilon}_{pq}^{fit} - \dot{\varepsilon}_{pq}^{obs}\right)V_{ij,pq}^{-1} + \sum\nolimits_1^M\left(u_i^{fit} - u_i^{obs}\right)\left(u_j^{fit} - u_j^{obs}\right)C_{ij}^{-1} \tag{7}$$

where ij, and pq denote tensor components of the strain rate tensor. The above equation suggest that "observed" strain rates can also be input, as was done in the previous GSRM, but this option was not used for the current GSRM. In any case, the strain rate variance covariance matrix V needs to be set. One could set the off-diagonal components of V such that preferred strain rate direction/style is imposed (as was done in the previous GSRM using earthquake focal mechanisms). However, for the new GSRM we only set the diagonal components of V, i.e., variances of the three strain rate components (see Section 4.3.2). The second part of (7) pertains to the fit of the M geodetic velocities, with the data covariance matrix given by C.

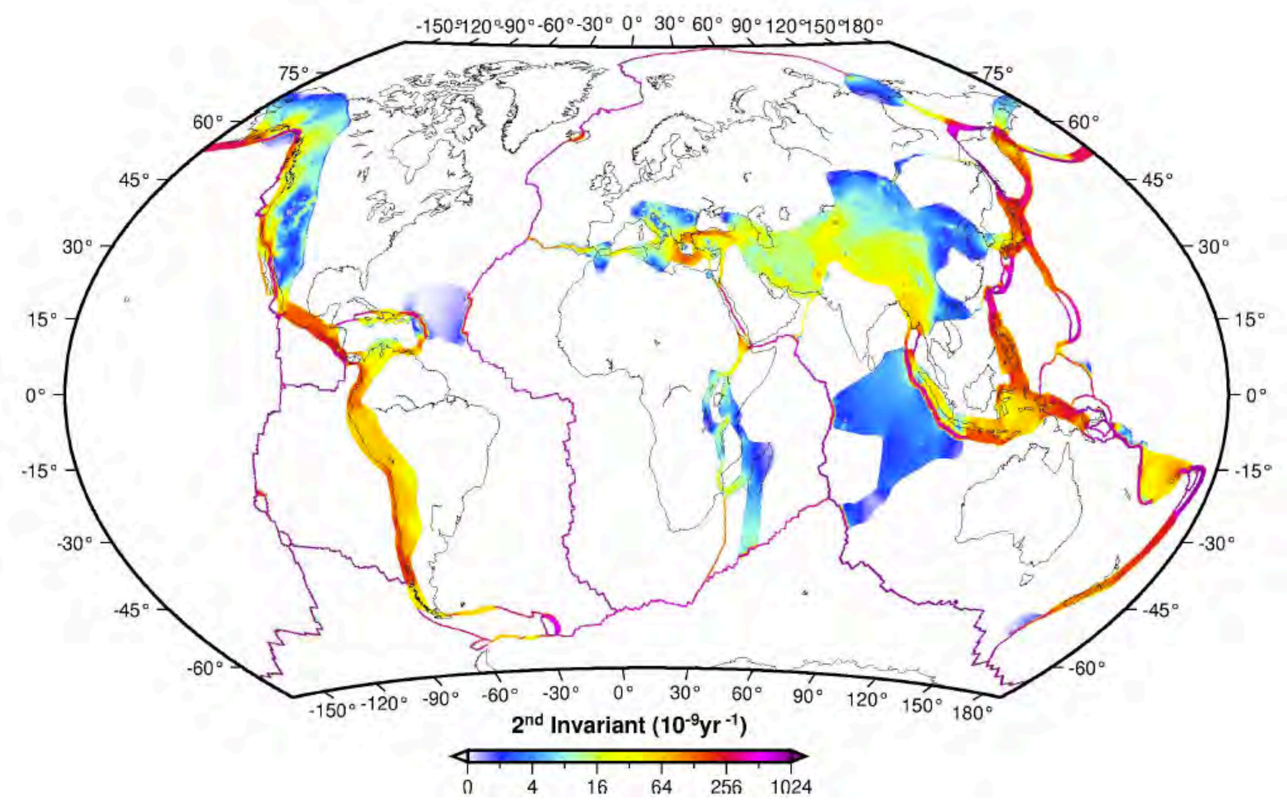

Figure 4.3 Second invariant of strain rates from step 1 (i.e., a spatially damped solution)

For the strain rate and velocity field to be self-consistent, St. Venant's compatibility relationships need to be satisfied everywhere. This strain rate compatibility equation for the horizontal strain rate tensor is (in Cartesian coordinates):

$$\frac{\partial^2 \varepsilon_{xx}}{\partial y^2} + \frac{\partial^2 \varepsilon_{yy}}{\partial x^2} - 2\frac{\partial^2 \varepsilon_{xy}}{\partial x \partial y} = 0 \tag{8}$$

This constraint avoids having incompatible strain rates from spurious velocity data and ensures that the velocity gradient between points A and B is independent of the path one takes through the deforming area from A to B.

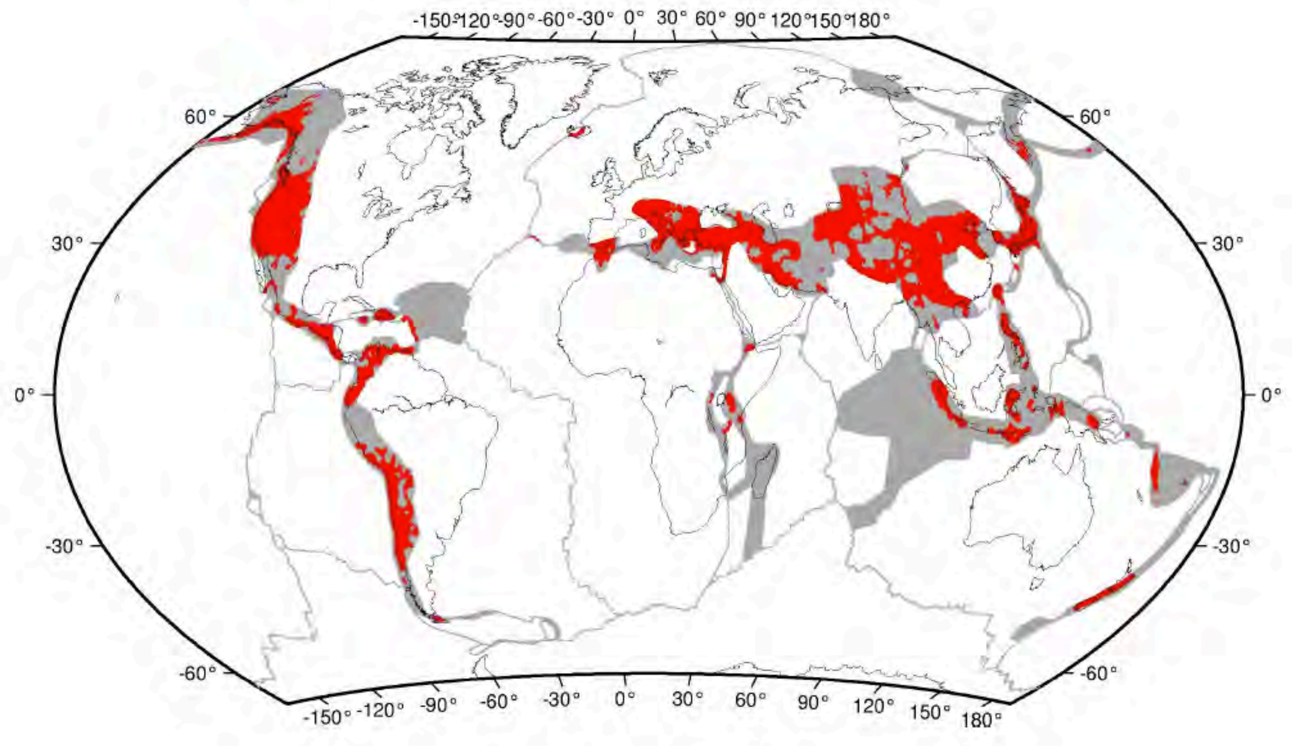

Figure 4.4 Red areas are parts of the plate boundary zone that are well constrained by GPS data (given our definition described in text), grey areas are not.

4.3.2 A priori strain rate variances

Following a Bayesian philosophy, the method requires us to assign *a priori* strain rate (co-)variances to each deforming grid cell. In order to properly fit the velocity gradient field in areas of high and low strain rates, and to avoid under- or over-fitting the geodetic velocities, respectively, we prefer to assign *a priori* variances that reflect the actual expected strain rates. To accomplish this, we decided on a two-step approach, modelling the strain rate field twice. In the first step, we assign the same standard deviations of 10^{-8}/yr for $\dot{\varepsilon}_{\varphi\varphi}$ and $\dot{\varepsilon}_{\theta\theta}$, and $1/\sqrt{2}\ 10^{-8}$/yr for $\dot{\varepsilon}_{\varphi\vartheta}$ to each cell, with zero covariances (i.e., assumed isotropy). However, if we would assign the same *a priori* values to each grid cell, we would create some erroneous results in the diffuse oceanic areas, where GPS data are largely absent. For instance, we can safely assume that in the Indian Ocean most of the deformation occurs along the spreading centres and not in the diffuse zone between the India, Capricorn and Australian plates. If we assign the same *a priori* variances to all grid cells, relatively high strain rates due to the relative plate motions will spread into the diffuse zone. To remedy this, we give all cells with transform and ridge segments very large *a priori* values. We do the same for the part of the Sunda subduction zone that borders the Indian Ocean diffuse deformation area. We follow a similar approach for the diffuse oceanic areas between the New Hebrides and Fiji, the one between the North and South America plates, and in the “armpit” of the easternmost Aleutian/Alaska subduction zone. For the diffuse boundary between Africa and Eurasia, south west of Portugal (as defined by *Chamot-Rooke and Rabaute* [2006]), the PB2002 boundary segments run through the middle of the diffuse zone and we set very high variances for the cells containing the PB2002 boundary segments. Figure 4.3 shows the second invariant of the model resulting from step 1.

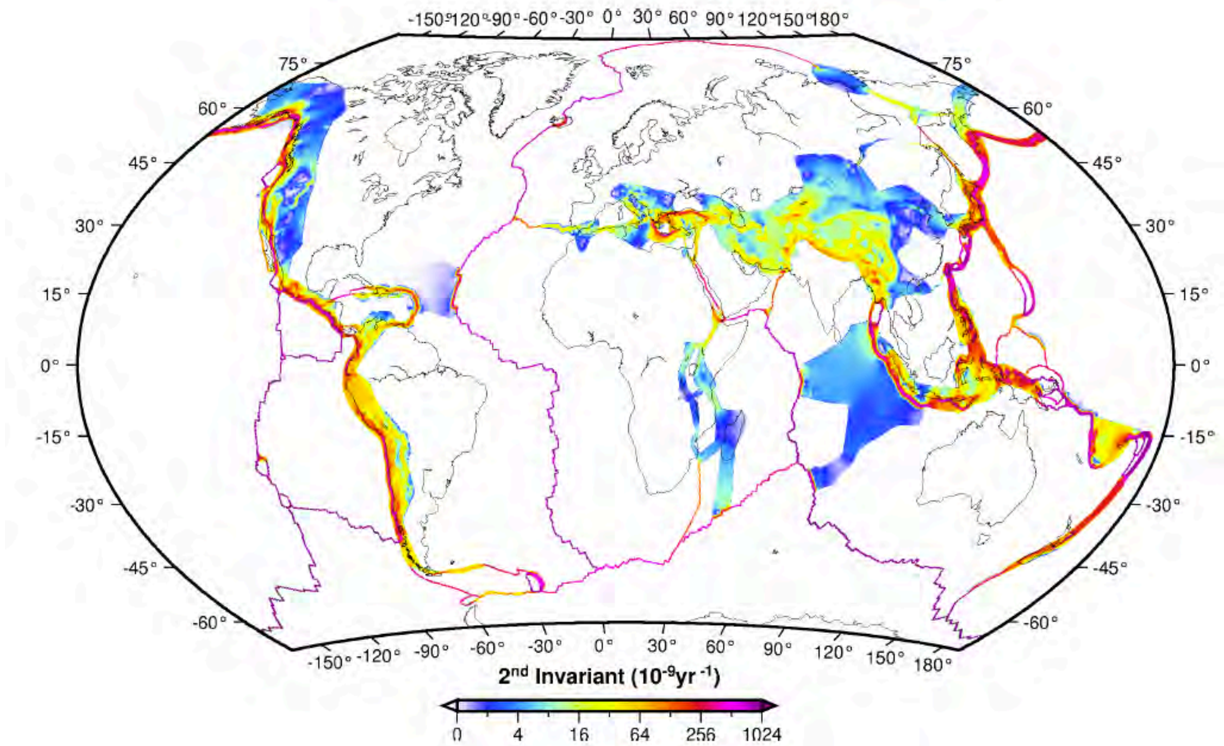

Figure 4.5 Contours of the second invariant of the strain rate tensor

In the second step, we take the modelled strain rate field from the first step and used it to constrain the *a priori* standard deviations. For this, we did not take-over the style or covariances but set the *a priori* standard deviation of $\dot{\varepsilon}_{\varphi\varphi}$ and $\dot{\varepsilon}_{\theta\theta}$ equal to the second invariant of the tensor modelled in step 1 ($\sqrt{\dot{\varepsilon}_{\varphi\varphi}{}^2 + \dot{\varepsilon}_{\theta\theta}{}^2 + 2\dot{\varepsilon}_{\varphi\theta}{}^2}$), and $\dot{\varepsilon}_{\varphi\vartheta}$ to the second invariant divided by the square-root of 2. However, we only want to apply these constraints to those cells that are reasonably well constrained by the GPS data so not to potentially "blow-up" the strain rates in areas where the data don't warrant it. We decided that a grid cell is constrained by the data if its midpoint lies within an ellipse defined by a pair of geodetic stations (within the deforming zones) less than 200 km apart with the data points situated at the endpoints of the major axis, and the length of the minor-axis being 3/4 of the major axis. Figure 4.4 shows the grid cells that we define as being well constrained by the data. All cells whose midpoints do not fall within any ellipse had their *a priori* standard deviations set to 0.35 times the second invariant of the tensor modelled in step 1 (to damp the model more where there are no data), unless that value is lower than the *a priori* standard deviations used in step 1 (i.e., 10^{-8}/yr), in which case those *a priori* standard deviations values are used. The latter exception is to avoid large signal-to-noise values in slowly deforming (<10^{-8}/yr), unconstrained, areas. A final exception was given to the Colorado Plateau area in the western United States. Because of how we define stable North America, we would obtain a band of elevated strain rates on the eastern edge of the Pacific-North America plate boundary zone (see discussion on the definition of the North America rotation vector in section 4.2) when following the procedure above. To avoid most of this artefact, we set the *a priori* strain rates in the second step to 5x 10^{-9}/yr in order to damp the model there.

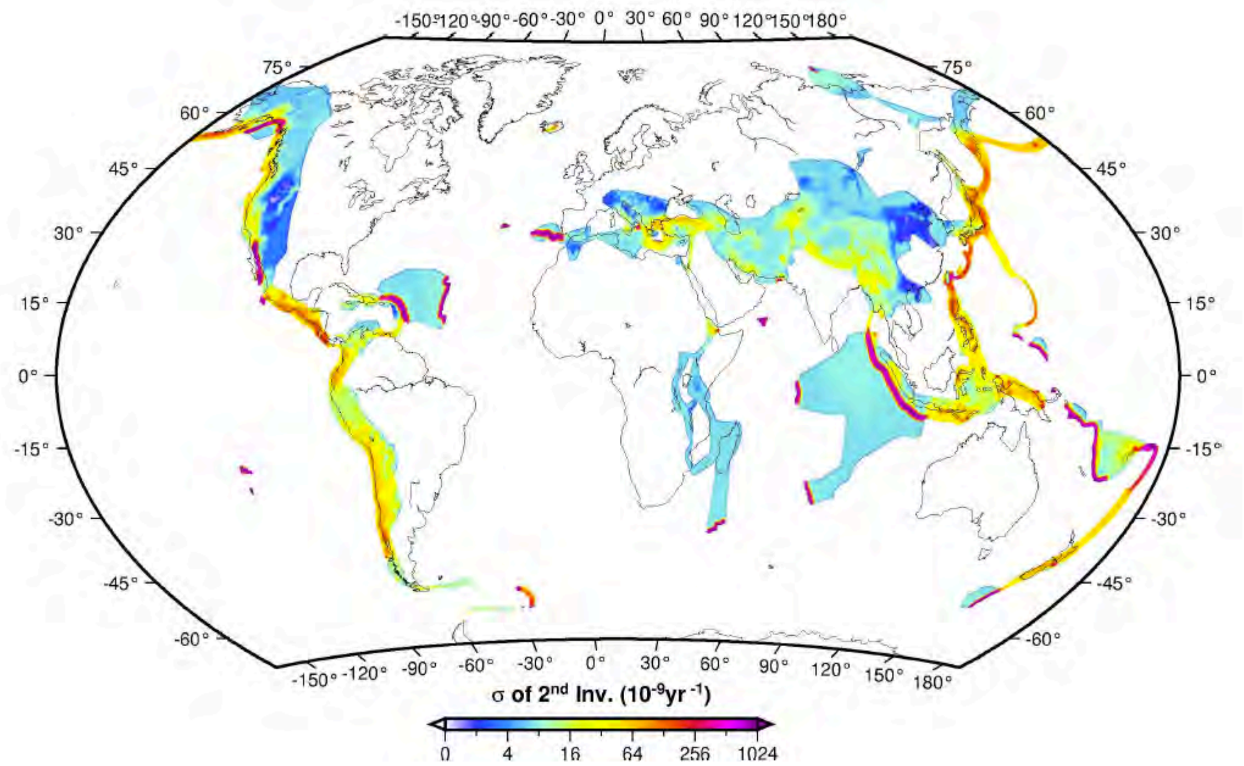

Figure 4.6 Contours of the standard deviation of the second invariant of the strain rate tensor

4.3.3 Results

The second invariant of strain rate of GSRM v.2 is shown in Figure 4.5. Note that the colour-scale is non-linear and that the high values are saturated. Strain rate contours for selected regions (where the model is well constrained by GPS data) are shown in Appendix A along with the input data.

A map with formal model uncertainties is shown in Figure 4.6 and a map with the signal-to-noise ratio in Figure 4.7. It is important to keep in mind that the shown uncertainties are indicative for uncertainty of the model at the scale of the 0.2° by 0.25° large cells. Because station spacing is for many areas (much) larger than the grid dimension, model uncertainties are correspondingly large. Also note that the strain rate uncertainties are zero for most spreading ridges and transform, because the deforming grid is only one grid cell wide, and thus the average model strain rates for those cells are exact.

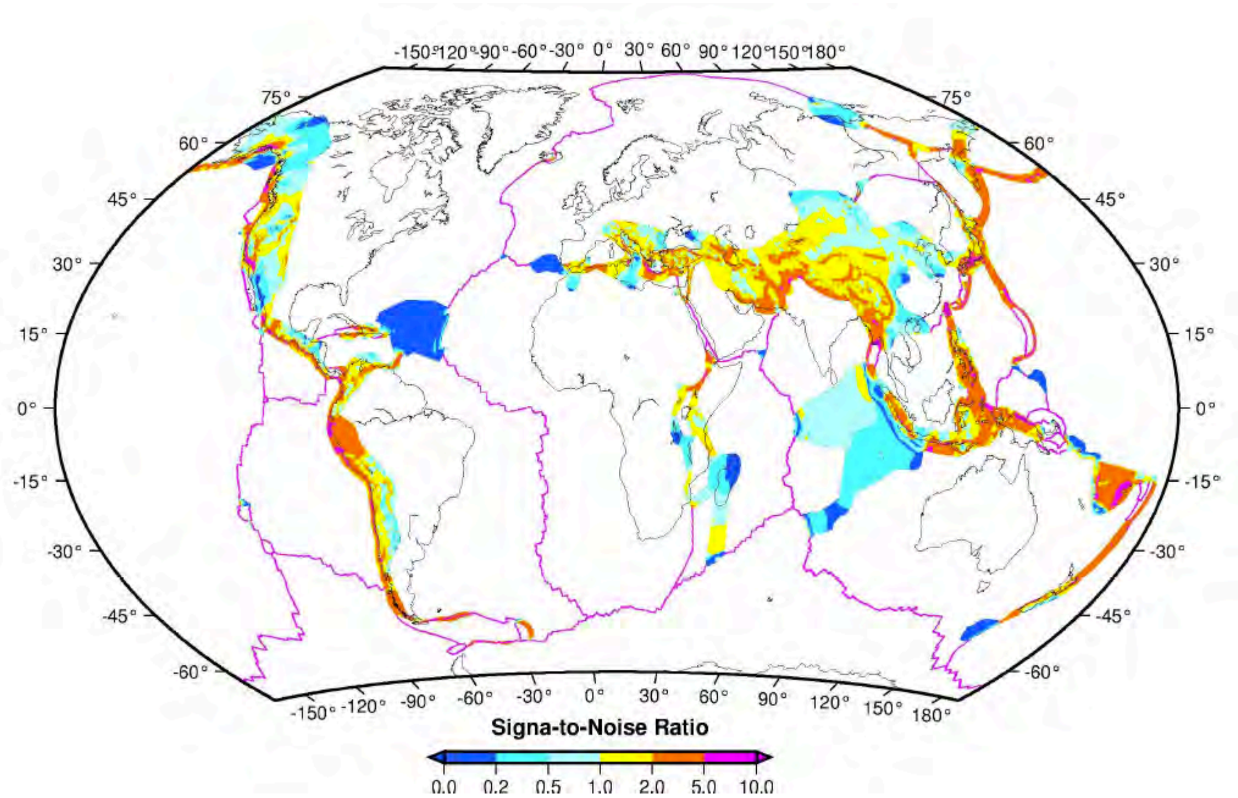

Figure 4.7 Contours of the signal-to-noise (results of Figure 4.5 divided by those in Figure 4.6)

5 Display and Archive of Data and Model

To dramatically show some of the GEM results around the globe, UNAVCO created and hosts a Google Earth representation of the GEM Strain Rate magnitude by images in a KMZ file, available online at http://gsrm2.unavco.org/images/GSRM_strain_magnitude.kmz (Figure 5.1). This Google Earth resource uses the tiling approach to show images of strain magnitude at progressively higher resolution as you zoom in towards the Earth surface. Images of GEM strain magnitude used in tiling, and the related logarithmic color scale, were created with UNAVCO's IDV visualization system (http://facility.unavco.org/software/idv/idv.html), which also made images for the GEM Strain Rate Model Project web site.

UNAVCO created, and hosts online, the "GEM GPS Velocity Viewer", available from the GEM SRM web site (Figure 5.2). This web tool shows the GPS velocity data and the user can control for map region and size, and for vector size, coloring , and decluttering. A user may also show the "error ellipses" for each station, a graphical depiction of data quality, and may show labels with information boxes for each station and its motion vector. GPS motion vectors can be defined relative to 53 reference frames, 50 of which are fixed plate reference frames, and additional frames are 1) a no-net-rotation reference frame, recomputed from the new model [after *Kreemer and Holt*, 2001; *Kreemer et al.*, 2006], 2) a frame that has the sub-asthenospheric mantle fixed [*Kreemer*, 2009], and IGS08 (the frame in which the original data was analysed).

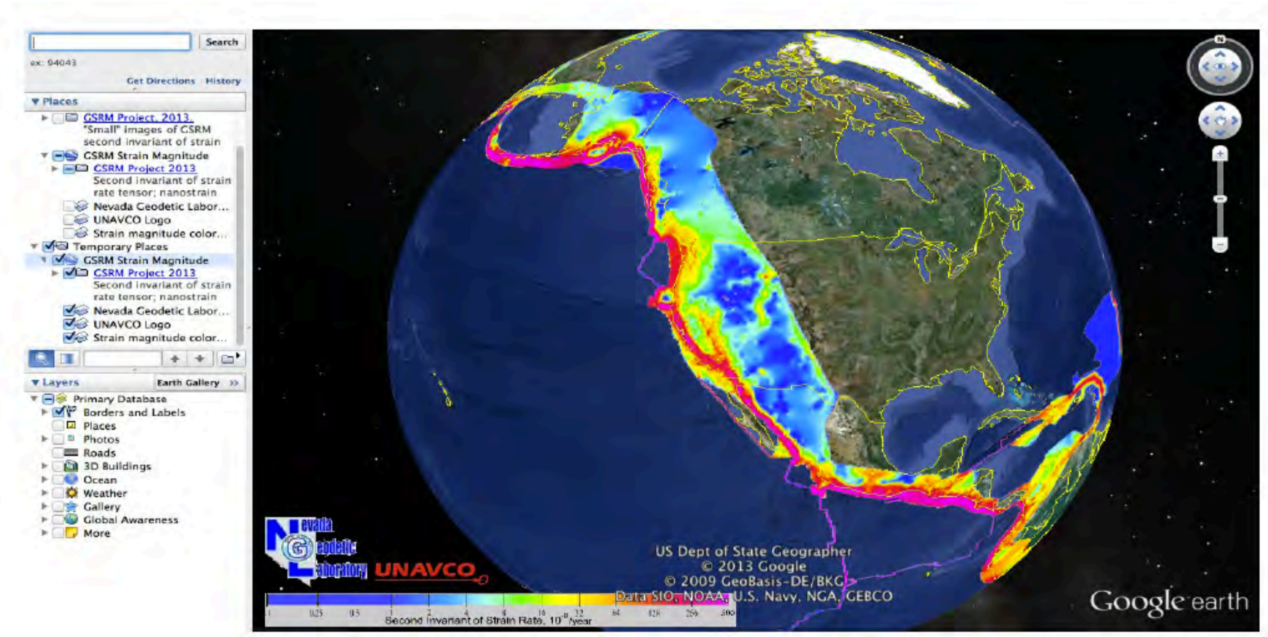

Figure 5.1 The GEM Strain Rate Model Project strain magnitude in Google Earth

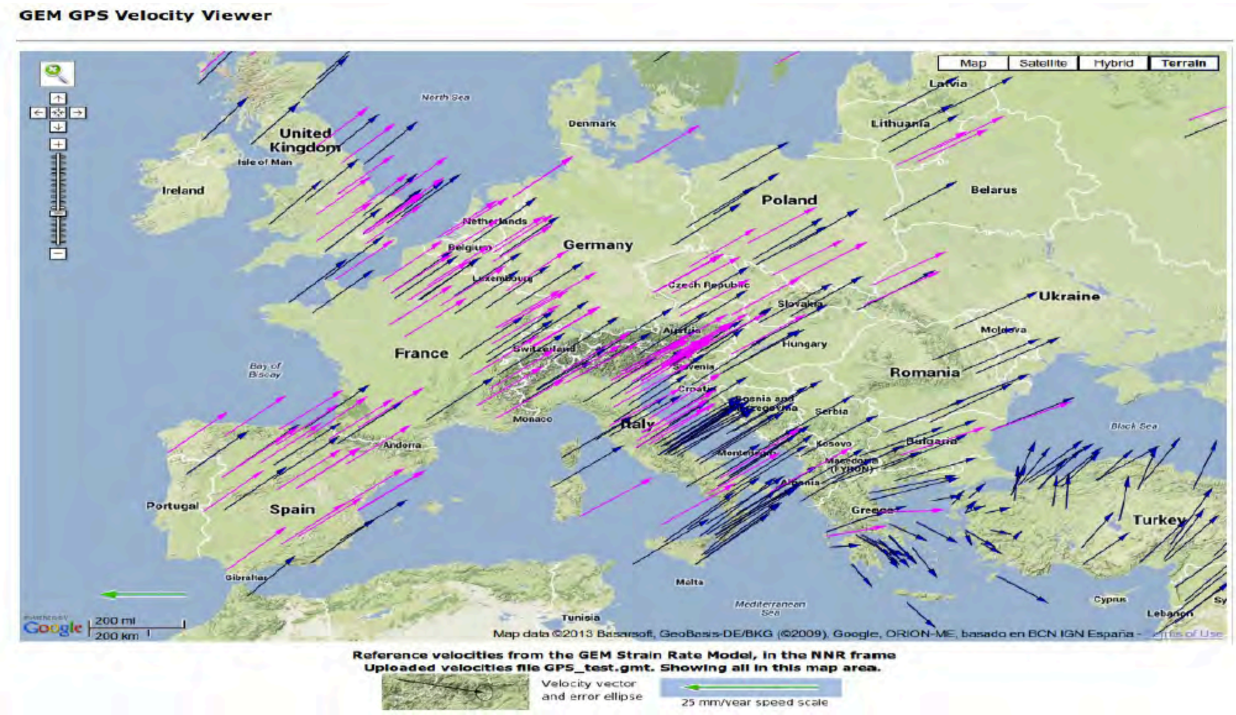

Figure 5.2 The GEM GPS velocity viewer map

The "GSRM GPS Velocity Viewer" also allows Earth scientists to to upload a file with their own velocity data of station motions observations and plot vectors for them. This allows side by side comparison of their data with the GPS velocity data used in GSRM v.2. Users may optionally change their data from any of the 53 GEM Strain Rate project reference frames, to any other reference frame. This tool can quickly reveal important parallels of differing data sets, indicating either important Earth behaviour or detecting obvious errors in measurements of velocities.

The GSRM data and model files were reformatted for input to Generic Mapping Tools (GMT) routines, which constitute the underlying engine for map image creation for the Voyager tools. The GEM GSRM edition also required modification of the Voyager Java applet (which runs on the user's browser, if Java is allowed) and creation of the needed Perl modules on the UNAVCO jules servers needed to construct the proper GMT commands for map images, made on demand, which are sent back to the user's browser.

The options for the JVV GEM GSRM edition can be found here: http://jules.unavco.org/Voyager/Docs/GEM_GSRM

For representation of the GSRM tensor field, the JVV GEM GSRM edition can display:

- the second-invariant of the strain rate tensor
- the principal strain axes
- the vertical strain rate, Ezz = -Exx-Eyy
- the strain style; for key, see:
- http://jules.unavco.org/Voyager/Anc/GEM_GSRM/strain_rate_style
- a "scaled" strain style, weighted by the second-invariant of the strain rate

Note: Currently, the JVV interface is a Java applet requiring the user to be using Java 6, not Java 7.

6 Concluding Remarks

GSRM v.2 is a vast improvement over GSRM v.1.2 in terms of data input and model resolution. However, only at a few places is the data input sufficient to obtain well-constrained strain rates at the resolution of the underlying grid. In the future we hope to use a dynamic grid that has the grid size adjusted to the station spacing, so that no computational power is wasted and no high-resolution model is pretended at places where the data are insufficient. However, we also hope that the recent surge in GPS data densification continues. About half of all studies included in our compilation were published since 2010 and the time-series of thousands of CGPS stations will mature over the next few years.

Some areas with great data coverage (western Europe, central and eastern U.S.) are currently not modelled. The main reason being that the strain rates there are expected to be at or below the uncertainty in the GPS velocity data. Furthermore, adding those regions to the area for which strain rates are currently modelled would add a significant computational burden. Hopefully in a future iteration of the GSRM, we can include those areas.

There are still many areas with insufficient GPS coverage surrounding important seismogenic faults, let alone unknown faults. This situation may not change for a long time, yet knowledge of the strain accumulation rate across these faults is essential to assess their activity rate. A potential solution in improving the spatial resolution in areas with limited GPS coverage is the use of InSAR. Most recent developments have been on using GPS to help improve the resolution and usefulness of InSAR maps of strain accumulation [e.g., *Wei et al.*, 2010; *Tong et al.*, 2013], however these improvements really only lead to images of the deformation in the direction of the line-of-sight (LOS) of the satellite. The main problem lies in 1) the ambiguity in the 3D velocity vector that can explain the LOS velocity, and 2) the fact that the LOS is insensitive to velocities along the direction of the satellite track. Therefore, InSAR alone can never recovery the velocity gradient tensor field needed to determine the strain rate. However, recent advances have shown strain rate fields from a combination of GPS and InSAR data [*Wang and Wright*, 2012].

It is our hope that GSRM will directly contribute to GEM's goals through the creation of earthquake activity rate maps. The previous GSRM was used to make such maps [*Bird et al.*, 2010], and new results based on the new GSRM are in development. Another contribution of the new GSRM is in assessing the correctness of the moment rate budget implied by GEM's Faulted Earth model. Indeed, we envision a future GSRM that is not only consistent with the GPS velocities, but also satisfies the geologic and seismologic data in terms of the spatial distribution of strain rate. This could be done by using the fault slip rates and earthquake rates as *a priori* estimates of the strain rate variances when inverting the GPS velocities.

Finally, some recommendations for those collecting GPS data and who would like to see their results included in future models:

For campaign measurements:

- Time-series length >3 years
- Each campaign several 24 hour sessions
- Each campaign held at approximately same time of year
- Velocity uncertainty should be “reasonable” and not the formal, white-noise, uncertainty
- Provide the time-span, useful to assess the possible effect of earthquakes

For continuous measurements:

- Time-series length >2.5 years
- Velocity uncertainty should be based on time-correlated noise model
- Also provide vertical velocity, which would help identify hydrologic effects
- Provide the time-span, useful to assess the possible effect of earthquakes

REFERENCES

Document References

Aktuğ, B., E. Parmaksız, M. Kurt, O. Lenk, A. Kılıçoğlu, M. A. Gürdal, and S. Özdemir (2013), Deformation of Central Anatolia: GPS implications, J. Geodyn., 67, 78–96, doi:10.1016/j.jog.2012.05.008.

Almuselmani, B., F. . Teferle, R. M. Bingley, and T. Moore (2008), New estimates of present-day Arabia plate motion and deformation from a dense GPS network in Saudi Arabia, vol. 89, p. G34A–02.

Altamimi, Z., L. Métivier, and X. Collilieux (2012), ITRF2008 plate motion model, J. Geophys. Res., 117(B7), B07402, doi:10.1029/2011JB008930.

Anderson, H., and J. Jackson (1987), Active tectonics of the Adriatic Region, Geophys. J. Int., 91(3), 937–983, doi:10.1111/j.1365-246X.1987.tb01675.x.

Antonelis, K., D. J. Johnson, M. M. Miller, and R. Palmer (1999), GPS determination of current Pacific–North American plate motion, Geology, 27(4), 299–302, doi:10.1130/0091-7613(1999)027<0299:GDOCPN>2.3.CO;2.

Apel, E. V., R. Bürgmann, G. Steblov, N. Vasilenko, R. King, and A. Prytkov (2006), Independent active microplate tectonics of northeast Asia from GPS velocities and block modeling, Geophys. Res. Lett., 33(11), L11303, doi:10.1029/2006GL026077.

Argus, D. F., and R. G. Gordon (1991), Current Sierra Nevada-North America motion from very long baseline interferometry:Implications for the kinematics of the western United States, Geology, 19(11), 1085–1088, doi:10.1130/0091-7613(1991)019<1085:CSNNAM>2.3.CO;2.

Argus, D. F., R. G. Gordon, M. B. Heflin, C. Ma, R. J. Eanes, P. Willis, W. R. Peltier, and S. E. Owen (2010), The angular velocities of the plates and the velocity of Earth's centre from space geodesy, Geophys. J. Int., 180(3), 913–960, doi:10.1111/j.1365-246X.2009.04463.x.

Asensio, E., G. Khazaradze, A. Echeverria, R. W. King, and I. Vilajosana (2012), GPS studies of active deformation in the Pyrenees, Geophys. J. Int., 190(2), 913–921, doi:10.1111/j.1365-246X.2012.05525.x.

Ashurkov, S. V., V. A. San'kov, A. I. Miroshnichenko, A. V. Lukhnev, A. P. Sorokin, M. A. Serov, and L. M. Byzov (2011), GPS geodetic constraints on the kinematics of the Amurian Plate, Russian Geology and Geophysics, 52(2), 239–249, doi:10.1016/j.rgg.2010.12.017.

Avouac, J. P., P. Tapponnier, M. Bai, H. You, and G. Wang (1993), Active thrusting and folding along the northern Tien Shan and Late Cenozoic rotation of the Tarim relative to Dzungaria and Kazakhstan, J. Geophys. Res., 98(B4), 6755–6804, doi:10.1029/92JB01963.

Bacolcol, T., E. Barrier, T. Duquesnoy, A. Aguilar, R. Jorgio, R. de la Cruz, and M. Lasala (2005), GPS constraints on Philippine Fault slip rate in Masbate Island, central Philippines, J. Geol. Soc. Phil., 1–7.

Baek, J., Y.-H. Shin, S.-H. Na, N. V. Shestakov, P.-H. Park, and S. Cho (2012), Coseismic and postseismic crustal deformations of the Korean Peninsula caused by the 2011 Mw 9.0 Tohoku earthquake, Japan, from global positioning system data, Terra Nova, 24(4), 295–300, doi:10.1111/j.1365-3121.2012.01062.x.

Battaglia, M., M. H. Murray, E. Serpelloni, and R. Bürgmann (2004), The Adriatic region: An independent microplate within the Africa-Eurasia collision zone, Geophys. Res. Lett., 31(9), L09605, doi:10.1029/2004GL019723.

Beavan, J., and J. Haines (2001), Contemporary horizontal velocity and strain rate fields of the Pacific-Australian plate boundary zone through New Zealand, J. Geophys. Res., 106(B1), 741–770, doi:10.1029/2000JB900302.

Benford, B., C. DeMets, B. Tikoff, P. Williams, L. Brown, and M. Wiggins-Grandison (2012), Seismic hazard along the southern boundary of the Gônave microplate: block modelling of GPS velocities from Jamaica and nearby islands, northern Caribbean, Geophys. J. Int., 190(1), 59–74, doi:10.1111/j.1365-246X.2012.05493.x.

Berglund, H. T., A. F. Sheehan, M. H. Murray, M. Roy, A. R. Lowry, R. S. Nerem, and F. Blume (2012), Distributed deformation across the Rio Grande Rift, Great Plains, and Colorado Plateau, Geology, 40(1), 23–26, doi:10.1130/G32418.1.

Bertiger, W., S. D. Desai, B. Haines, N. Harvey, A. W. Moore, S. Owen, and J. P. Weiss (2010), Single receiver phase ambiguity resolution with GPS data, J Geod, 84(5), 327–337, doi:10.1007/s00190-010-0371-9.

Bettinelli, P., J.-P. Avouac, M. Flouzat, F. Jouanne, L. Bollinger, P. Willis, and G. Chitrakar (2006), Plate Motion of India and Interseismic Strain in the Nepal Himalaya from GPS and DORIS Measurements, J. Geodesy, 80(8), 567–589, doi:10.1007/s00190-006-0030-3.

Bird, P. (2003), An updated digital model of plate boundaries, Geochemistry, Geophysics, Geosystems, 4(3), 1027, doi:10.1029/2001GC000252.

Bird, P., C. Kreemer, and W. E. Holt (2010), A long-term forecast of shallow seismicity based on the global strain rate map, Seismol. Res. Lett., 81(2), 184–194, doi:10.1785/gssrl.81.2.184.

Blewitt, G. (1989), Carrier phase ambiguity resolution for the Global Positioning System applied to geodetic baselines up to 2000 km, J. Geophys. Res., 94(B8), 10187–10203, doi:10.1029/JB094iB08p10187.

Blewitt, G. (1990), An Automatic Editing Algorithm for GPS data, Geophys. Res. Lett., 17(3), 199–202, doi:10.1029/GL017i003p00199.

Blewitt, G., and D. Lavallée (2002), Effect of annual signals on geodetic velocity, J. Geophys. Res., 107(B7), B72145, doi:10.1029/2001JB000570.

Blewitt, G., W. C. Hammond, and C. Kreemer (2009), Geodetic observation of contemporary deformation in the northern Walker Lane: 1. Semipermanent GPS strategy, Geological Society of America Special Papers, 447, 1–15, doi:10.1130/2009.2447(01).

Bock, Y., L. Prawirodirdjo, J. F. Genrich, C. W. Stevens, R. McCaffrey, C. Subarya, S. S. O. Puntodewo, and E. Calais (2003), Crustal motion in Indonesia from Global Positioning System measurements, J. Geophys. Res., 108(B8), 2367, doi:10.1029/2001JB000324.

Boehm, J., A. Niell, P. Tregoning, and H. Schuh (2006), Global Mapping Function (GMF): A new empirical mapping function based on numerical weather model data, Geophys. res. Lett., 33(7), L07304, doi:10.1029/2005GL025546.

Ten Brink, U. S., and A. M. López-Venegas (2012), Plate interaction in the NE Caribbean subduction zone from continuous GPS observations, Geophys. Res. Lett., 39, L10304, doi:10.1029/2012GL051485.

Brooks, B. A., M. Bevis, R. S. Jr, E. Kendrick, R. Manceda, E. Lauría, R. Maturana, and M. Araujo (2003), Crustal motion in the Southern Andes (26°–36°S): Do the Andes behave like a microplate?, Geochem. Geophys. Geosyst., 4(10), 1085, doi:10.1029/2003GC000505.

Calais, E., J. Y. Han, C. DeMets, and J. M. Nocquet (2006a), Deformation of the North American plate interior from a decade of continuous GPS measurements, J. Geophys. Res., 111(B6), B06402, doi:10.1029/2005JB004253.

Calais, E., C. Ebinger, C. Hartnady, and J.-M. Nocquet (2006b), Kinematics of the East African rift from GPS and earthquake slip vector data, in The Afar Volcanic Province within the East African Rift System, vol. 259, edited by C. J. Ebinger, G. Yirgu, and P. K. . Maguire, pp. 9–22.

Chamot-Rooke, N., and A. Rabaute (2006), Plate tectonics from space, Commission for the Geological Map of the World, scale: 1:50000000,

Chlieh, M., H. Perfettini, H. Tavera, J.-P. Avouac, D. Remy, J.-M. Nocquet, F. Rolandone, F. Bondoux, G. Gabalda, and S. Bonvalot (2011), Interseismic coupling and seismic potential along the Central Andes subduction zone, J. Geophys. Res., 116(B12), B12405, doi:10.1029/2010JB008166.

Conder, J. A., and D. W. Forsyth (2001), Seafloor spreading on the Southeast Indian Ridge over the last one million years: a test of the Capricorn plate hypothesis, Earth Planet. Sci. Lett., 188(1), 91–105, doi:10.1016/S0012-821X(01)00326-0.

Cook, D. B., K. Fujita, and C. A. McMullen (1986), Present-day plate interactions in Northeast Asia: North American, Eurasian, and Okhotsk plates, J. Geodyn., 6(1–4), 33–51, doi:10.1016/0264-3707(86)90031-1.

Cross, R. S., and J. T. Freymueller (2008), Evidence for and implications of a Bering plate based on geodetic measurements from the Aleutians and western Alaska, J. Geophys. Res., 113(B7), B07405, doi:10.1029/2007JB005136.

D'Agostino, N., A. Avallone, D. Cheloni, E. D'Anastasio, S. Mantenuto, and G. Selvaggi (2008), Active tectonics of the Adriatic region from GPS and earthquake slip vectors, J. Geophys. Res., 113(B12), B12413, doi:10.1029/2008JB005860.

Dawson, J., G. Luton, and R. Govind (2004), Permanent Committee for GIS Infrastructure for Asia and the Pacific, 1997, 1998, 1999, 2000, 2001, 2002 GPS Campaign Analysis, Geoscience Australia.

DeMets, C., R. G. Gordon, and D. F. Argus (2010), Geologically current plate motions, Geophys. J. Int., 181(1), 1–80, doi:10.1111/j.1365-246X.2009.04491.x.

Dietrich, R., A. Rülke, J. Ihde, K. Lindner, H. Miller, W. Niemeier, H.-W. Schenke, and G. Seeber (2004), Plate kinematics and deformation status of the Antarctic Peninsula based on GPS, Global and Planetary Change, 42(1–4), 313–321, doi:10.1016/j.gloplacha.2003.12.003.

Dixon, T. H., M. Miller, F. Farina, H. Wang, and D. Johnson (2000), Present-day motion of the Sierra Nevada block and some tectonic implications for the Basin and Range province, North American Cordillera, Tectonics, 19(1), 1–24, doi:10.1029/1998TC001088.

Drewes, H., and O. Heidbach (2012), The 2009 horizontal velocity field for South America and the Caribbean, in Geodesy for Planet Earth, vol. 136, edited by S. Kenyon, M. C. Pacino, and U. Marti, pp. 657–664, Springer Berlin Heidelberg.

Duquesnoy, T., M. Kasser, M. Aurelio, R. Gaulon, R. S. Punongbayan, and C. Rangin (1994), Detection of creep along the Philippine Fault: First results of geodetic measurements on Leyte Island, central Philippine, Geophys. Res. Lett., 21(11), 975–978, doi:10.1029/94GL00640.

Elliott, J., J. T. Freymueller, and C. F. Larsen (2013), Active tectonics of the St. Elias Orogen, Alaska, observed with GPS measurements, J. Geophys. Res., in press, doi:10.1002/jgrb.50341.

Elliott, J. L., C. F. Larsen, J. T. Freymueller, and R. J. Motyka (2010), Tectonic block motion and glacial isostatic adjustment in southeast Alaska and adjacent Canada constrained by GPS measurements, J. Geophys. Res., 115(B9), B09407, doi:10.1029/2009JB007139.

Floyd, M. A. et al. (2010), A new velocity field for Greece: Implications for the kinematics and dynamics of the Aegean, J. Geophys. Res., 115(B10), B10403, doi:10.1029/2009JB007040.

Gagnon, K., C. D. Chadwell, and E. Norabuena (2005), Measuring the onset of locking in the Peru-Chile trench with GPS and acoustic measurements, Nature, 434(7030), 205–208, doi:10.1038/nature03412.

Ganas, A., A. Marinou, D. Anastasiou, D. Paradissis, K. Papazissi, P. Tzavaras, and G. Drakatos (2013), GPS-derived estimates of crustal deformation in the central and north Ionian Sea, Greece: 3-yr results from NOANET continuous network data, J. Geodyn., 67, 62–71, doi:10.1016/j.jog.2012.05.010.

Gan, W., P. Zhang, Z.-K. Shen, Z. Niu, M. Wang, Y. Wan, D. Zhou, and J. Cheng (2007), Present-day crustal motion within the Tibetan Plateau inferred from GPS measurements, J. Geophys. Res., 112(B8), B08416, doi:10.1029/2005JB004120.

Genrich, J. F., Y. Bock, R. McCaffrey, L. Prawirodirdjo, C. W. Stevens, S. S. O. Puntodewo, C. Subarya, and S. Wdowinski (2000), Distribution of slip at the northern Sumatran fault system, J. Geophys. Res., 105(B12), 28327–28341, doi:10.1029/2000JB900158.

Haines, A. J., and W. E. Holt (1993), A procedure for obtaining the complete horizontal motions within zones of distributed deformation from the inversion of strain rate data, J. Geophys. Res., 98(B7), 12057–12082, doi:10.1029/93JB00892.

Hammond, W. C., G. Blewitt, and C. Kreemer (2011), Block modeling of crustal deformation of the northern Walker Lane and Basin and Range from GPS velocities, J. Geophys. Res., 116(B4), B04402, doi:10.1029/2010JB007817.

Harada, Y. (2000), The motion of the Pacific plate determined by a GPS network of Pacific Islands, Bull. Geogr. Surv. Inst., 46, 11–15.

Hartnady, C. J. H. (2002), Earthquake hazard in Africa: perspectives on the Nubia-Somalia boundary, South African Journal of Science, 98(9-10), 425–428.

Henton, J. A., M. R. Craymer, R. Ferland, H. Dragert, S. Mazzotti, and D. L. Forbes (2006), Crustal motion and deformation monitoring of the Canadian landmass, Geomatica, 60(2), 173–191.

Hill, E. M., and G. Blewitt (2006), Testing for fault activity at Yucca Mountain, Nevada, using independent GPS results from the BARGEN network, Geophys. Res. Lett., 33(14), L14302, doi:10.1029/2006GL026140.

Van der Hoeven, A. G. A., V. Mocanu, W. Spakman, M. Nutto, A. Nuckelt, L. Matenco, L. Munteanu, C. Marcu, and B. A. C. Ambrosius (2005), Observation of present-day tectonic motions in the Southeastern Carpathians: Results of the ISES/CRC-461 GPS measurements, Earth Planet. Sci. Lett., 239(3–4), 177–184, doi:10.1016/j.epsl.2005.09.018.

Holt, W. E., B. Shen-Tu, J. Haines, and J. Jackson (2000), On the determination of self-consistent strain rate fields within zones of distributed continental deformation, in Geophysical Monograph Series, vol. 121, edited by M. A. Richards, R. G. Gordon, and R. D. van der Hilst, pp. 113–141, American Geophysical Union, Washington, D. C.

Holt, W. E., C. Kreemer, A. J. Haines, L. Estey, C. Meertens, G. Blewitt, and D. Lavallée (2005), Project helps constrain continental dynamics and seismic hazards, Eos, Transactions American Geophysical Union, 86(41), 383–387, doi:10.1029/2005EO410002.

Horner-Johnson, B. C., R. G. Gordon, and D. F. Argus (2007), Plate kinematic evidence for the existence of a distinct plate between the Nubian and Somalian plates along the Southwest Indian Ridge, J. Geophys. Res., 112(B5), B05418, doi:10.1029/2006JB004519.

Jackson, J., and D. McKenzie (1984), Active tectonics of the Alpine—Himalayan Belt between western Turkey and Pakistan, Geophys. J. Int., 77(1), 185–264, doi:10.1111/j.1365-246X.1984.tb01931.x.

Jansma, P. E., G. S. Mattioli, A. Lopez, C. DeMets, T. H. Dixon, P. Mann, and E. Calais (2000), Neotectonics of Puerto Rico and the Virgin Islands, northeastern Caribbean, from GPS geodesy, Tectonics, 19(6), 1021–1037, doi:10.1029/1999TC001170.

Jiang, W.-P., D.-C. E, B.-W. Zhan, and Y.-W. Liu (2009), New model of Antarctic plate motion and its analysis, Chin. j. Geophys., 52(1), 23–32.

Kato, T., J. Beavan, T. Matsushima, Y. Kotake, J. T. Camacho, and S. Nakao (2003), Geodetic evidence of back-arc spreading in the Mariana Trough, Geophys. Res. Lett., 30(12), 1625, doi:10.1029/2002GL016757.

Kendrick, E., M. Bevis, R. Smalley Jr., B. Brooks, R. B. Vargas, E. Lauría, and L. P. S. Fortes (2003), The Nazca–South America Euler vector and its rate of change, J. South Am. Earth Sci., 16(2), 125–131, doi:10.1016/S0895-9811(03)00028-2.

Kierulf, H. P., M. Ouassou, M. J. R. Simpson, and O. Vestøl (2013), A continuous velocity field for Norway, J Geod, 87(4), 337–349, doi:10.1007/s00190-012-0603-2.

Kogan, M. G., and G. M. Steblov (2008), Current global plate kinematics from GPS (1995–2007) with the plate-consistent reference frame, J. Geophys. Res., 113(B4), B04416, doi:10.1029/2007JB005353.

Kreemer, C. (2009), Absolute plate motions constrained by shear wave splitting orientations with implications for hot spot motions and mantle flow, J. Geophys. Res., 114, B10405, doi:10.1029/2009JB006416.

Kreemer, C., and W. E. Holt (2001), A no-net-rotation model of present-day surface motions, Geophys. Res. Lett., 28(23), 4407–4410, doi:10.1029/2001GL013232.

Kreemer, C., J. Haines, W. Holt, G. Blewitt, and D. Lavallée (2000), On the determination of a global strain rate model., Geophys. J. Int., 52(10), 765–770.

Kreemer, C., W. E. Holt, and A. J. Haines (2003), An integrated global model of present-day plate motions and plate boundary deformation, Geophys. J. Int., 154(1), 8–34, doi:10.1046/j.1365-246X.2003.01917.x.

Kreemer, C., D. A. Lavallée, G. Blewitt, and W. E. Holt (2006), On the stability of a geodetic no-net-rotation frame and its implication for the International Terrestrial Reference Frame, Geophys. Res. Lett., 33, L17306, doi:10.1029/2006GL027058.

Kreemer, C., G. Blewitt, and W. C. Hammond (2010a), Evidence for an active shear zone in southern Nevada linking the Wasatch fault to the Eastern California shear zone, Geology, 38(5), 475–478, doi:10.1130/G30477.1.

Kreemer, C., G. Blewitt, and R. A. Bennett (2010b), Present-day motion and deformation of the Colorado Plateau, Geophys. Res. Lett., 37(10), L10311, doi:10.1029/2010GL043374.

Kreemer, C., R. G. Gordon, and J. K. Mishra (2010c), The effect of horizontal thermal contraction on oceanic intraplate deformation: examples for the Pacific, in EGU General Assembly Conference Abstracts, vol. 12, p. 13918.

Kreemer, C., W. C. Hammond, G. Blewitt, A. A. Holland, and R. A. Bennett (2012), A geodetic strain rate model for the Pacific-North American plate boundary, western United States, Nevada Bureau of Mines and Geolog Map 178, scale 1:1,500,000.

Kumar, R. R., and R. G. Gordon (2009), Horizontal thermal contraction of oceanic lithosphere: The ultimate limit to the rigid plate approximation, J. Geophys. Res., 114(B1), B01403, doi:10.1029/2007JB005473.

Lidberg, M., J. M. Johansson, H.-G. Scherneck, and G. A. Milne (2010), Recent results based on continuous GPS observations of the GIA process in Fennoscandia from BIFROST, J. Geodyn., 50(1), 8–18, doi:10.1016/j.jog.2009.11.010.

De Lis Mancilla, F., D. Stich, M. Berrocoso, R. Martín, J. Morales, A. Fernandez-Ros, R. Páez, and A. Pérez-Peña (2013), Delamination in the Betic Range: Deep structure, seismicity, and GPS motion, Geology, 41(3), 307–310, doi:10.1130/G33733.1.

Lyard, F., F. Lefevre, T. Letellier, and O. Francis (2006), Modelling the global ocean tides: modern insights from FES2004, Ocean Dynamics, 56(5-6), 394–415, doi:10.1007/s10236-006-0086-x.

Mackey, K. G., K. Fujita, L. V. Gunbina, V. N. Kovalev, V. S. Imaev, B. M. Koz'min, and L. P. Imaeva (1997), Seismicity of the Bering Strait region: Evidence for a Bering block, Geology, 25(11), 979–982, doi:10.1130/0091-7613(1997)025<0979:SOTBSR>2.3.CO;2.

Mahmoud, S., R. Reilinger, S. McClusky, P. Vernant, and A. Tealeb (2005), GPS evidence for northward motion of the Sinai Block: Implications for E. Mediterranean tectonics, Earth and Planetary Science Letters, 238(1–2), 217–224, doi:10.1016/j.epsl.2005.06.063.

Manaker, D. M., E. Calais, A. M. Freed, S. T. Ali, P. Przybylski, G. Mattioli, P. Jansma, C. Petit, and J. B. de Chabalier (2008), Interseismic plate coupling and strain partitioning in the Northeastern Caribbean, Geophys. J. Int., 174(3), 889–903.

Mann, P., F. W. Taylor, R. L. Edwards, and T.-L. Ku (1995), Actively evolving microplate formation by oblique collision and sideways motion along strike-slip faults: An example from the northeastern Caribbean plate margin, Tectonophysics, 246(1–3), 1–69, doi:10.1016/0040-1951(94)00268-E.

Matson, S. E. (2007), Arc kinematics of the Northern Lesser Antilles from GPS geodesy, M.S., University of Arkansas.

Mazzotti, S., T. S. James, J. Henton, and J. Adams (2005), GPS crustal strain, postglacial rebound, and seismic hazard in eastern North America: The Saint Lawrence valley example, J. Geophys. Res., 110(B11), B11301, doi:10.1029/2004JB003590.

McCaffrey, R. (2005), Block kinematics of the Pacific–North America plate boundary in the southwestern United States from inversion of GPS, seismological, and geologic data, Journal of Geophysical Research, 110(B7), B07401, doi:10.1029/2004JB003307.

McCaffrey, R., R. W. King, S. J. Payne, and M. Lancaster (2013), Active tectonics of northwestern U.S. inferred from GPS-derived surface velocities, J. Geophys. Res., 118, doi:10.1029/2012JB009473.

McCann, W. R. (1985), On the earthquake hazards of Puerto Rico and the Virgin Islands, Bull. Seismol. Soc. Amer., 75(1), 251–262.

McClusky, S. et al. (2000), Global Positioning System constraints on plate kinematics and dynamics in the eastern Mediterranean and Caucasus, J. Geophys. Res., 105(B3), 5695–5719, doi:10.1029/1999JB900351.

McClusky, S. et al. (2010), Kinematics of the southern Red Sea–Afar Triple Junction and implications for plate dynamics, Geophys. Res. Lett., 37(5), L05301, doi:10.1029/2009GL041127.

McKenzie, D. P. (1970), Plate tectonics of the Mediterranean region, Nature, 226(5242), 239–243, doi:10.1038/226239a0.

Meade, B. J. (2007), Present-day kinematics at the India-Asia collision zone, Geology, 35(1), 81–84, doi:10.1130/G22924A.1.

Medak, D., and B. Pribicevic (2006), Processing of geodynamic GPS neworks in Croatia with GAMIT software, in The Adriatic Microplate: GPS Geodesy, Tectonics and Hazards, vol. 61, edited by N. Pinter, pp. 247–256, Springer.

Mendes, V. B., J. Madeira, A. Brum da Silveira, A. Trota, P. Elosegui, and J. Pagarete (2013), Present-day deformation in São Jorge Island, Azores, from episodic GPS measurements (2001–2011), Adv. Space Res., 51(8), 1581–1592, doi:10.1016/j.asr.2012.10.019.

Meng, G. J., X. H. Shen, S. Vladimir, A. R. Eugene, and J. C. Wu (2009), Research on characteristics of present-day crustal motion and deformation in Kamchatka area, Chin. J. Geophys., 52(3), 720–731.

Miranda, J. M., A. Navarro, J. Catalão, and R. M. S. Fernandes (2012), Surface displacement field at Terceira island deduced from repeated GPS measurements, J. Volc. Geoth. Res., 217–218, 1–7, doi:10.1016/j.jvolgeores.2011.10.009.

Müller, M. D., A. Geiger, H.-G. Kahle, G. Veis, H. Billiris, D. Paradissis, and S. Felekis (2013), Velocity and deformation fields in the North Aegean domain, Greece, and implications for fault kinematics, derived from GPS data 1993–2009, Tectonophysics, 597-598, 34–49, doi:10.1016/j.tecto.2012.08.003.

Mullick, M., F. Riguzzi, and D. Mukhopadhyay (2009), Estimates of motion and strain rates across active faults in the frontal part of eastern Himalayas in North Bengal from GPS measurements, Terra Nova, 21(5), 410–415, doi:10.1111/j.1365-3121.2009.00898.x.

Munekane, H., and Y. Fukuzaki (2006), A plate motion model around Japan, Bull. Geogr. Surv. Inst., 35-41, 35.

Nishimura, S., M. Hashimoto, and M. Ando (2004), A rigid block rotation model for the GPS derived velocity field along the Ryukyu arc, Phys. Earth Planet. Inter., 142(3–4), 185–203, doi:10.1016/j.pepi.2003.12.014.

Nocquet, J.-M. (2012), Present-day kinematics of the Mediterranean: A comprehensive overview of GPS results, Tectonophysics, 579, 220–242, doi:10.1016/j.tecto.2012.03.037.

Peltier, W. R., and R. Drummond (2008), Rheological stratification of the lithosphere: A direct inference based upon the geodetically observed pattern of the glacial isostatic adjustment of the North American continent, Geophys. Res. Lett., 35(16), L16314, doi:10.1029/2008GL034586.

Plattner, C., R. Malservisi, T. H. Dixon, P. LaFemina, G. F. Sella, J. Fletcher, and F. Suarez-Vidal (2007), New constraints on relative motion between the Pacific Plate and Baja California microplate (Mexico) from GPS measurements, Geophys. J. Int., 170(3), 1373–1380, doi:10.1111/j.1365-246X.2007.03494.x.

Prawirodirdjo, L., and Y. Bock (2004), Instantaneous global plate motion model from 12 years of continuous GPS observations, J. Geophys. Res., 109(B8), B08405, doi:10.1029/2003JB002944.

Rebischung, P., J. Griffiths, J. Ray, R. Schmid, X. Collilieux, and B. Garayt (2012), IGS08: the IGS realization of ITRF2008, GPS Solut., 16(4), 483–494, doi:10.1007/s10291-011-0248-2.

Reilinger, R., and S. McClusky (2011), Nubia–Arabia–Eurasia plate motions and the dynamics of Mediterranean and Middle East tectonics, Geophys. J. Int., 186(3), 971–979, doi:10.1111/j.1365-246X.2011.05133.x.

Riegel, S. A., K. Fujita, B. M. Koz'min, V. S. Imaev, and D. B. Cook (1993), Extrusion tectonics of the Okhotsk Plate, northeast Asia, Geophys. Res. Lett., 20(7), 607–610, doi:10.1029/93GL00267.

Rodriguez, A. (2007), Global Positioning System (GPS) determination of motions, neotectonics, and seismic hazard in Trinidad and Tobago, M.S. Thesis, Grand Valley State University.

Royer, J.-Y., and R. G. Gordon (1997), The motion and boundary between the Capricorn and Australian plates, Science, 277(5330), 1268–1274, doi:10.1126/science.277.5330.1268.

Salamon, A., A. Hofstetter, Z. Garfunkel, and H. Ron (2003), Seismotectonics of the Sinai subplate – the eastern Mediterranean region, Geophys. J. Int., 155(1), 149–173, doi:10.1046/j.1365-246X.2003.02017.x.

Saria, E., E. Calais, Z. Altamimi, P. Willis, and H. Farah (2013), A new velocity field for Africa from combined GPS and DORIS space geodetic solutions: contribution to the definition of the African Reference Frame (AFREF), J. Geophys. Res., in press, doi:10.1002/jgrb.50137.

Sato, M., M. Fujita, Y. Matsumoto, T. Ishikawa, H. Saito, M. Mochizuki, and A. Asada (2013), Interplate coupling off northeastern Japan before the 2011 Tohoku-oki earthquake, inferred from seafloor geodetic data, J. Geophys. Res., in press, doi:10.1002/jgrb.50275.

Scherneck, H.-G. (1991), A parametrized solid earth tide model and ocean tide loading effects for global geodetic baseline measurements, Geophys. J. Int., 106(3), 677–694, doi:10.1111/j.1365-246X.1991.tb06339.x.

Schmid, R., P. Steigenberger, G. Gendt, M. Ge, and M. Rothacher (2007), Generation of a consistent absolute phase-center correction model for GPS receiver and satellite antennas, J. Geod., 81(12), 781–798, doi:10.1007/s00190-007-0148-y.

Sella, G. F., T. H. Dixon, and A. Mao (2002), REVEL: A model for Recent plate velocities from space geodesy, Journal of Geophysical Research: Solid Earth, 107(B4), 2081, doi:10.1029/2000JB000033.

Sella, G. F., S. Stein, T. H. Dixon, M. Craymer, T. S. James, S. Mazzotti, and R. K. Dokka (2007), Observation of glacial isostatic adjustment in "stable" North America with GPS, Geophys. Res. Lett., 34(2), L02306, doi:10.1029/2006GL027081.

Bar-Sever, Y. E., P. M. Kroger, and J. A. Borjesson (1998), Estimating horizontal gradients of tropospheric path delay with a single GPS receiver, J. Geophys. Res., 103(B3), 5019–5035, doi:10.1029/97JB03534.

Shen, Z.-K., C. Zhao, A. Yin, Y. Li, D. D. Jackson, P. Fang, and D. Dong (2000), Contemporary crustal deformation in east Asia constrained by Global Positioning System measurements, J. Geophys. Res., 105(B3), 5721–5734, doi:10.1029/1999JB900391.

Shen, Z.-K., M. Wang, Y. Li, D. D. Jackson, A. Yin, D. Dong, and P. Fang (2001), Crustal deformation along the Altyn Tagh fault system, western China, from GPS, J. Geophys. Res., 106(B12), 30,607–30,621, doi:10.1029/2001JB000349.

Shen, Z.-K., J. Lü, M. Wang, and R. Bürgmann (2005), Contemporary crustal deformation around the southeast borderland of the Tibetan Plateau, J. Geophys. Res., 110(B11), B11409, doi:10.1029/2004JB003421.

Shen, Z.-K., R. W. King, D. C. Agnew, M. Wang, T. A. Herring, D. Dong, and P. Fang (2011), A unified analysis of crustal motion in Southern California, 1970–2004: The SCEC crustal motion map, J. Geophys. Res., 116(B11), B11402, doi:10.1029/2011JB008549.

Simons, W. J. F. et al. (2007), A decade of GPS in Southeast Asia: Resolving Sundaland motion and boundaries, J. Geophys. Res., 112(B6), B06420, doi:10.1029/2005JB003868.

Storchak, D., D. Di Giacomo, I. Bondar, J. Harris, E. R. Engdahl, W. H. K. Lee, A. Villasenor, P. Bormann, and G. Ferrari (2012), ISC-GEM Global Instrumental Earthquake Catalogue (1900-2009), GEM Final Report.

Tadokoro, K., R. Ikuta, T. Watanabe, M. Ando, T. Okuda, S. Nagai, K. Yasuda, and T. Sakata (2012), Interseismic seafloor crustal deformation immediately above the source region of anticipated megathrust earthquake along the Nankai Trough, Japan, Geophys. Res. Lett., 39(10), L10306, doi:10.1029/2012GL051696.

Taylor, F. W., M. G. Bevis, I. W. D. Dalziel, R. S. Jr, C. Frohlich, E. Kendrick, J. Foster, D. Phillips, and K. Gudipati (2008), Kinematics and segmentation of the South Shetland Islands-Bransfield basin system, northern Antarctic Peninsula, Geochem. Geophys. Geosyst., 9(4), Q04035, doi:10.1029/2007GC001873.

Teferle, F. N. et al. (2009), Crustal motions in Great Britain: evidence from continuous GPS, absolute gravity and Holocene sea level data, Geophys. J. Int., 178(1), 23–46, doi:10.1111/j.1365-246X.2009.04185.x.

Tong, X., D. T. Sandwell, and B. Smith-Konter (2013), High-resolution interseismic velocity data along the San Andreas Fault from GPS and InSAR, J. Geophys. Res., 118(1), 369–389, doi:10.1029/2012JB009442.

Tregoning, P. (2002), Plate kinematics in the western Pacific derived from geodetic observations, J. Geophys. Res., 107(B1), 2020, doi:10.1029/2001JB000406.

Tregoning, P. et al. (1998), Estimation of current plate motions in Papua New Guinea from Global Positioning System observations, J. Geophys. Res., 103(B6), 12,181–12,203, doi:10.1029/97JB03676.

Tregoning, P., R. Burgette, S. C. McClusky, S. Lejeune, C. S. Watson, and H. McQueen (2013), A decade of horizontal deformation from great earthquakes, J. Geophys. Res., 118, 2371–2381, doi:10.1002/jgrb.50154.

Trenkamp, R., J. N. Kellogg, J. T. Freymueller, and H. P. Mora (2002), Wide plate margin deformation, southern Central America and northwestern South America, CASA GPS observations, J. South Am. Earth Sci., 15(2), 157–171, doi:10.1016/S0895-9811(02)00018-4.

Tserolas, V., S. P. Mertikas, and X. Frantzis (2013), The Western Crete geodetic infrastructure: Long-range power-law correlations in GPS time series using Detrended Fluctuation Analysis, Adv. Space Res., 51(8), 1448–1467, doi:10.1016/j.asr.2012.08.002.

Umhoefer, P. J., and R. J. Dorsey (1997), Translation of terranes: Lessons from central Baja California, Mexico, Geology, 25(11), 1007–1010, doi:10.1130/0091-7613(1997)025<1007:TOTLFC>2.3.CO;2.

Vernant, P. et al. (2004), Present-day crustal deformation and plate kinematics in the Middle East constrained by GPS measurements in Iran and northern Oman, Geophysical Journal International, 157(1), 381–398, doi:10.1111/j.1365-246X.2004.02222.x.

Wallace, L. M., J. Beavan, R. McCaffrey, and D. Darby (2004), Subduction zone coupling and tectonic block rotations in the North Island, New Zealand, J. Geophys. Res., 109(B12), B12406, doi:10.1029/2004JB003241.

Walpersdorf, A., S. Baize, E. Calais, P. Tregoning, and J.-M. Nocquet (2006), Deformation in the Jura Mountains (France): First results from semi-permanent GPS measurements, Earth and Planetary Science Letters, 245(1–2), 365–372, doi:10.1016/j.epsl.2006.02.037.

Wang, H., and T. J. Wright (2012), Satellite geodetic imaging reveals internal deformation of western Tibet, Geophys Res. Lett., 39(7), L07303, doi:10.1029/2012GL051222.

Wang, K., Y. Hu, M. Bevis, E. Kendrick, R. Smalley, R. B. Vargas, and E. Lauría (2007), Crustal motion in the zone of the 1960 Chile earthquake: Detangling earthquake-cycle deformation and forearc-sliver translation, Geochemistry, Geophysics, Geosystems, 8(10), Q10010, doi:10.1029/2007GC001721.

Wang, Q. et al. (2001), Present-Day Crustal Deformation in China Constrained by Global Positioning System Measurements, Science, 294(5542), 574–577, doi:10.1126/science.1063647.

Ward, S. N. (1994), Constraints on the seismotectonics of the central Mediterranean from Very Long Baseline Interferometry, Geophys. J. Int., 117(2), 441–452, doi:10.1111/j.1365-246X.1994.tb03943.x.

Wdowinski, S., Y. Bock, G. Baer, L. Prawirodirdjo, N. Bechor, S. Naaman, R. Knafo, Y. Forrai, and Y. Melzer (2004), GPS measurements of current crustal movements along the Dead Sea Fault, J. Geophys. Res., 109(B5), B05403, doi:10.1029/2003JB002640.

Weber, J. C., T. H. Dixon, C. DeMets, W. B. Ambeh, P. Jansma, G. Mattioli, J. Saleh, G. Sella, R. Bilham, and O. Pérez (2001), GPS estimate of relative motion between the Caribbean and South American plates, and geologic implications for Trinidad and Venezuela, Geology, 29(1), 75–78, doi:10.1130/0091-7613(2001)029<0075:GEORMB>2.0.CO;2.

Weber, J. C., J. Saleh, S. Balkaransingh, T. Dixon, W. Ambeh, T. Leong, A. Rodriguez, and K. Miller (2011), Triangulation-to-GPS and GPS-to-GPS geodesy in Trinidad, West Indies: Neotectonics, seismic risk, and geologic implications, Marine and Petroleum Geology, 28(1), 200–211.

Wei, M., D. Sandwell, and B. Smith-Konter (2010), Optimal combination of InSAR and GPS for measuring interseismic crustal deformation, Adv. Space Res., 46(2), 236–249, doi:10.1016/j.asr.2010.03.013.

Wernicke, B., J. L. Davis, R. A. Bennett, J. E. Normandeau, A. M. Friedrich, and N. A. Niemi (2004), Tectonic implications of a dense continuous GPS velocity field at Yucca Mountain, Nevada, J. Geophys. Res., 109, B12404, B12404, doi:10.1029/2003JB002832.

Yu, S.-B., Y.-J. Hsu, T. Bacolcol, C.-C. Yang, Y.-C. Tsai, and R. Solidum (2013), Present-day crustal deformation along the Philippine Fault in Luzon, Philippines, J. Asian Earth Sci., 65, 64–74, doi:10.1016/j.jseaes.2010.12.007.

Zhang, P.-Z., and W. Gan (2008), Combined model of rigid-block motion with continuous deformation: Patterns of present-day deformation in continental China, in Investigations into the tectonics of the Tibetan plateau, vol. 444, edited by B. C. Burchfiel and E. Wang, pp. 59–71, Geological Society of America Special Papers.

Zhang, P.-Z. et al. (2004), Continuous deformation of the Tibetan Plateau from global positioning system data, Geology, 32(9), 809–812, doi:10.1130/G20554.1.

Zumberge, J. F., M. B. Heflin, D. C. Jefferson, M. M. Watkins, and F. H. Webb (1997), Precise point positioning for the efficient and robust analysis of GPS data from large networks, J. Geophys. Res., 102(B3), 5005–5017, doi:10.1029/96JB03860.

APPENDIX A Figures with Regional Results

a) GPS velocities in regional reference frame (indicated in legend). Blue velocities are derived in this project, black velocities are from the literature. b) Contour of second invariant of modelled strain rates. Black and white vectors are the average contractional and extensional principal strain rate vectors, respectively, for sampled grid cells (scaled relatively to the highest principal values shown in plot). Open circles are epicentres for all events in ISC-GEM catalogue with depths ≤70 km [*Storchak et al.*, 2012].

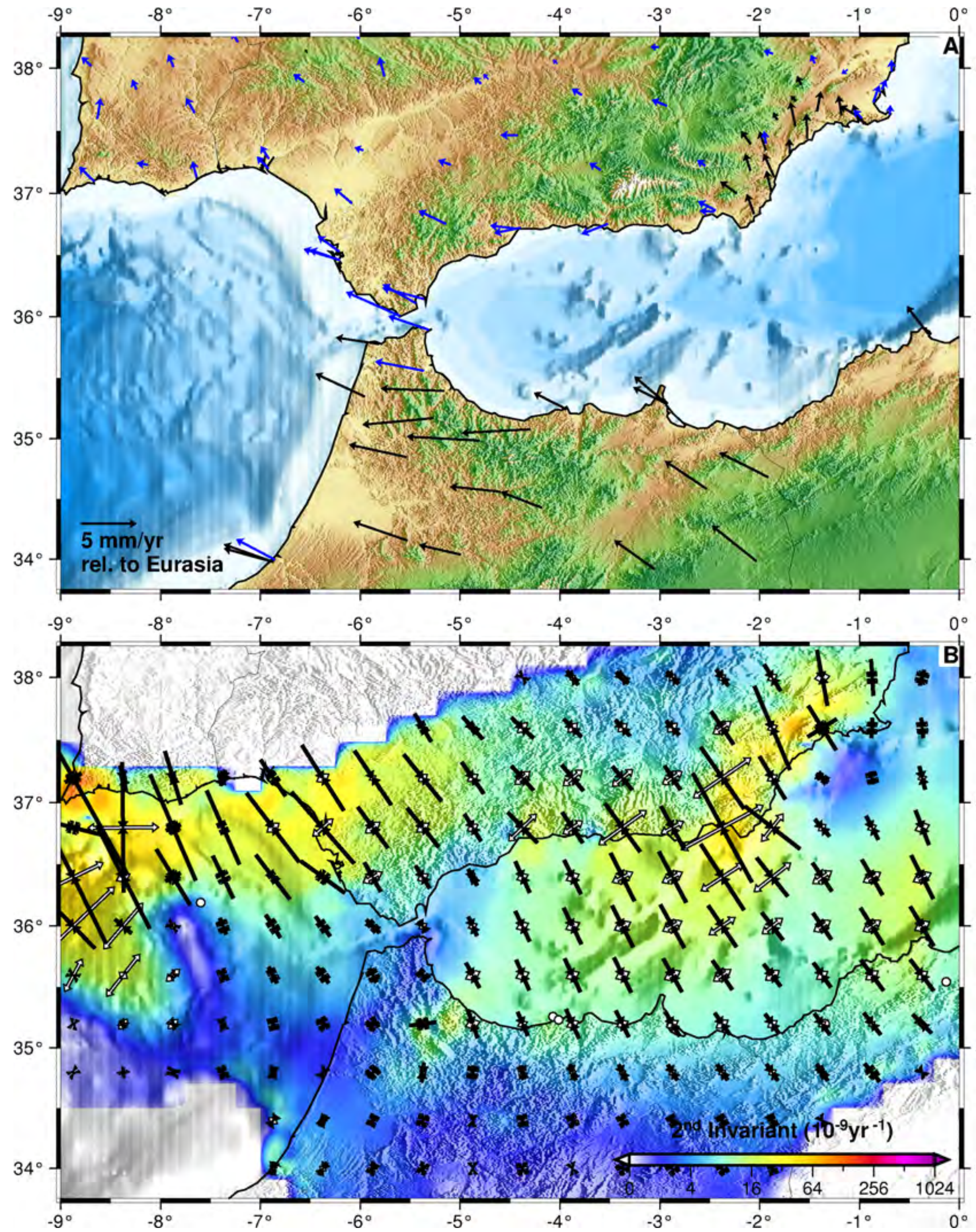
A
5 mm/yr
rel. to Eurasia
B
2nd Invariant (10-9yr-1)
0
4
16
64
256
1024
-9°
-8°
-7°
-6°
-5°
-4°
-3°
-2°
-1°
0°
38°
37°
36°
35°
34°

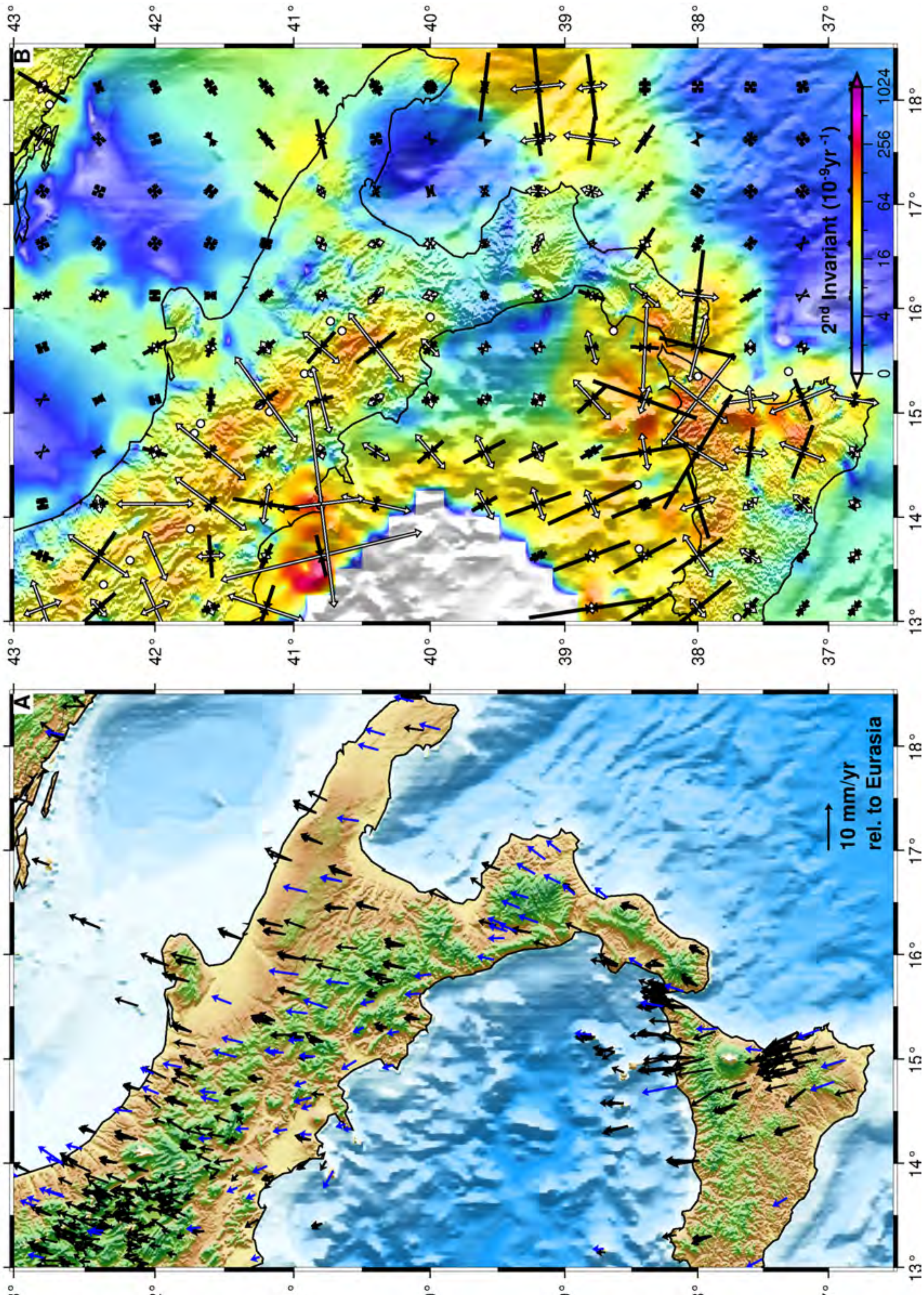
A
B
10 mm/yr
rel. to Eurasia
2nd Invariant (10-9yr-1)
0
4
16
64
256
1024

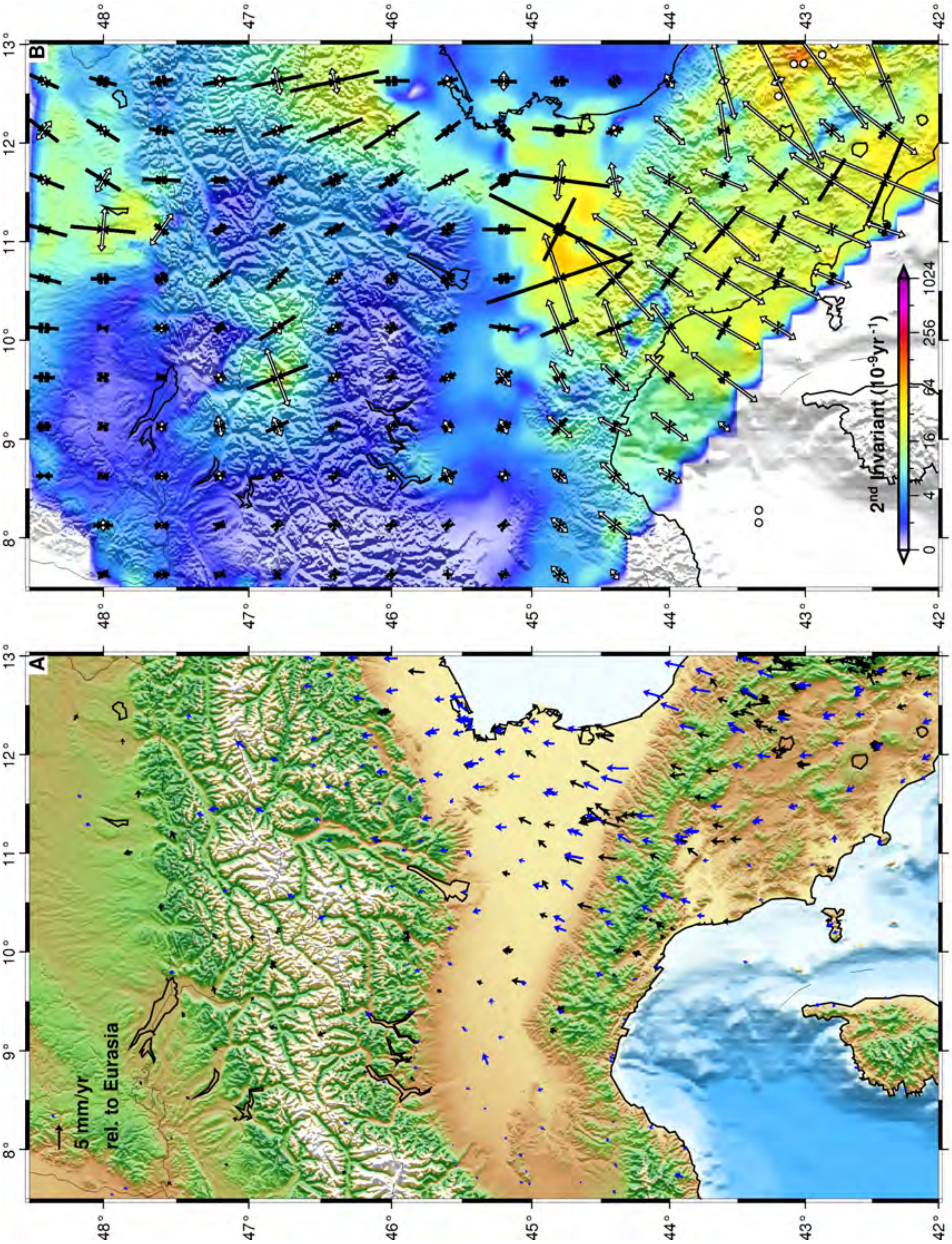
A
5 mm/yr
rel. to Eurasia
B
2nd Invariant (10⁻⁹yr⁻¹)
0
4
16
64
256
1024

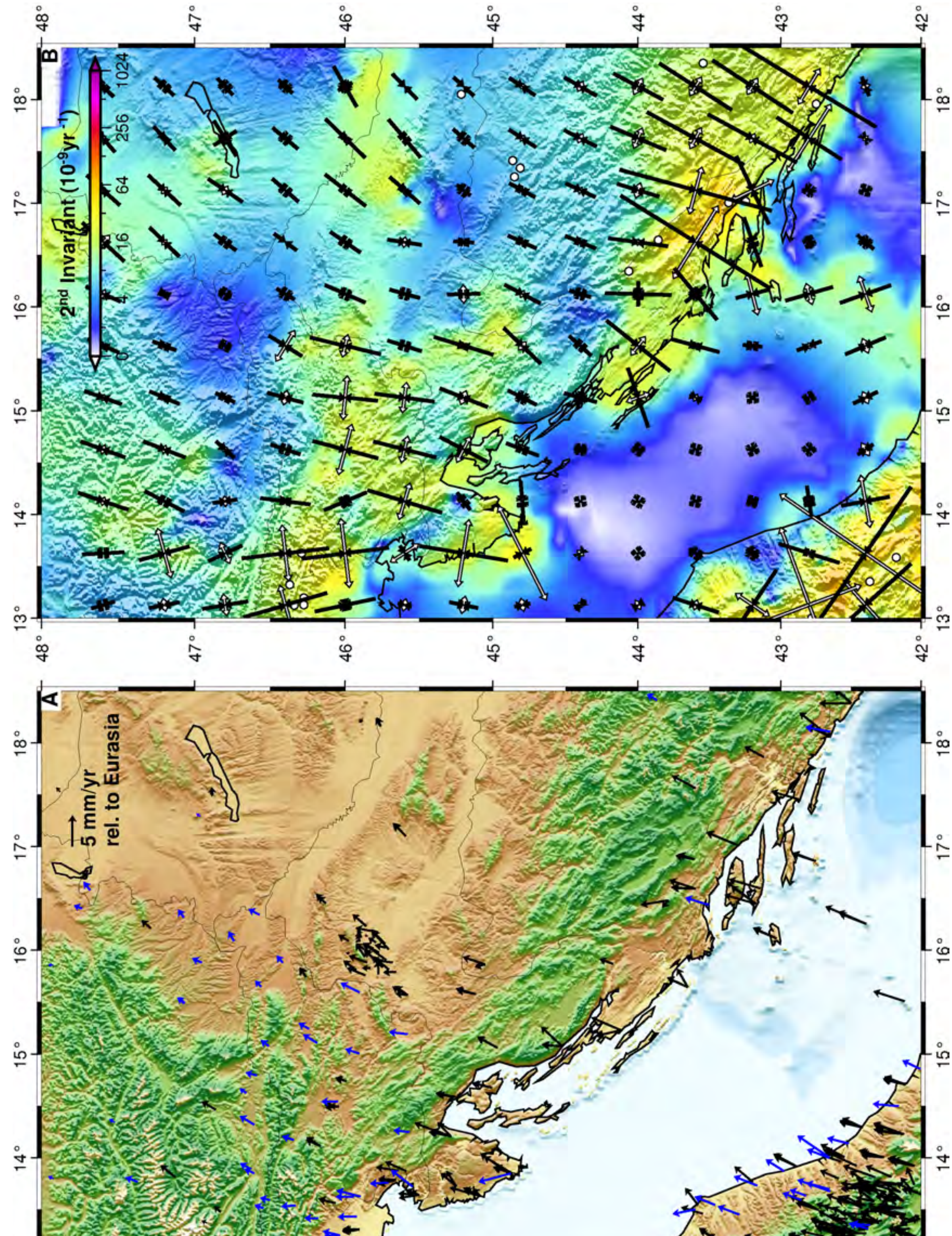
A
5 mm/yr
rel. to Eurasia
B
2nd Invariant (10-9yr-1)
1024
256
64
16
4
0
13°
14°
15°
16°
17°
18°
42°
43°
44°
45°
46°
47°
48°

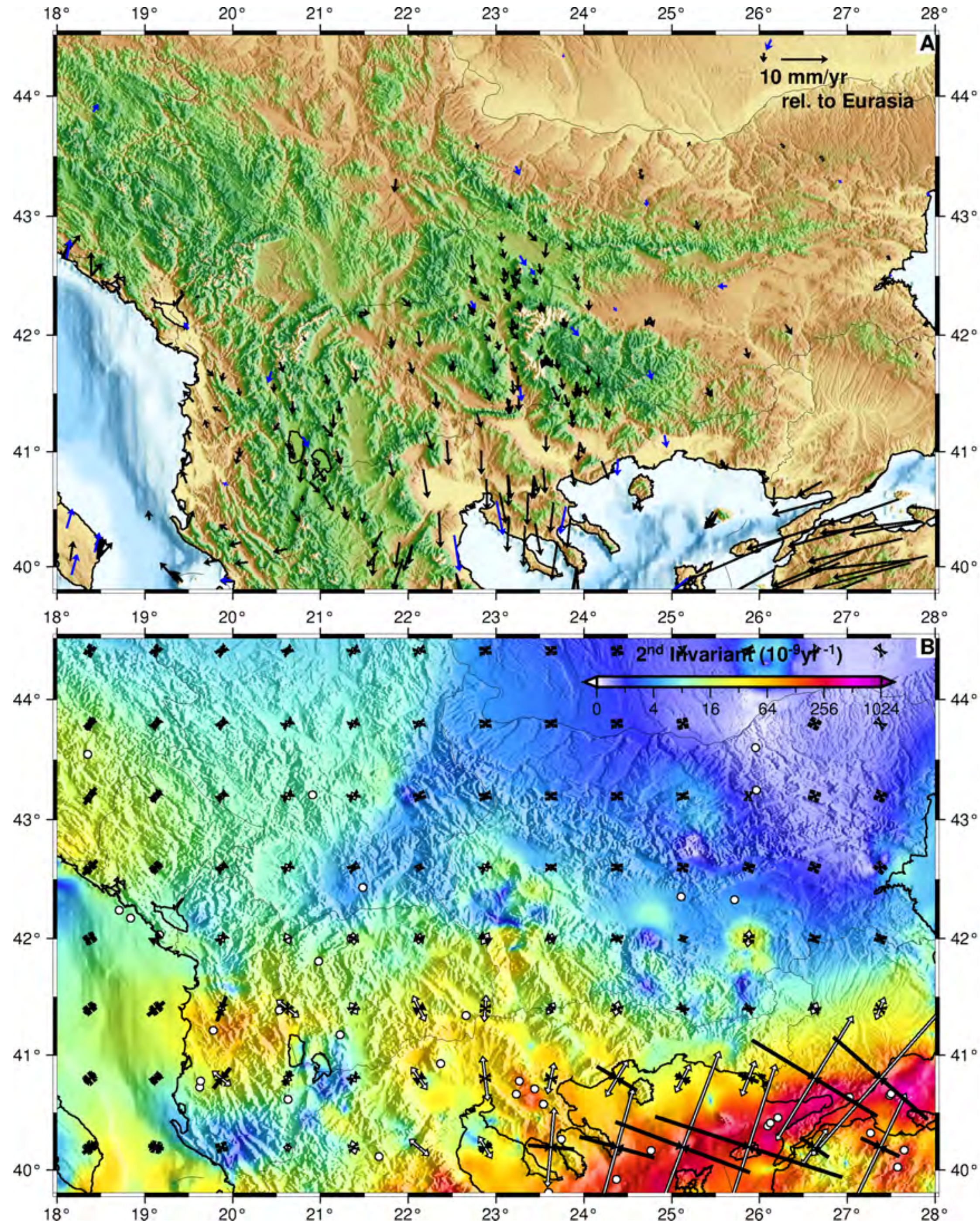
A
10 mm/yr
rel. to Eurasia
B
2nd Invariant ($10^{-9}yr^{-1}$)
0
4
16
64
256
1024
18°
19°
20°
21°
22°
23°
24°
25°
26°
27°
28°
40°
41°
42°
43°
44°

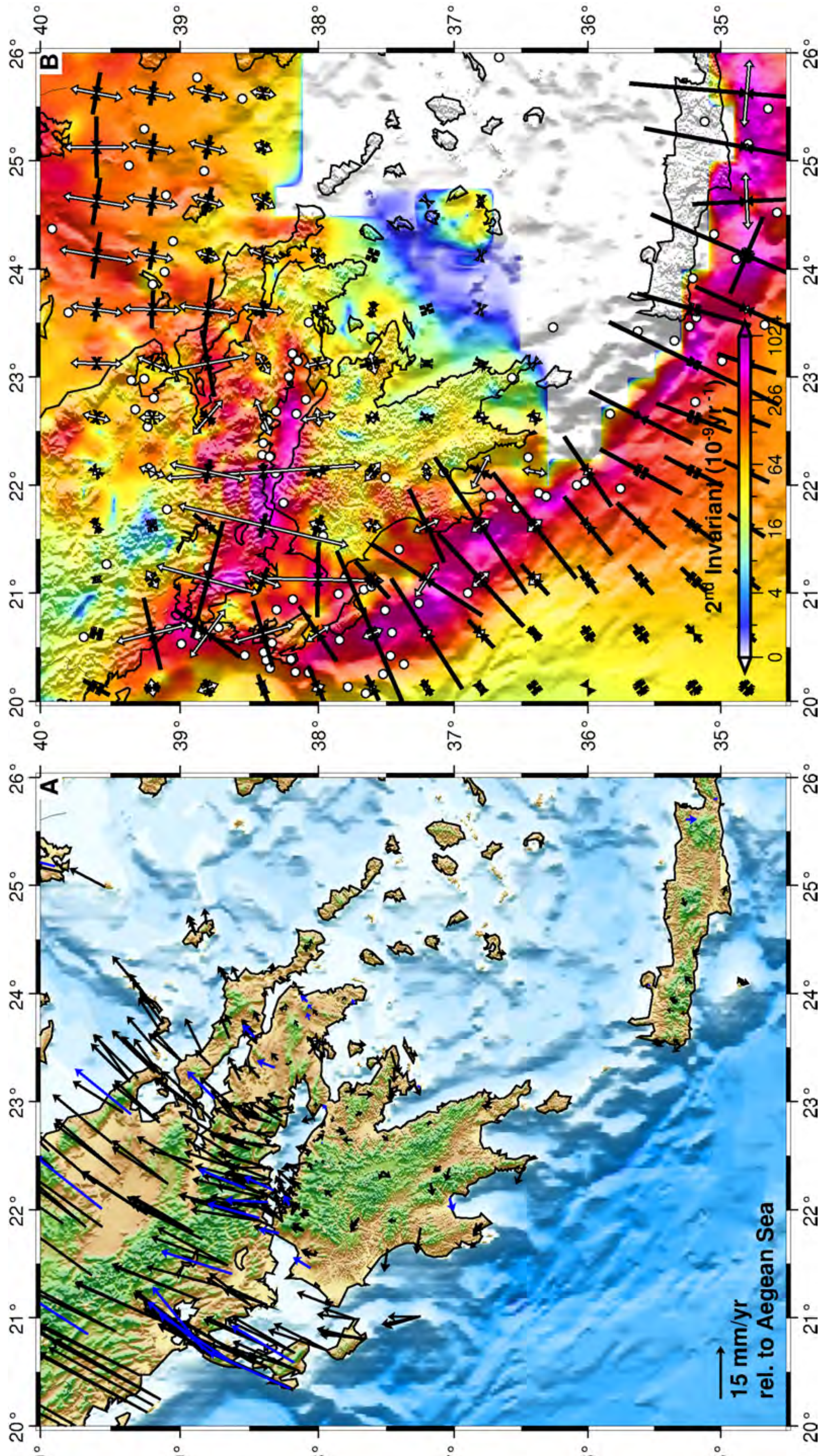
A
B
15 mm/yr
rel. to Aegean Sea
2nd Invariant (10-9/yr-1)
0
4
16
64
256
1024
20°
21°
22°
23°
24°
25°
26°
35°
36°
37°
38°
39°
40°

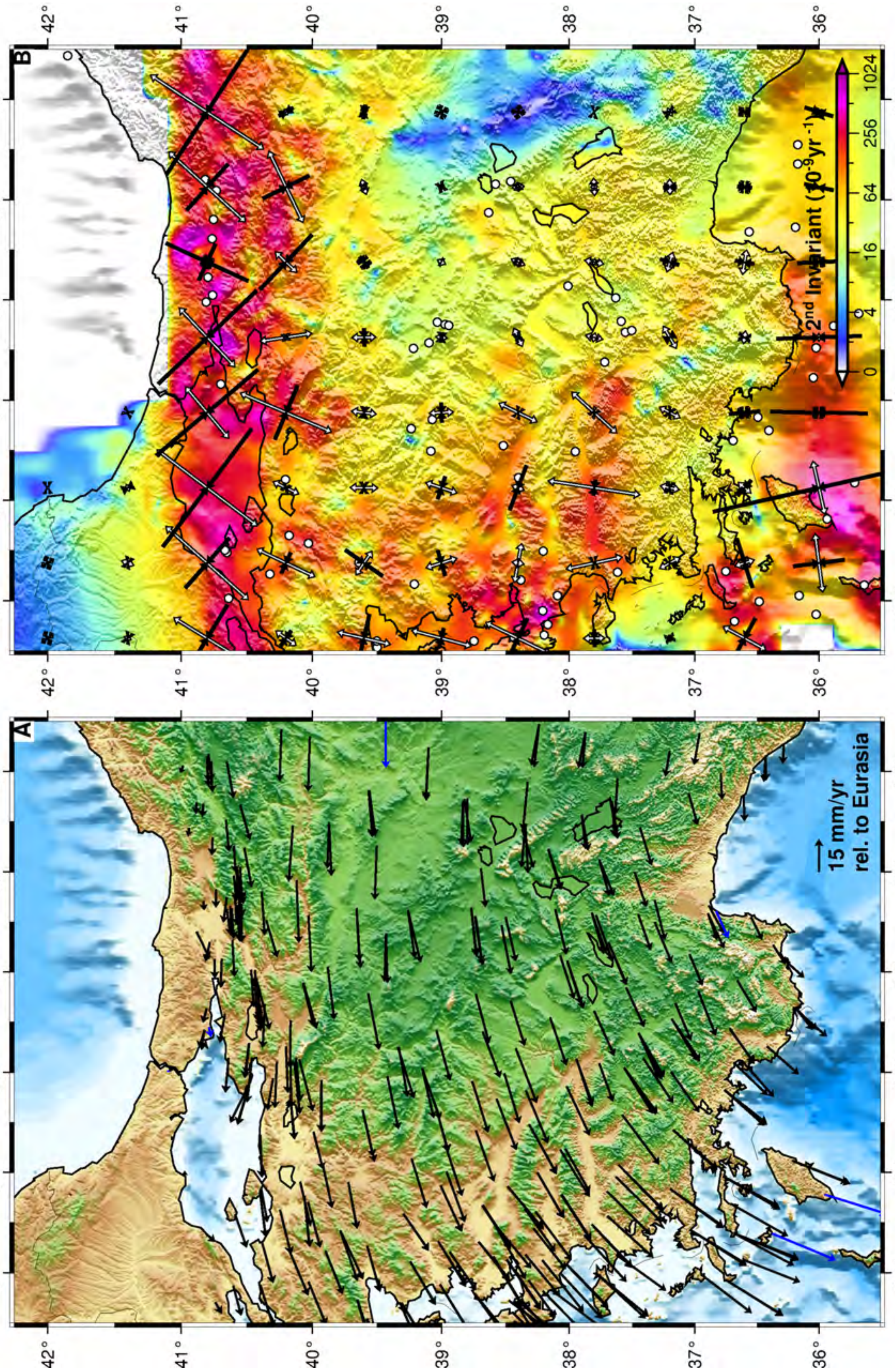
A
B
15 mm/yr
rel. to Eurasia
2nd Invariant (10^-9 yr^-1)
0
4
16
64
256
1024
27°
28°
29°
30°
31°
32°
36°
37°
38°
39°
40°
41°
42°

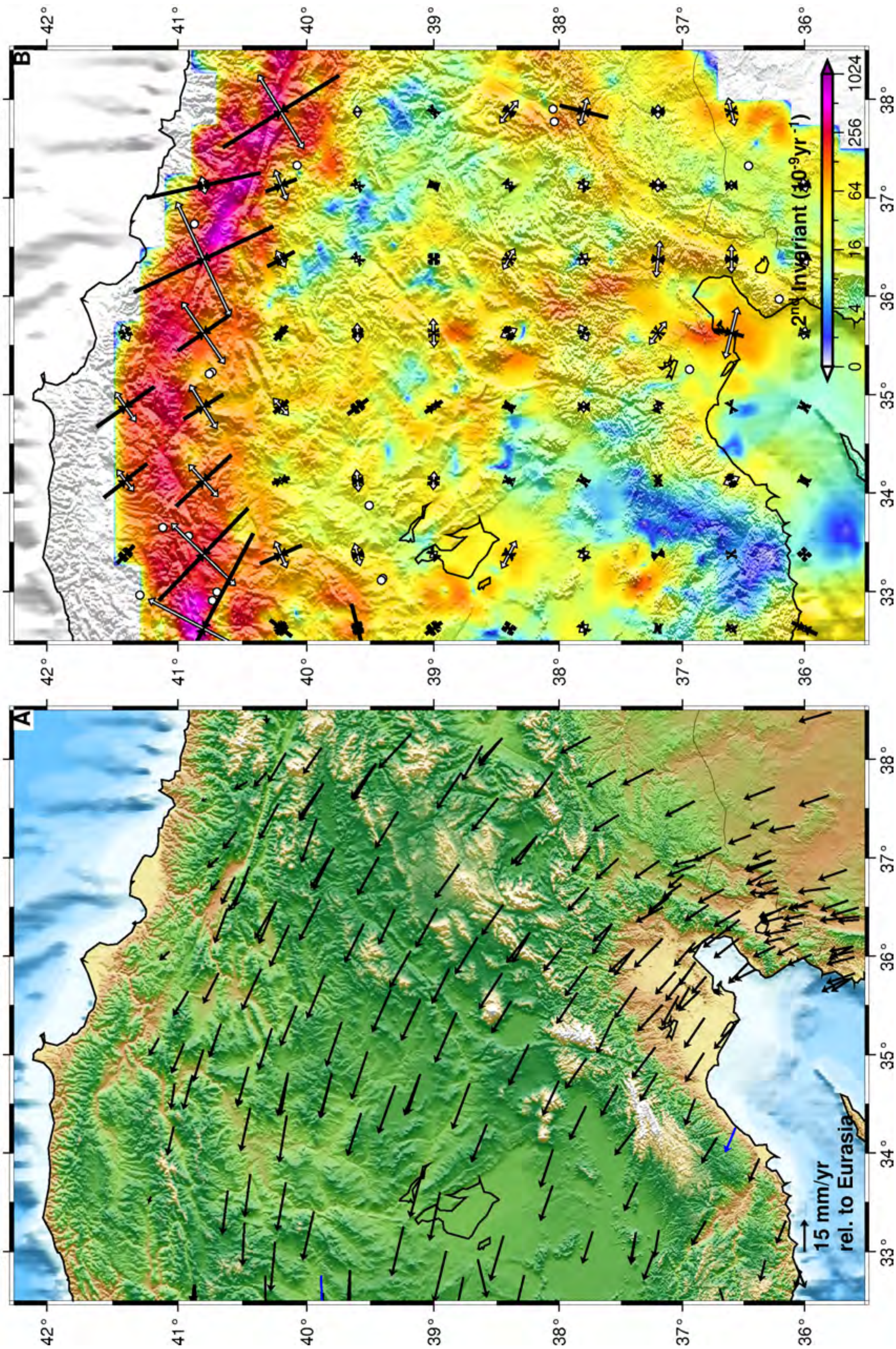
A
B
15 mm/yr
rel. to Eurasia
2nd Invariant (10-9yr-1)
0
4
16
64
256
1024
33°
34°
35°
36°
37°
38°
36°
37°
38°
39°
40°
41°
42°

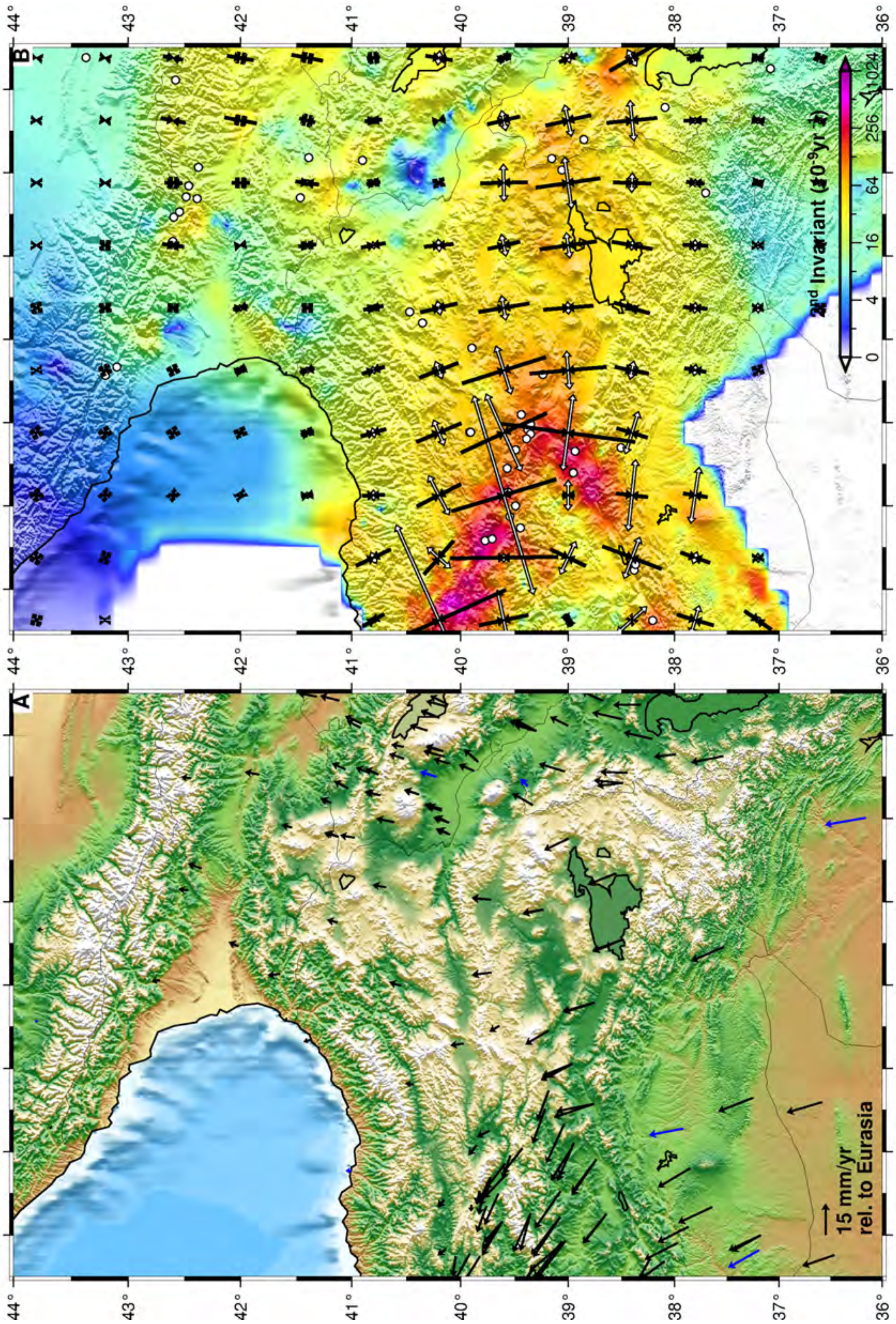
A
B
2nd Invariant (10^-9 yr^-1)
0
4
16
64
256
1024
15 mm/yr
rel. to Eurasia

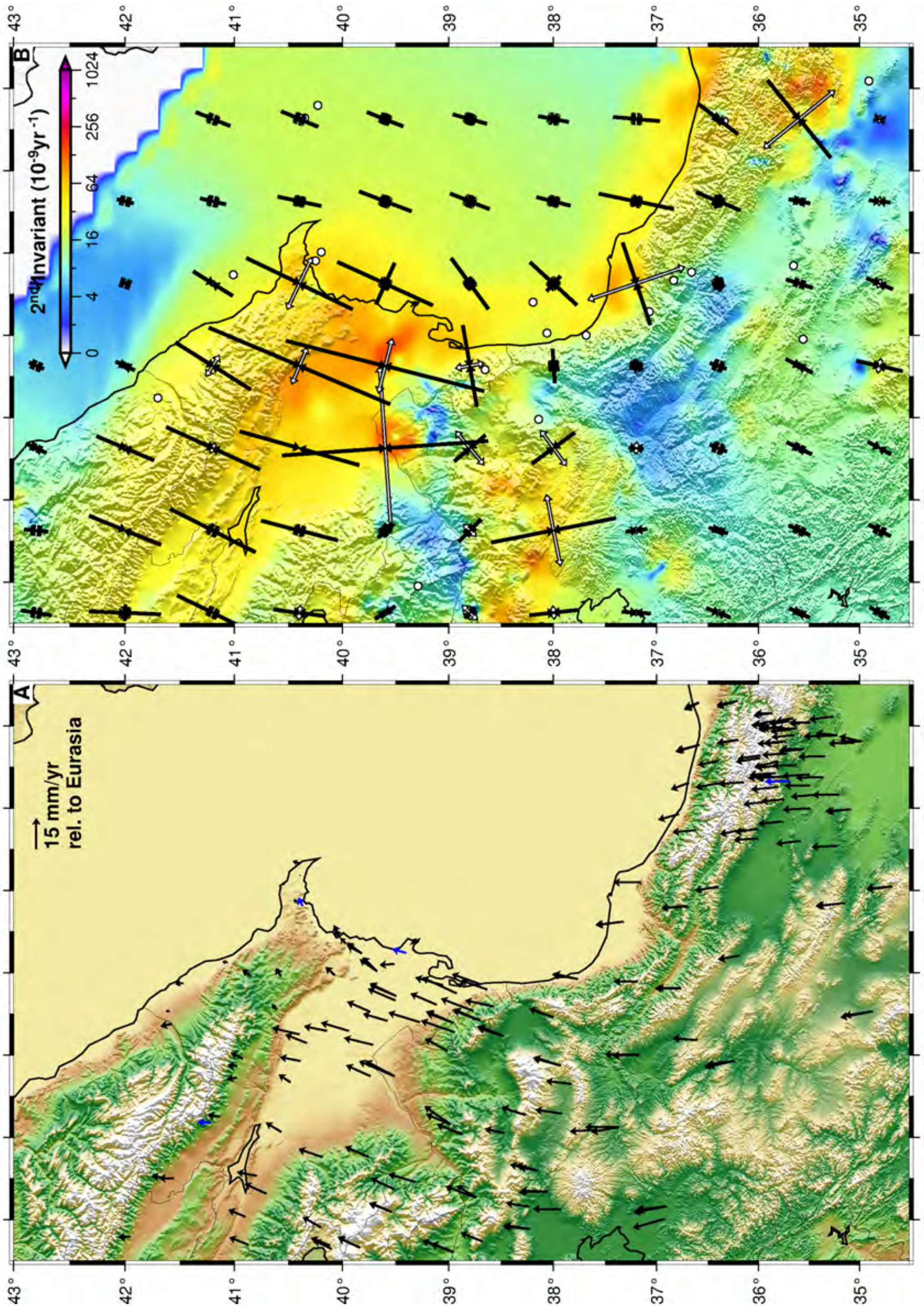
A
15 mm/yr
rel. to Eurasia
B
2nd Invariant (10-9yr-1)
0
4
16
64
256
1024
46°
47°
48°
49°
50°
51°
52°
35°
36°
37°
38°
39°
40°
41°
42°
43°

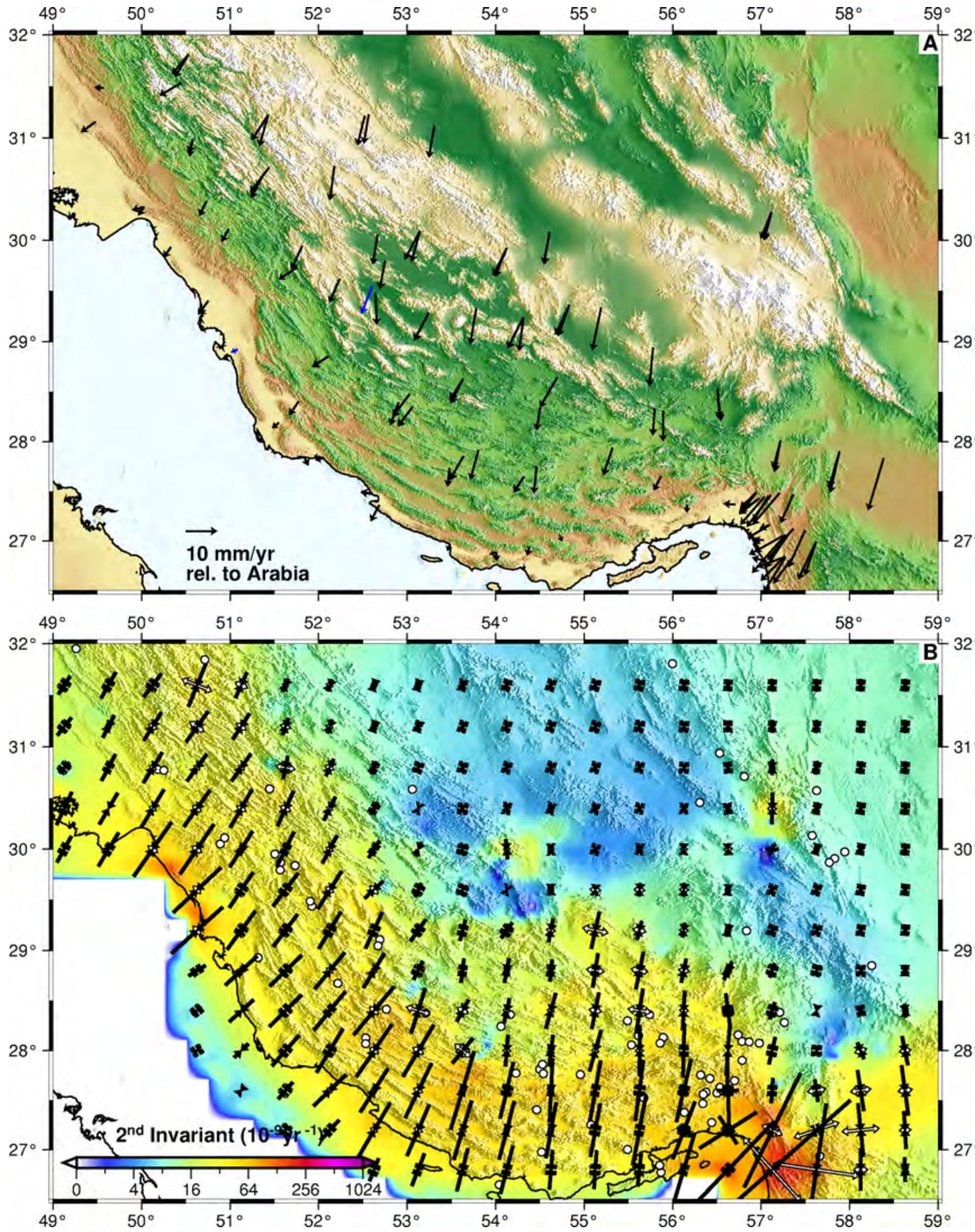
A
B
10 mm/yr
rel. to Arabia
2nd Invariant (10⁻⁹ yr⁻¹)
0
4
16
64
256
1024
49°
50°
51°
52°
53°
54°
55°
56°
57°
58°
59°
27°
28°
29°
30°
31°
32°

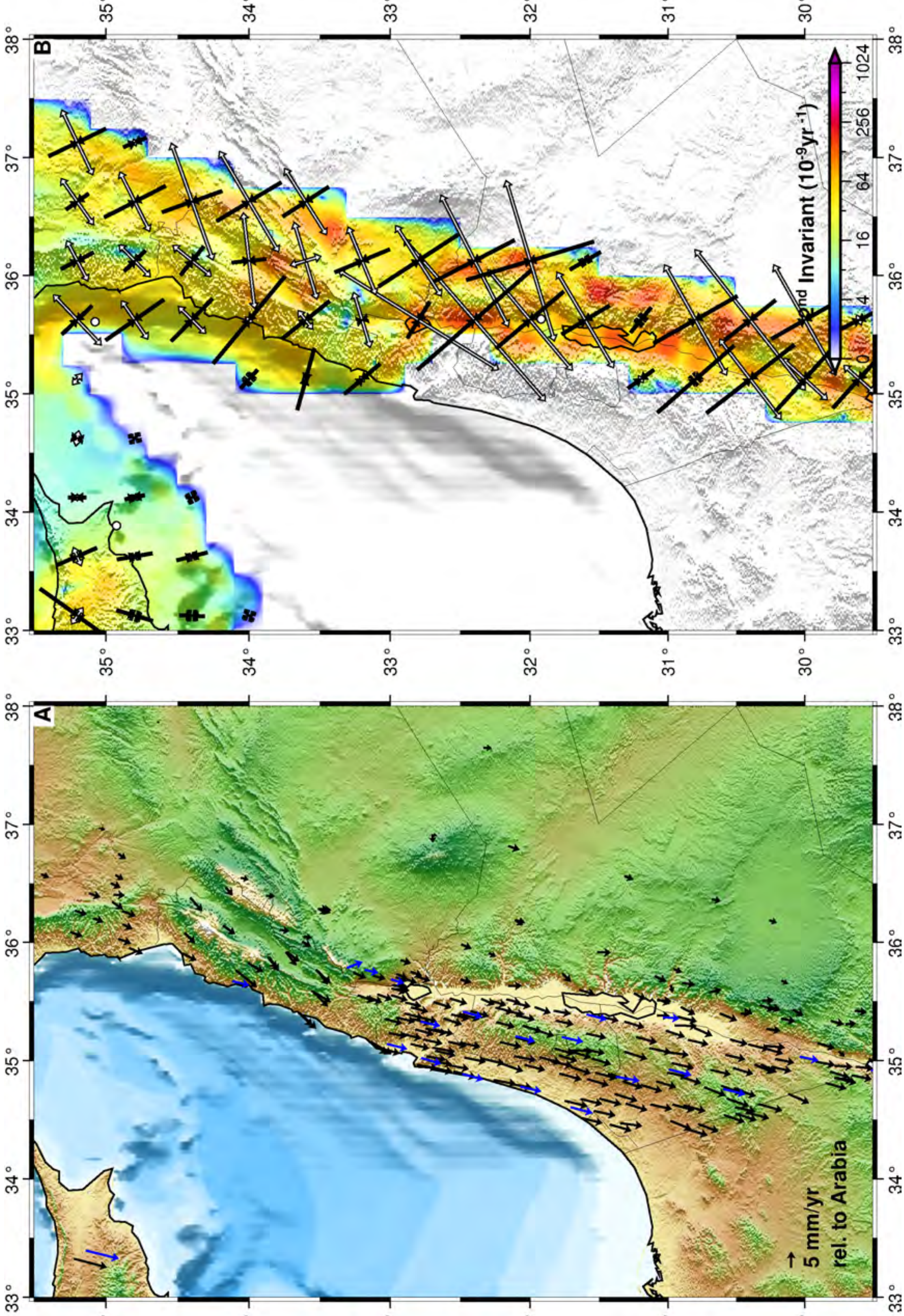
A
B
5 mm/yr
rel. to Arabia
2nd Invariant ($10^{-9}yr^{-1}$)
0
4
16
64
256
1024

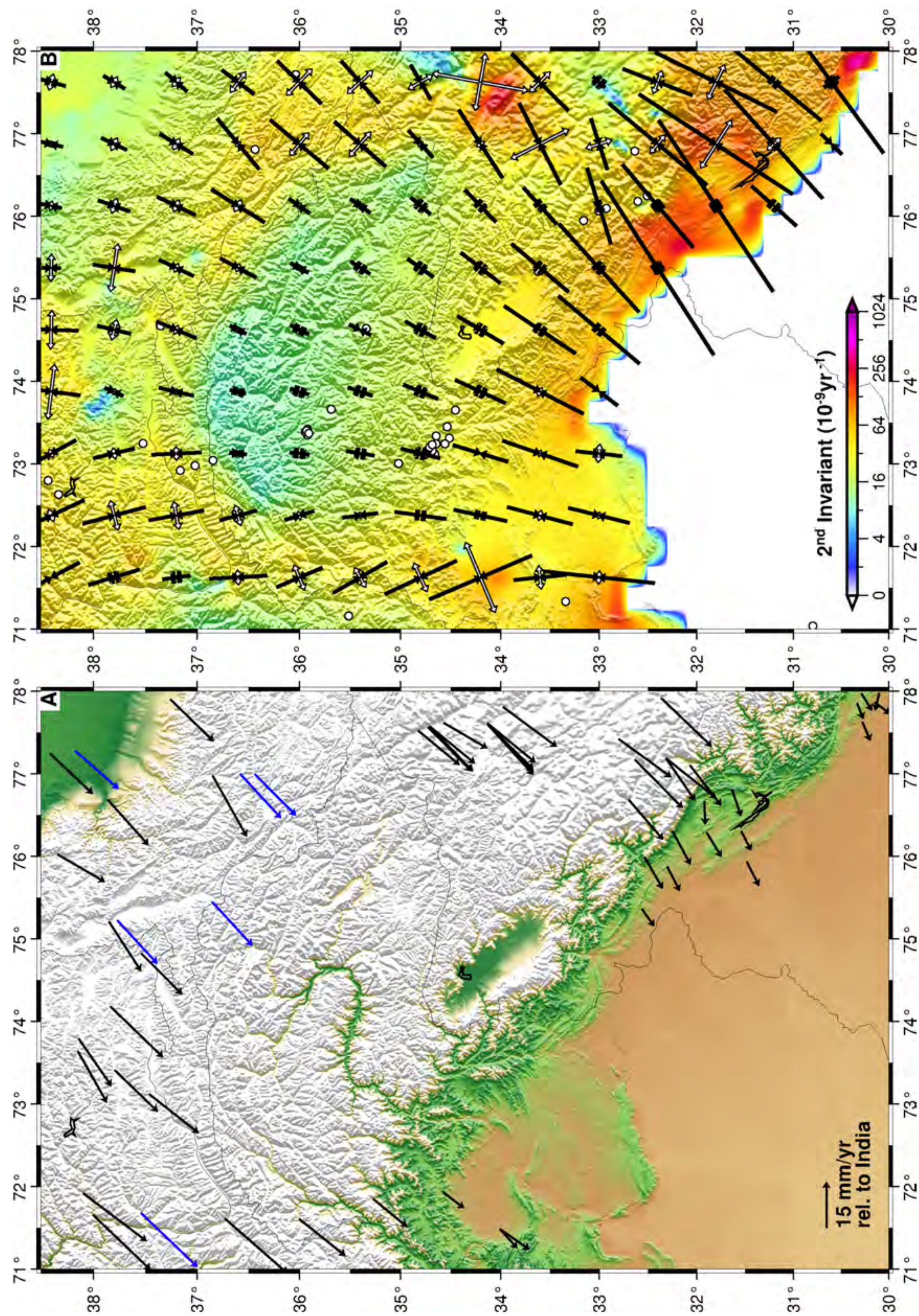
A
B
15 mm/yr
rel. to India
2nd Invariant (10-9yr-1)
0
4
16
64
256
1024
71°
72°
73°
74°
75°
76°
77°
78°
30°
31°
32°
33°
34°
35°
36°
37°
38°

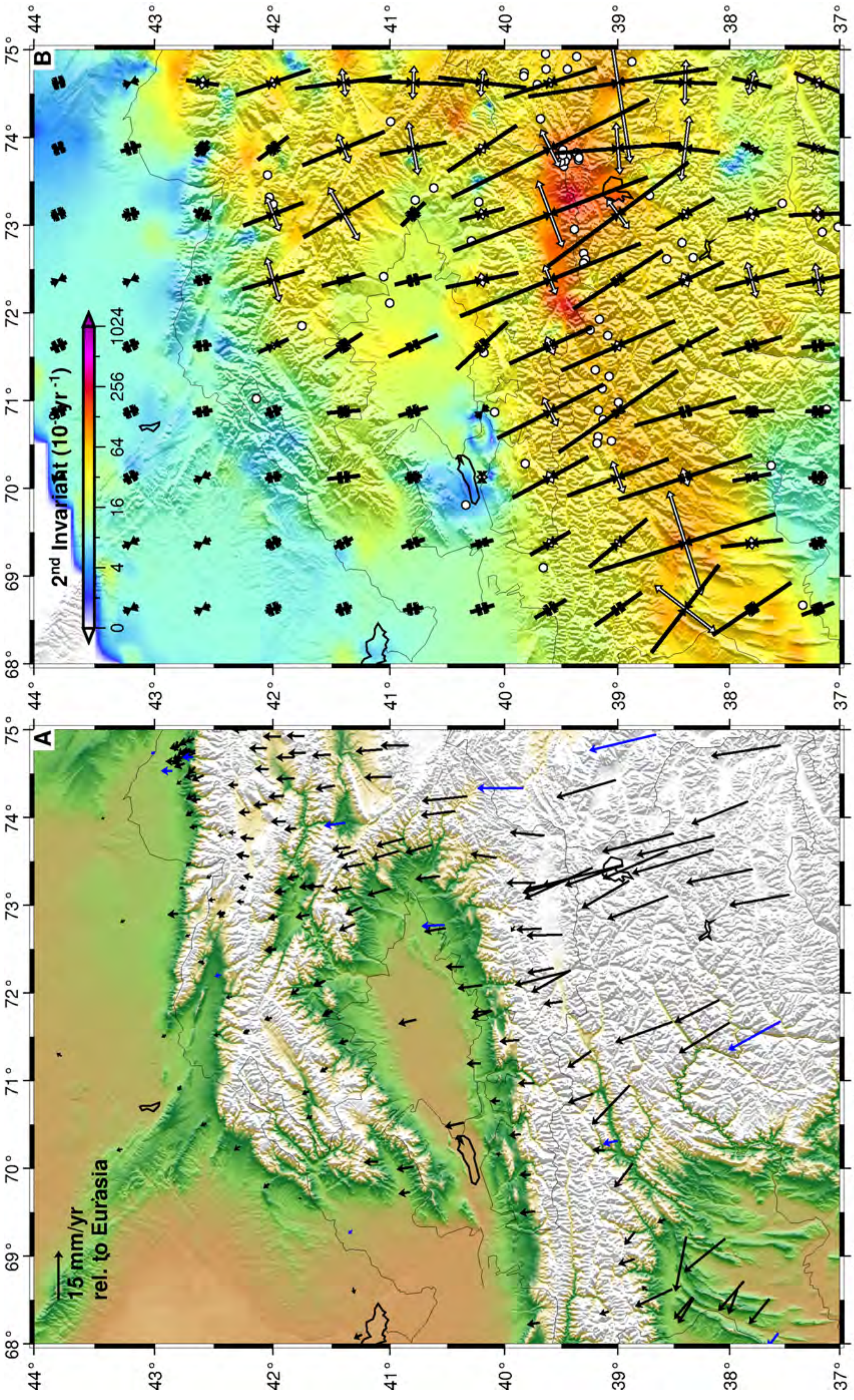
A
15 mm/yr
rel. to Eurasia
B
2nd Invariant (10-9 yr-1)
0
4
16
64
256
1024
68°
69°
70°
71°
72°
73°
74°
75°
37°
38°
39°
40°
41°
42°
43°
44°

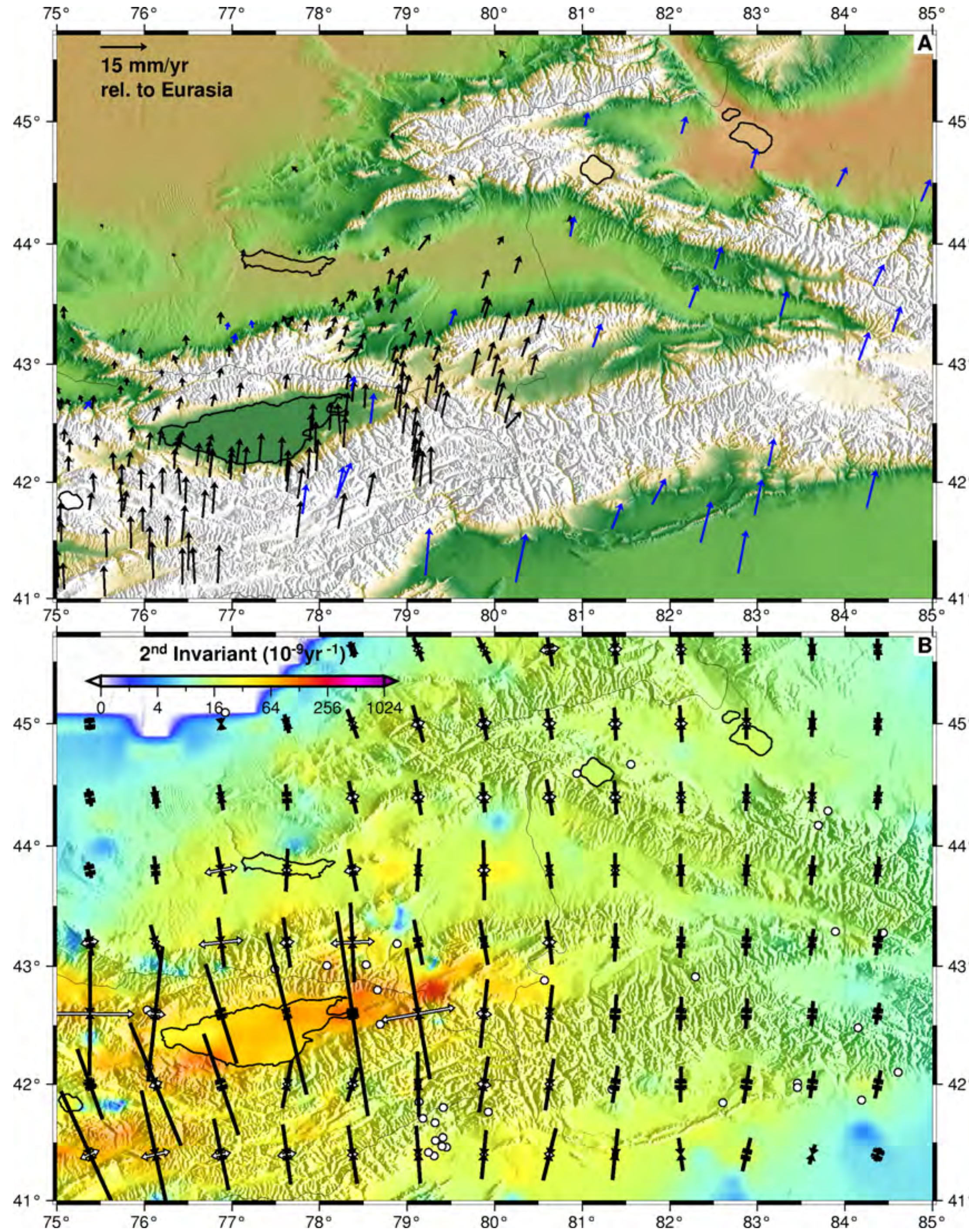
A
15 mm/yr
rel. to Eurasia
B
2nd Invariant (10-9yr-1)
0
4
16
64
256
1024
75°
76°
77°
78°
79°
80°
81°
82°
83°
84°
85°
41°
42°
43°
44°
45°

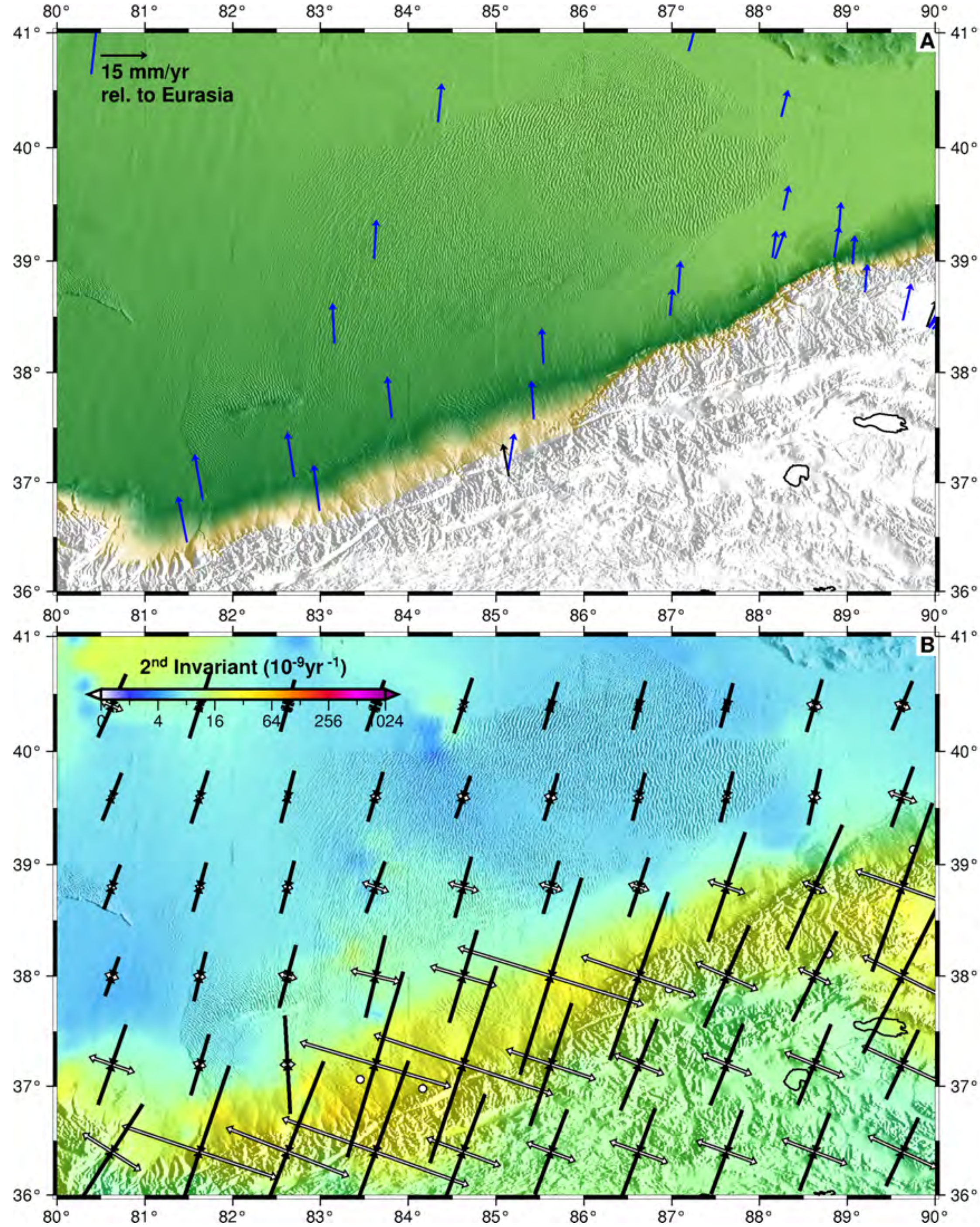

A
15 mm/yr
rel. to Eurasia
B
2nd Invariant (10-9yr-1)
0
4
16
64
256
1024
80°
81°
82°
83°
84°
85°
86°
87°
88°
89°
90°
36°
37°
38°
39°
40°
41°

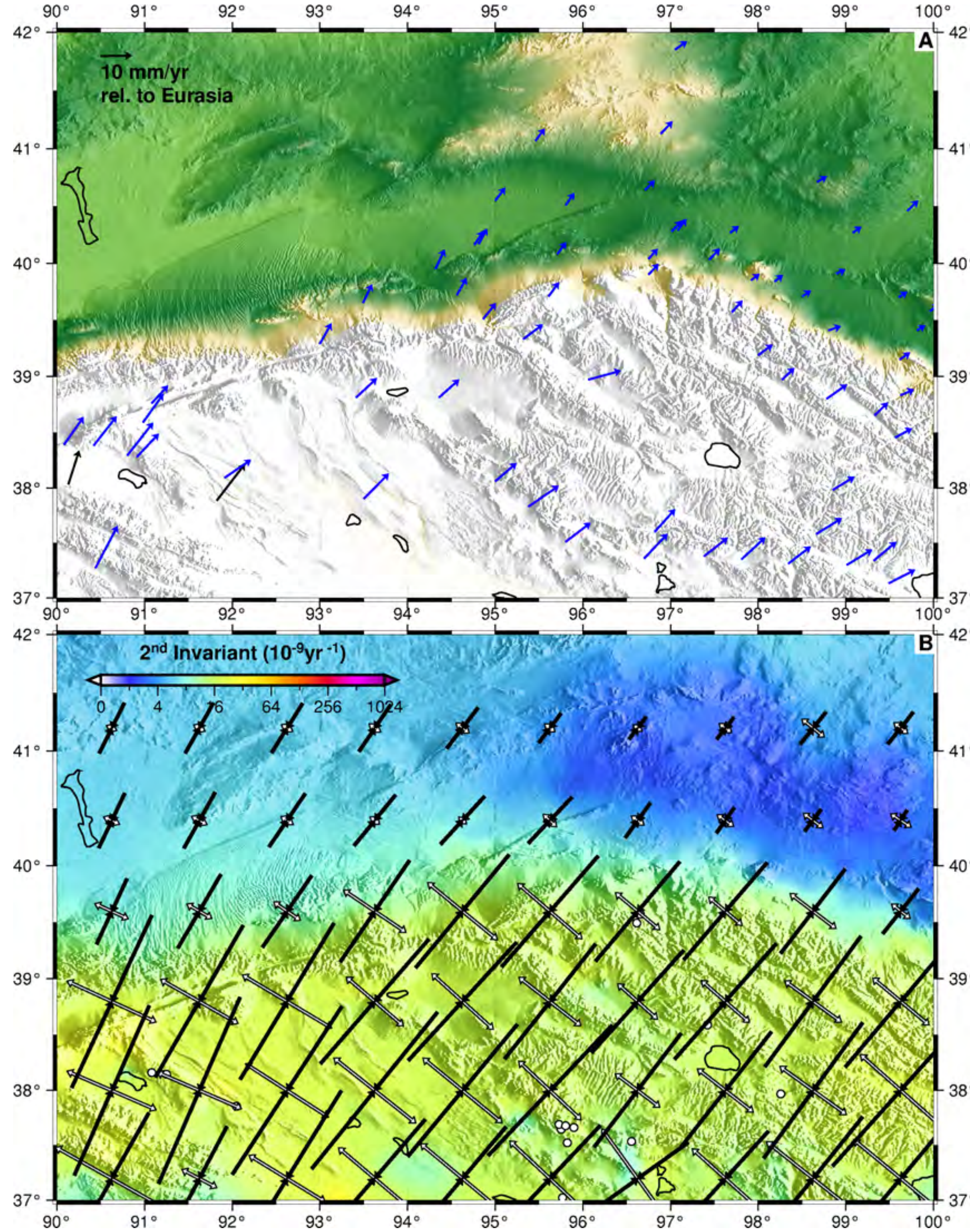
A
10 mm/yr
rel. to Eurasia
B
2nd Invariant (10-9yr-1)
0
4
16
64
256
1024
90°
91°
92°
93°
94°
95°
96°
97°
98°
99°
100°
37°
38°
39°
40°
41°
42°

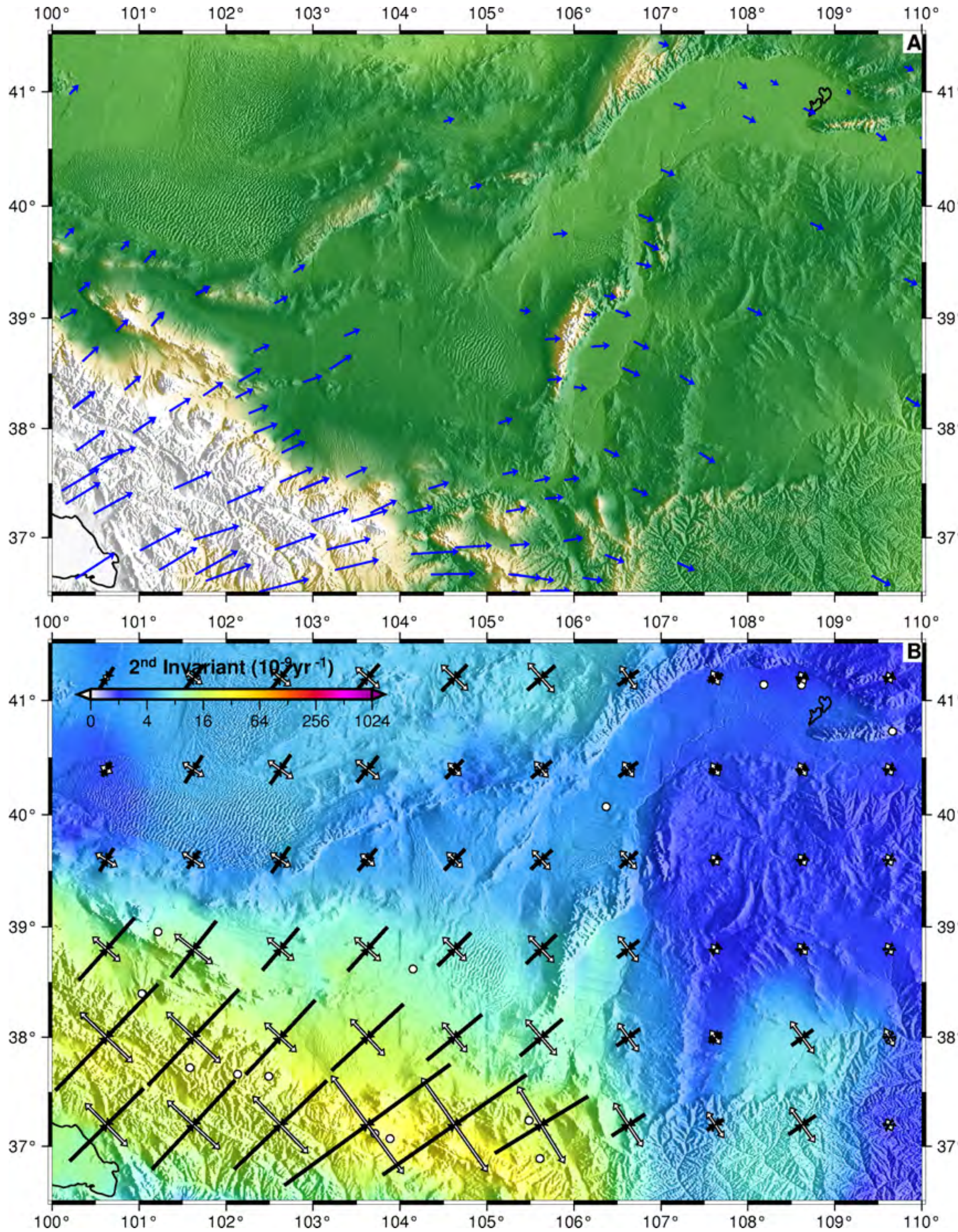
A
B
2nd Invariant (10-9yr-1)
0
4
16
64
256
1024
100°
101°
102°
103°
104°
105°
106°
107°
108°
109°
110°
37°
38°
39°
40°
41°

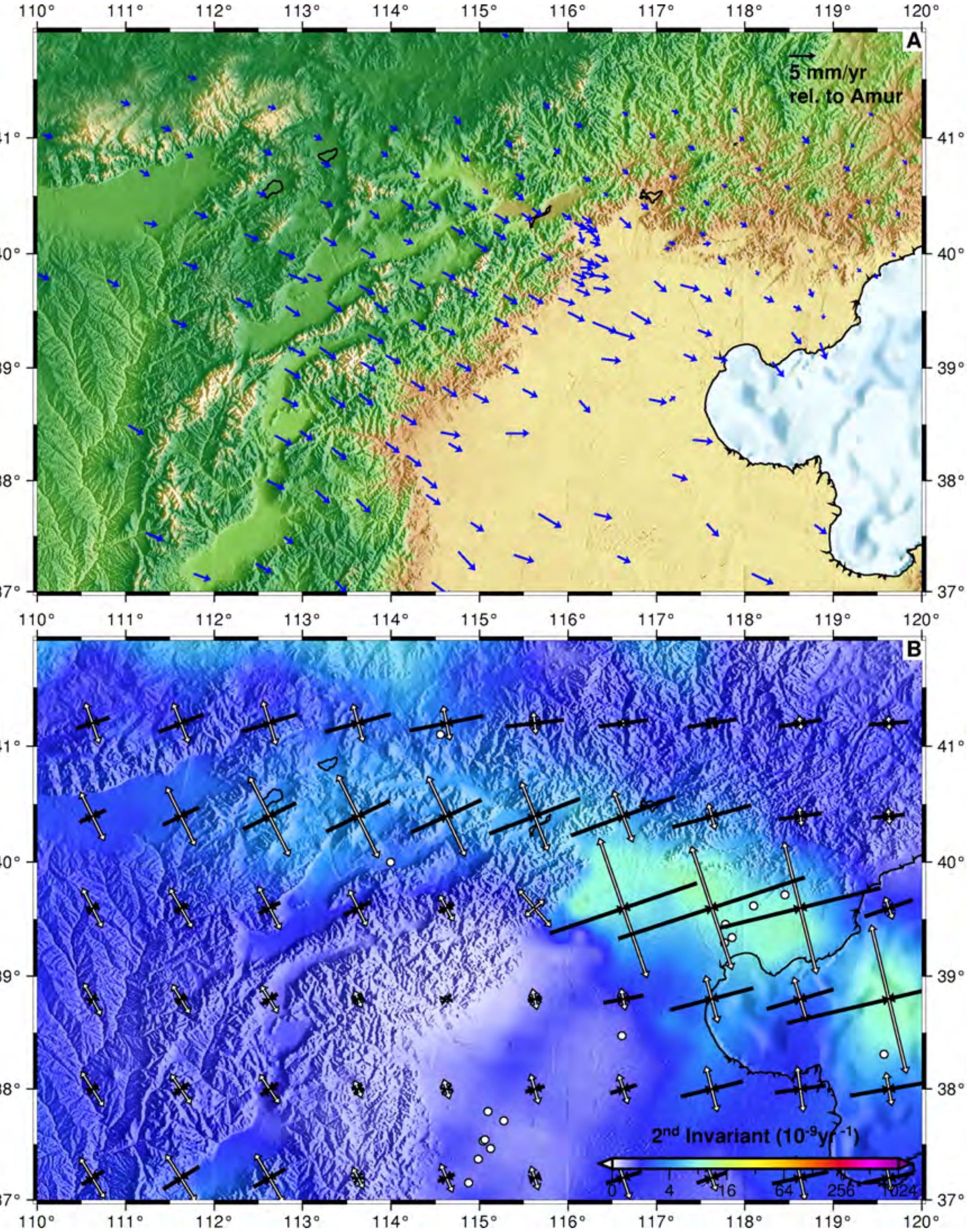
A
5 mm/yr
rel. to Amur
B
2nd Invariant (10-9yr-1)
0
4
16
64
256
1024
110°
111°
112°
113°
114°
115°
116°
117°
118°
119°
120°
37°
38°
39°
40°
41°

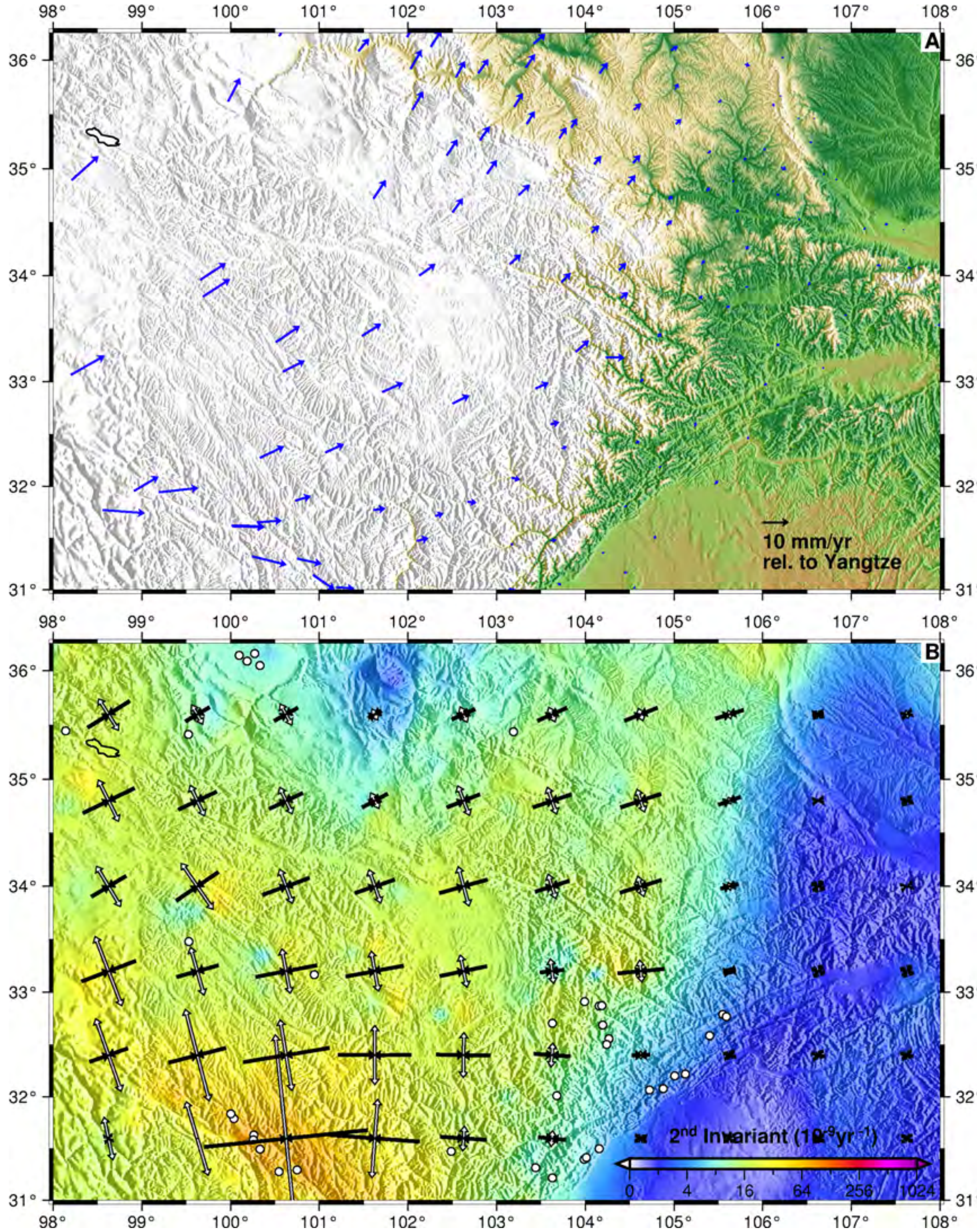
A
10 mm/yr
rel. to Yangtze
B
2nd Invariant (10-9yr-1)
0
4
16
64
256
1024
98°
99°
100°
101°
102°
103°
104°
105°
106°
107°
108°
31°
32°
33°
34°
35°
36°

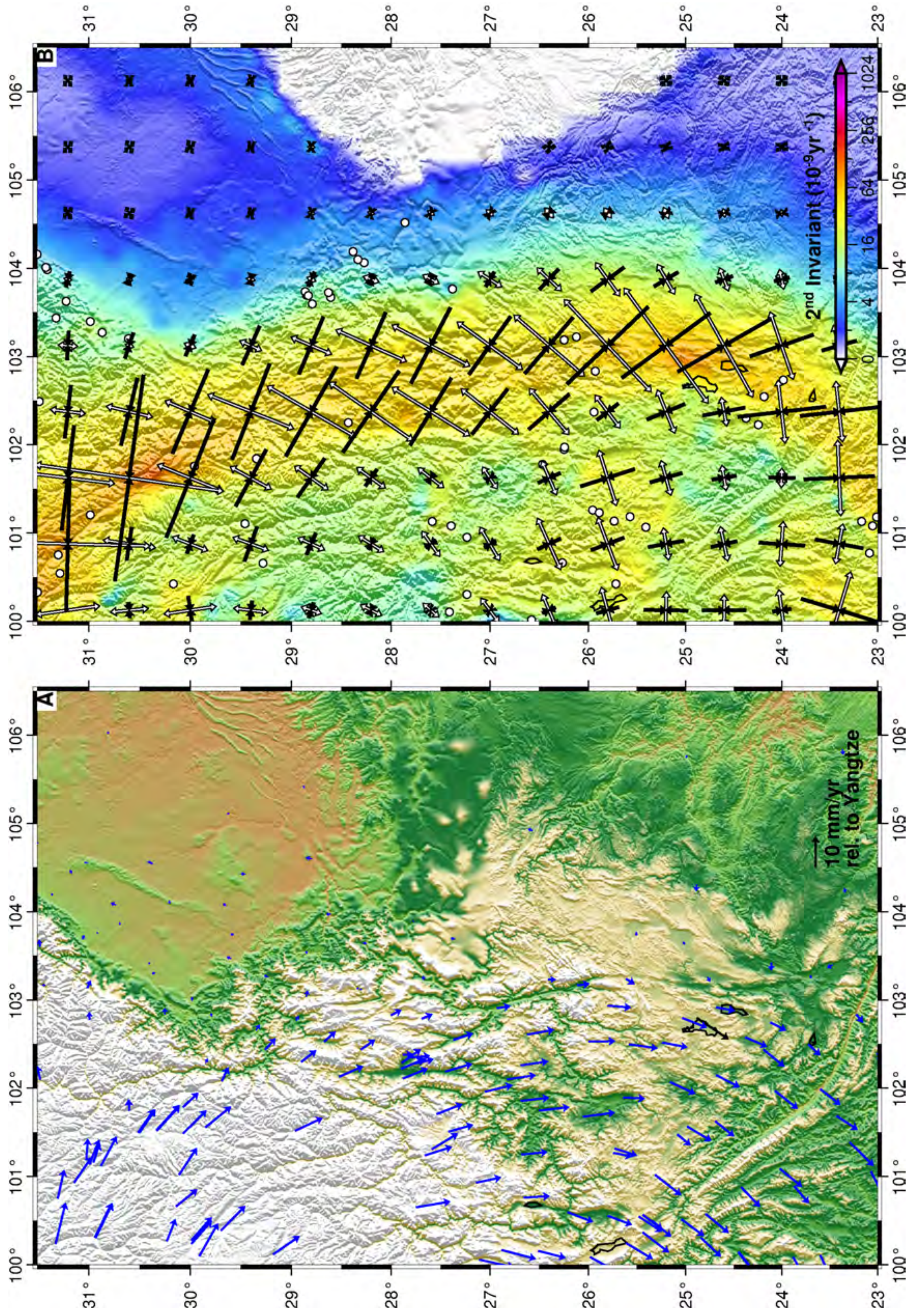
A
B
10 mm/yr
rel. to Yangtze
2nd Invariant (10⁻⁹yr⁻¹)
0
4
16
64
256
1024
100°
101°
102°
103°
104°
105°
106°
23°
24°
25°
26°
27°
28°
29°
30°
31°

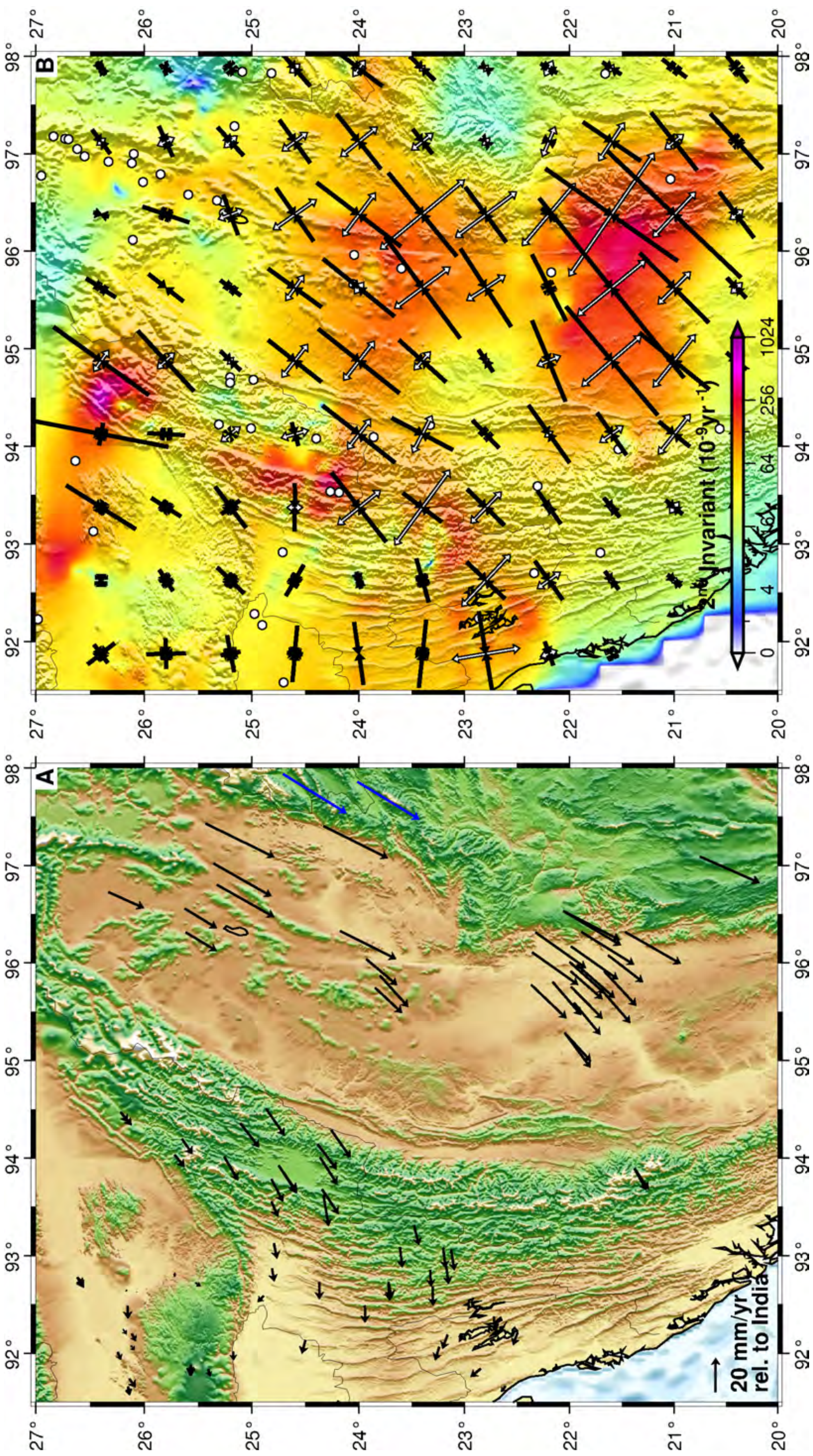

A
B
20 mm/yr
rel. to India
2nd Invariant (10⁻⁹yr⁻¹)
0
4
64
256
1024

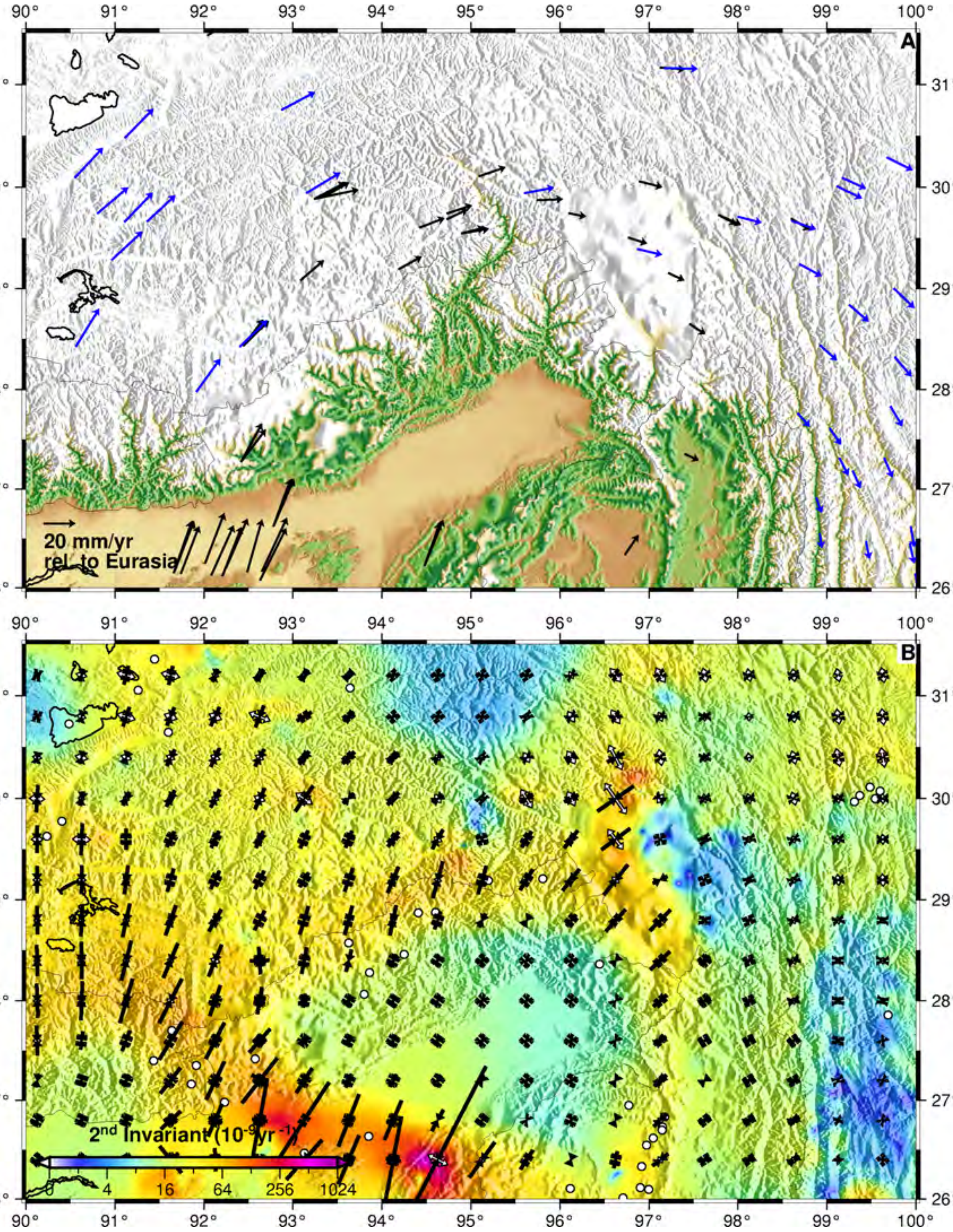
A
20 mm/yr
rel. to Eurasia
B
2nd Invariant (10-9 yr-1)
4
16
64
256
1024
90°
91°
92°
93°
94°
95°
96°
97°
98°
99°
100°
26°
27°
28°
29°
30°
31°

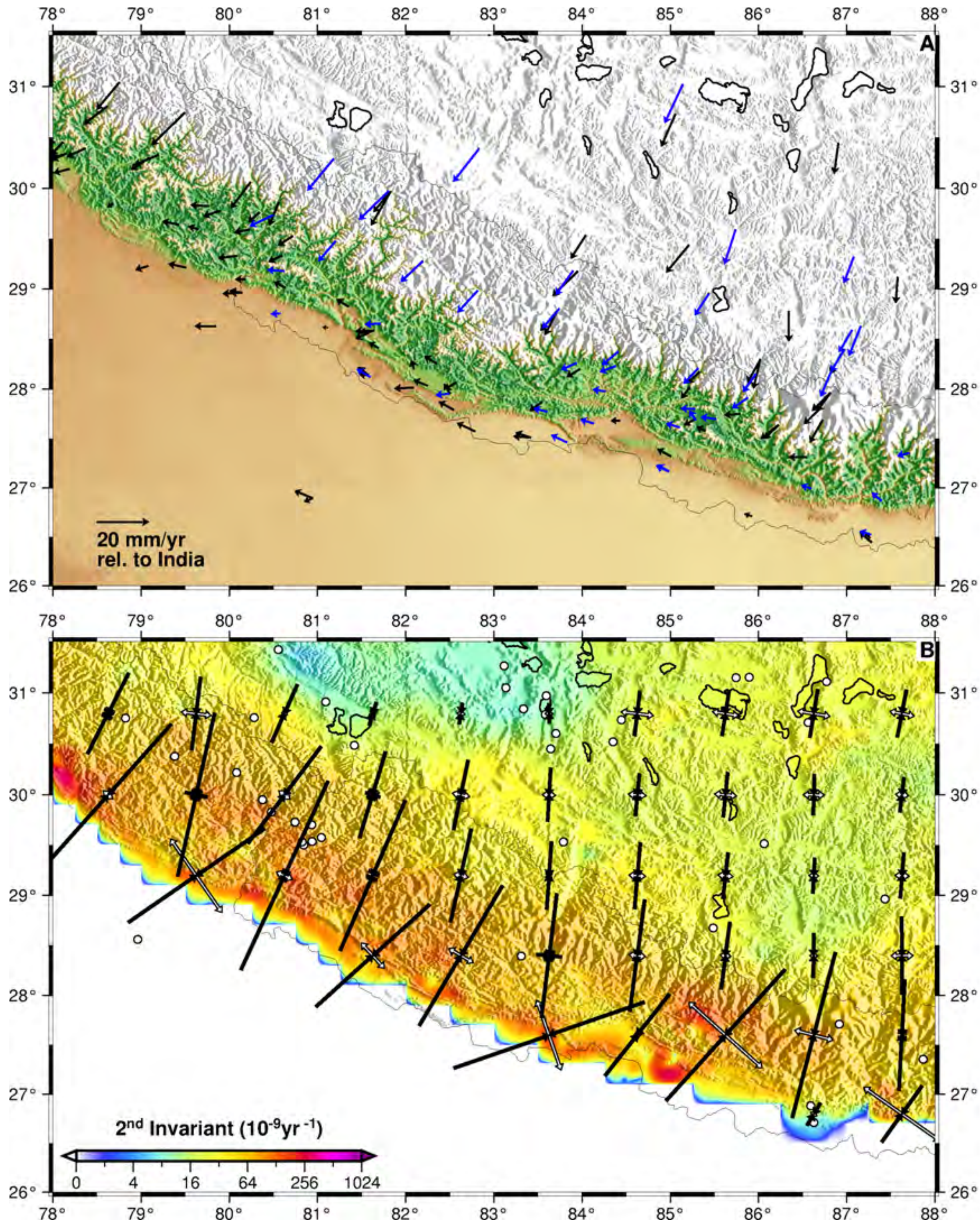

A
B
20 mm/yr
rel. to India
2nd Invariant (10-9yr -1)
0
4
16
64
256
1024
78°
79°
80°
81°
82°
83°
84°
85°
86°
87°
88°
26°
27°
28°
29°
30°
31°

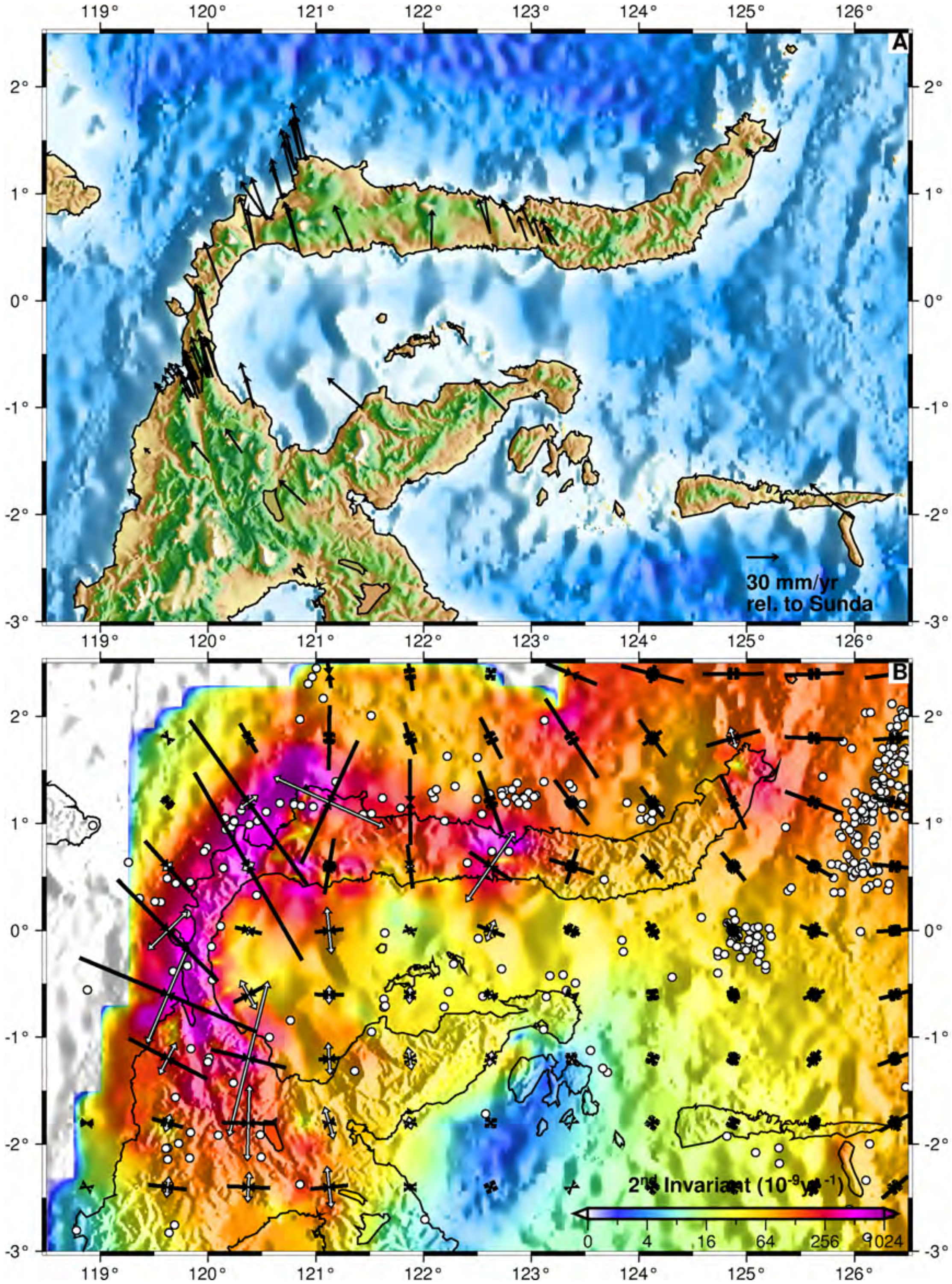
A
30 mm/yr
rel. to Sunda
B
2nd Invariant (10^{-9} yr^{-1})
0
4
16
64
256
1024

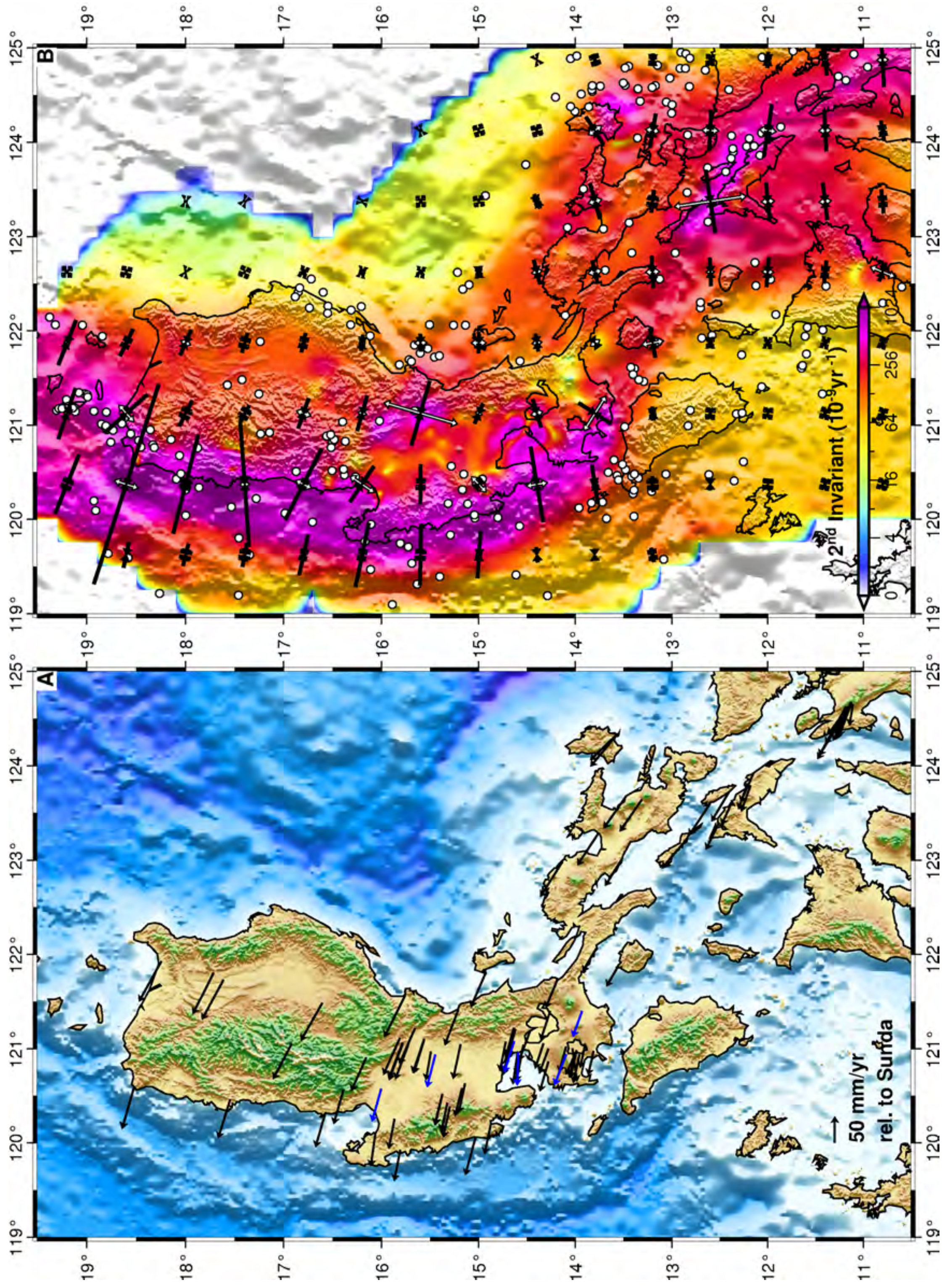
A
B
50 mm/yr
rel. to Sunda
2nd Invariant (10-9yr-1)
0
4
16
64
256
1024

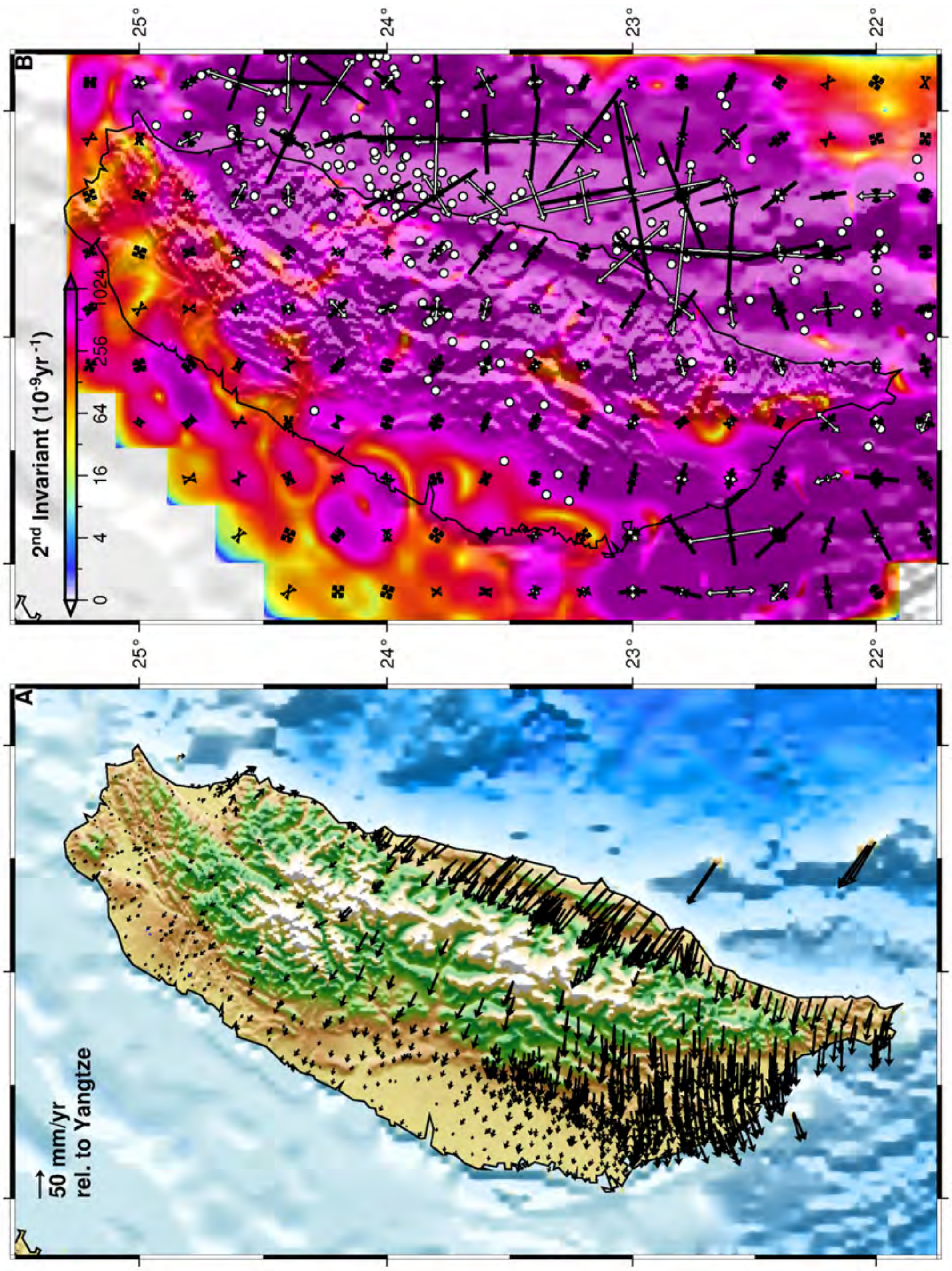
A
B
50 mm/yr
rel. to Yangtze
2nd Invariant (10-9yr-1)
0
4
16
64
256
1024
120°
121°
122°
22°
23°
24°
25°

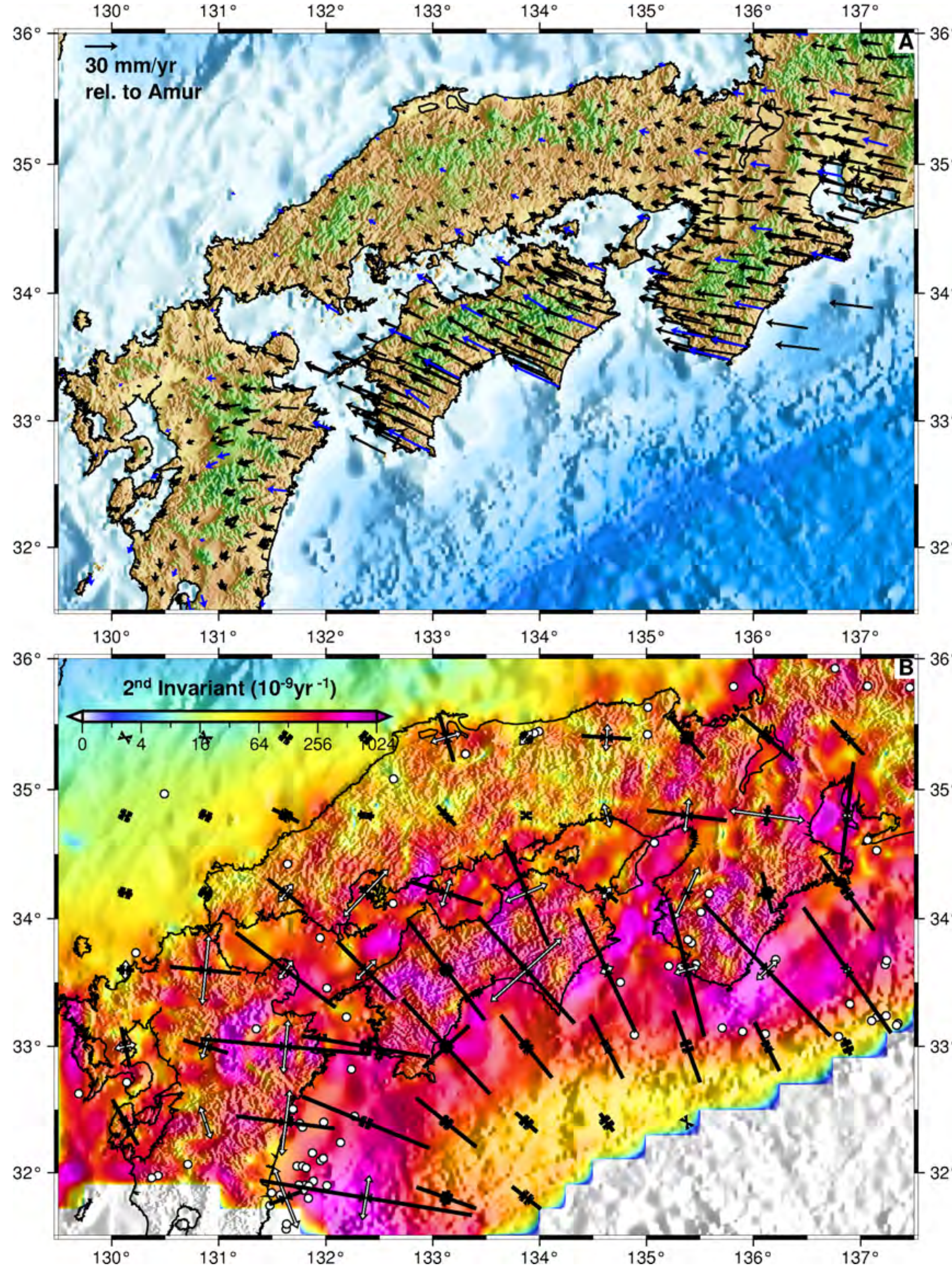
A
30 mm/yr
rel. to Amur
B
2nd Invariant (10-9yr -1)
0
4
16
64
256
1024
130°
131°
132°
133°
134°
135°
136°
137°
36°
35°
34°
33°
32°

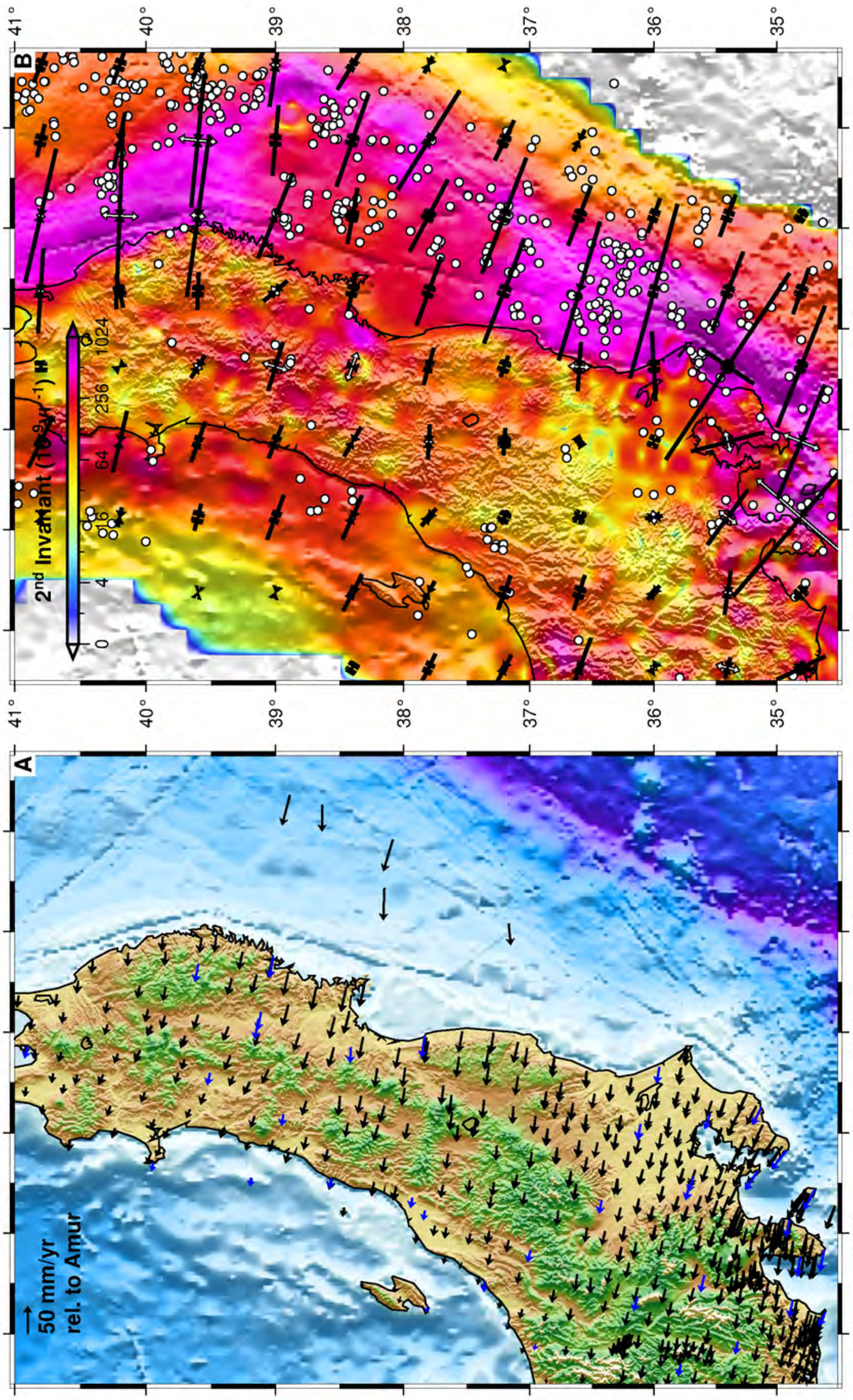
A
50 mm/yr
rel. to Amur
B
2nd Invariant (10-9 yr-1)
0
4
16
64
256
1024
138°
139°
140°
141°
142°
143°
35°
36°
37°
38°
39°
40°
41°

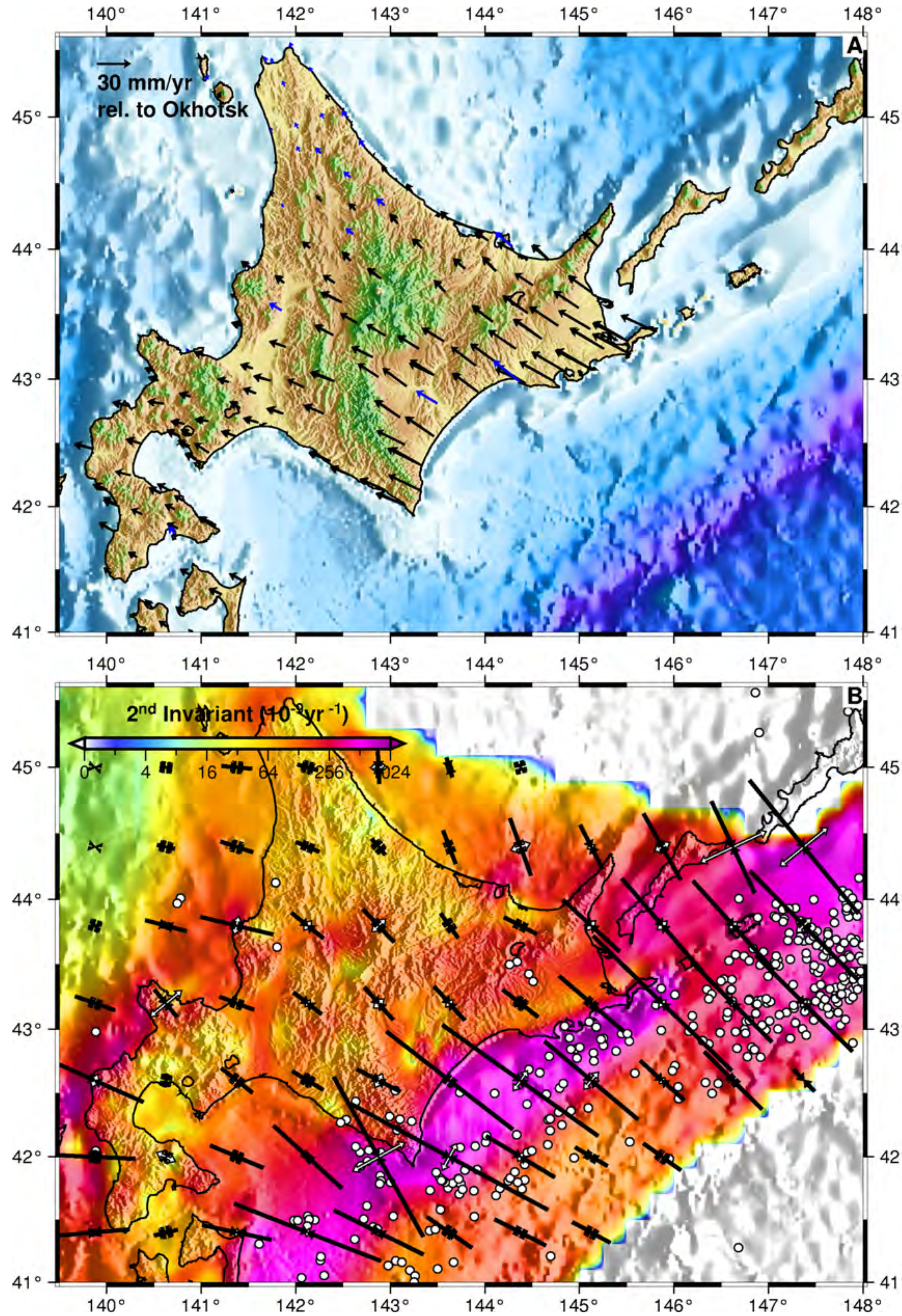
A
30 mm/yr
rel. to Okhotsk
B
2nd Invariant (10^{-9}yr^{-1})
0
4
16
64
256
1024
140°
141°
142°
143°
144°
145°
146°
147°
148°
41°
42°
43°
44°
45°

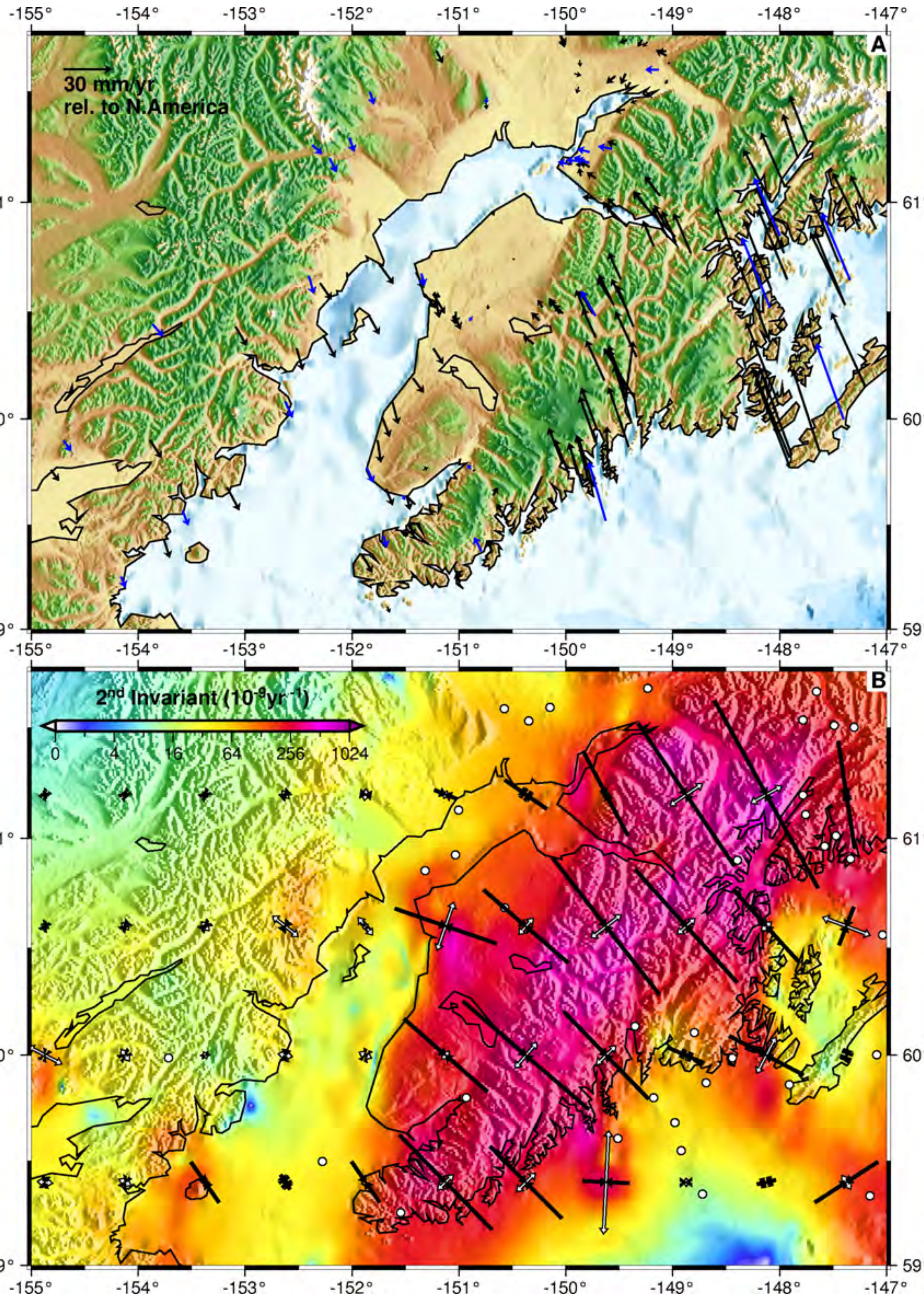
A
30 mm/yr
rel. to N.America
B
2nd Invariant (10-9yr-1)
0
4
16
64
256
1024
-155°
-154°
-153°
-152°
-151°
-150°
-149°
-148°
-147°
59°
60°
61°

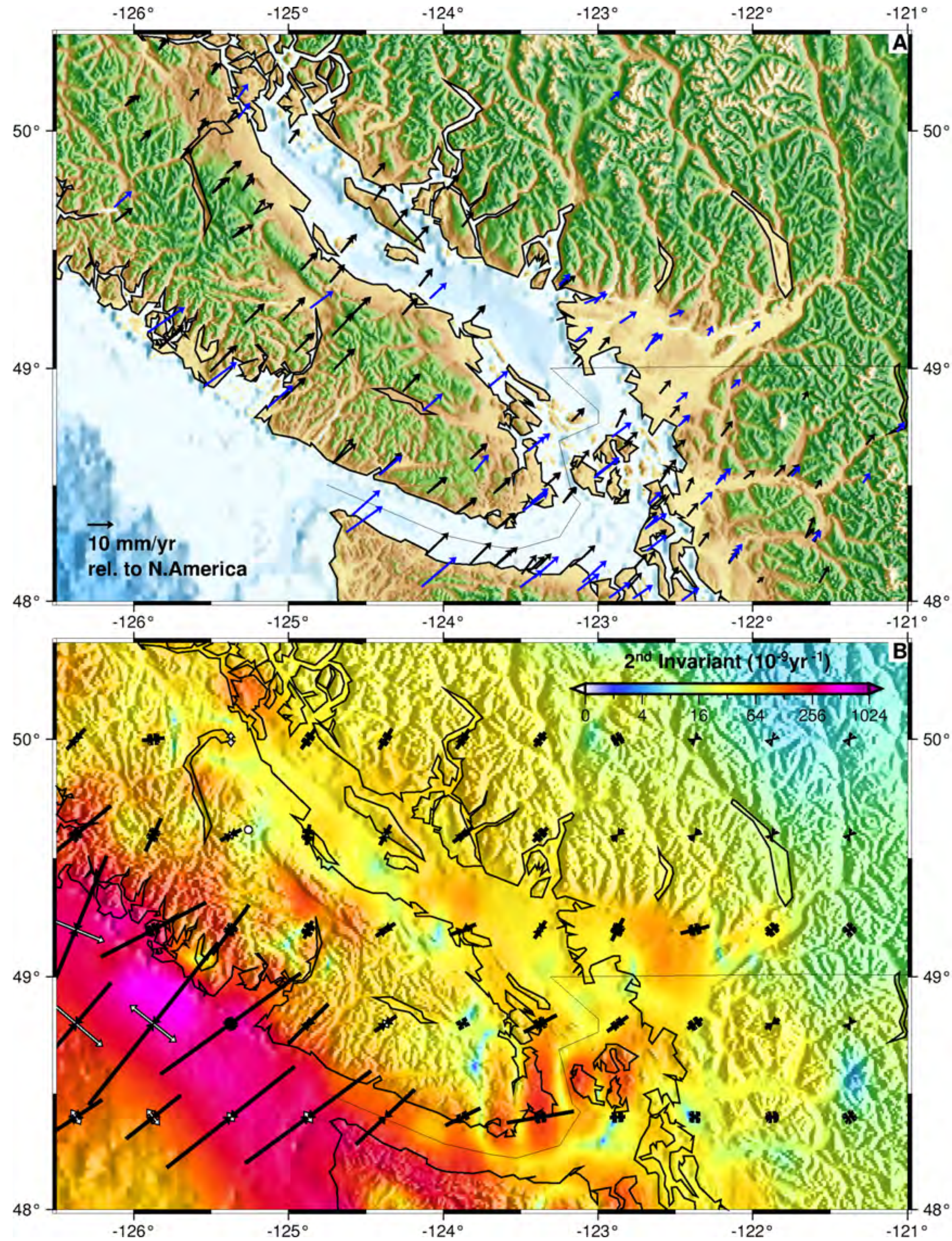
-126°
-125°
-124°
-123°
-122°
-121°
50°
49°
48°
A
10 mm/yr
rel. to N.America
B
2nd Invariant (10-9yr-1)
0
4
16
64
256
1024

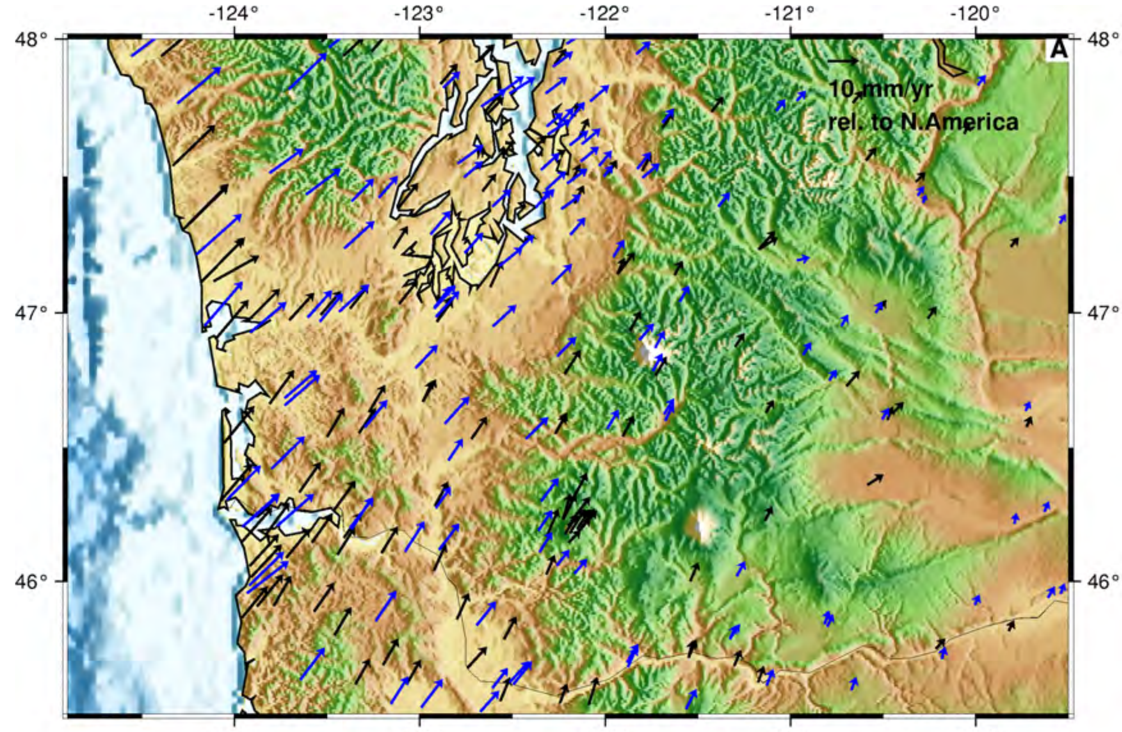
A
10 mm/yr
rel. to N.America
48°
47°
46°
-124°
-123°
-122°
-121°
-120°

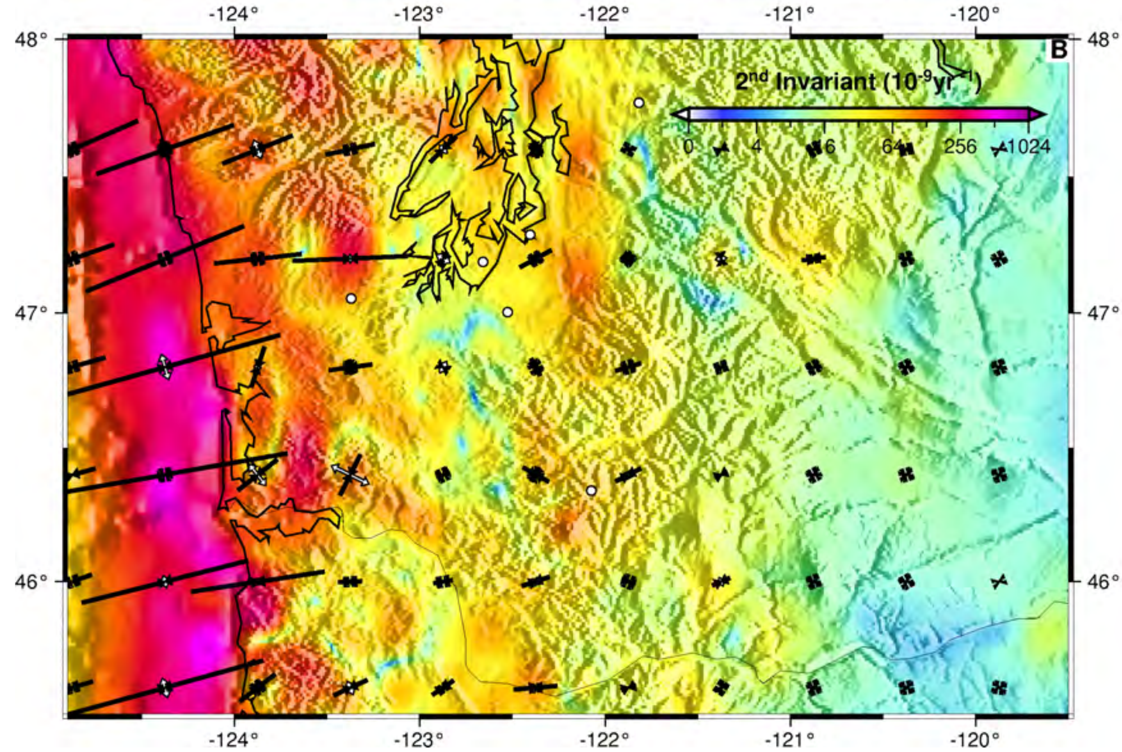
B
2nd Invariant (10-9yr-1)
0
4
16
64
256
1024
48°
47°
46°
-124°
-123°
-122°
-121°
-120°

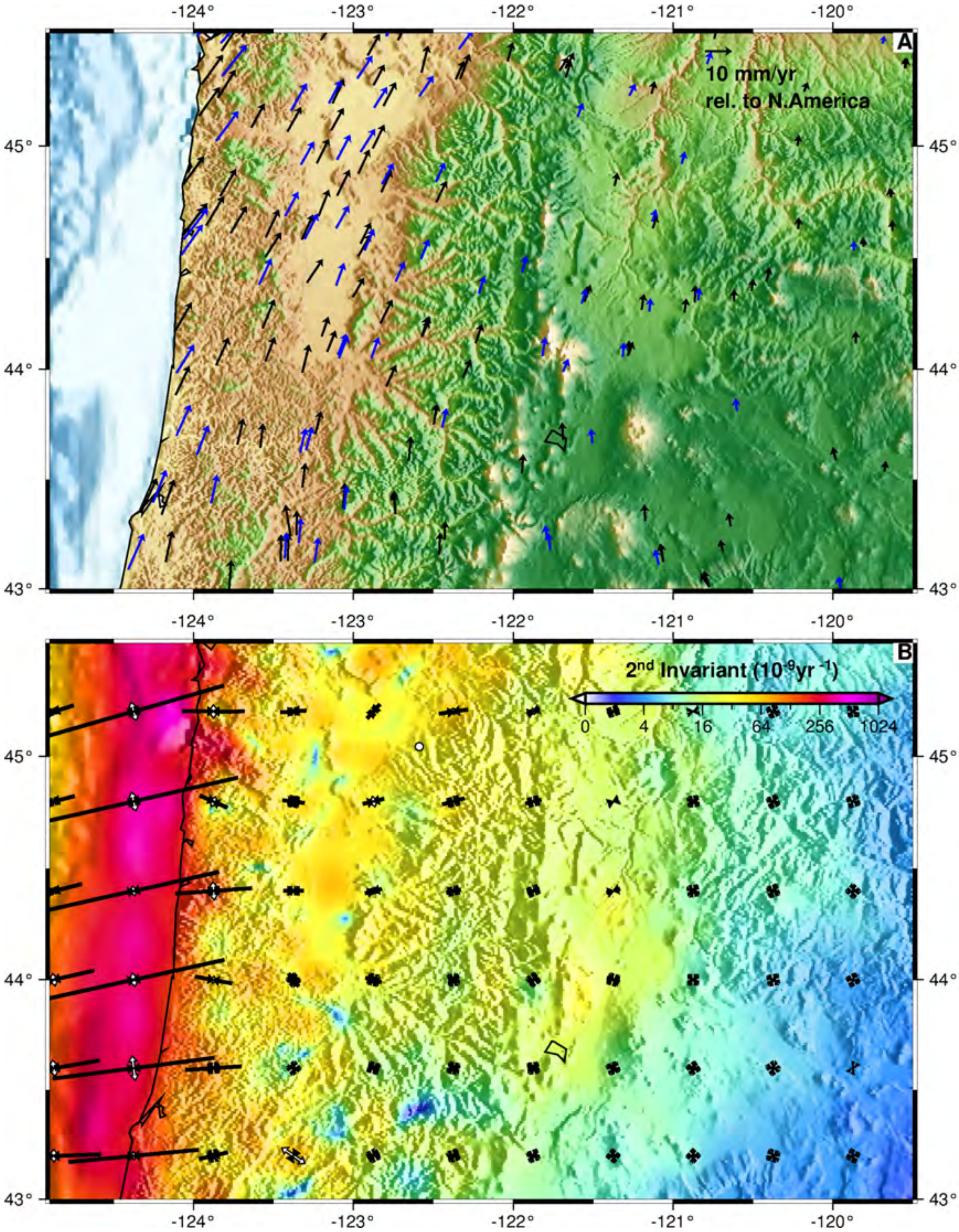
A
10 mm/yr
rel. to N.America
B
2nd Invariant (10-9yr-1)
0
4
16
64
256
1024
-124°
-123°
-122°
-121°
-120°
45°
44°
43°

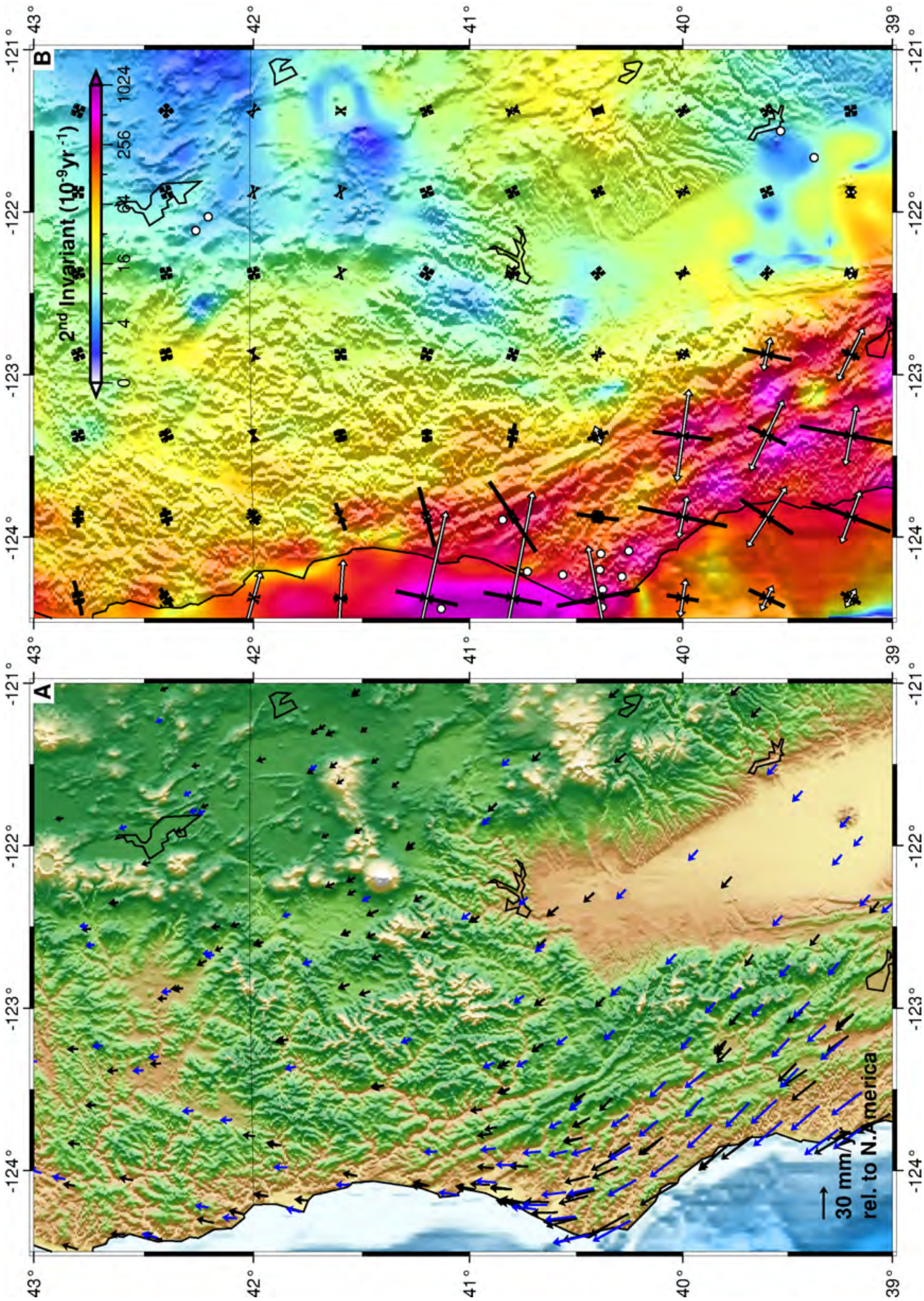
A
B
2nd Invariant (10^{-9} yr^{-1})
0
4
16
64
256
1024
30 mm/yr
rel. to N.America
43°
42°
41°
40°
39°
-121°
-122°
-123°
-124°

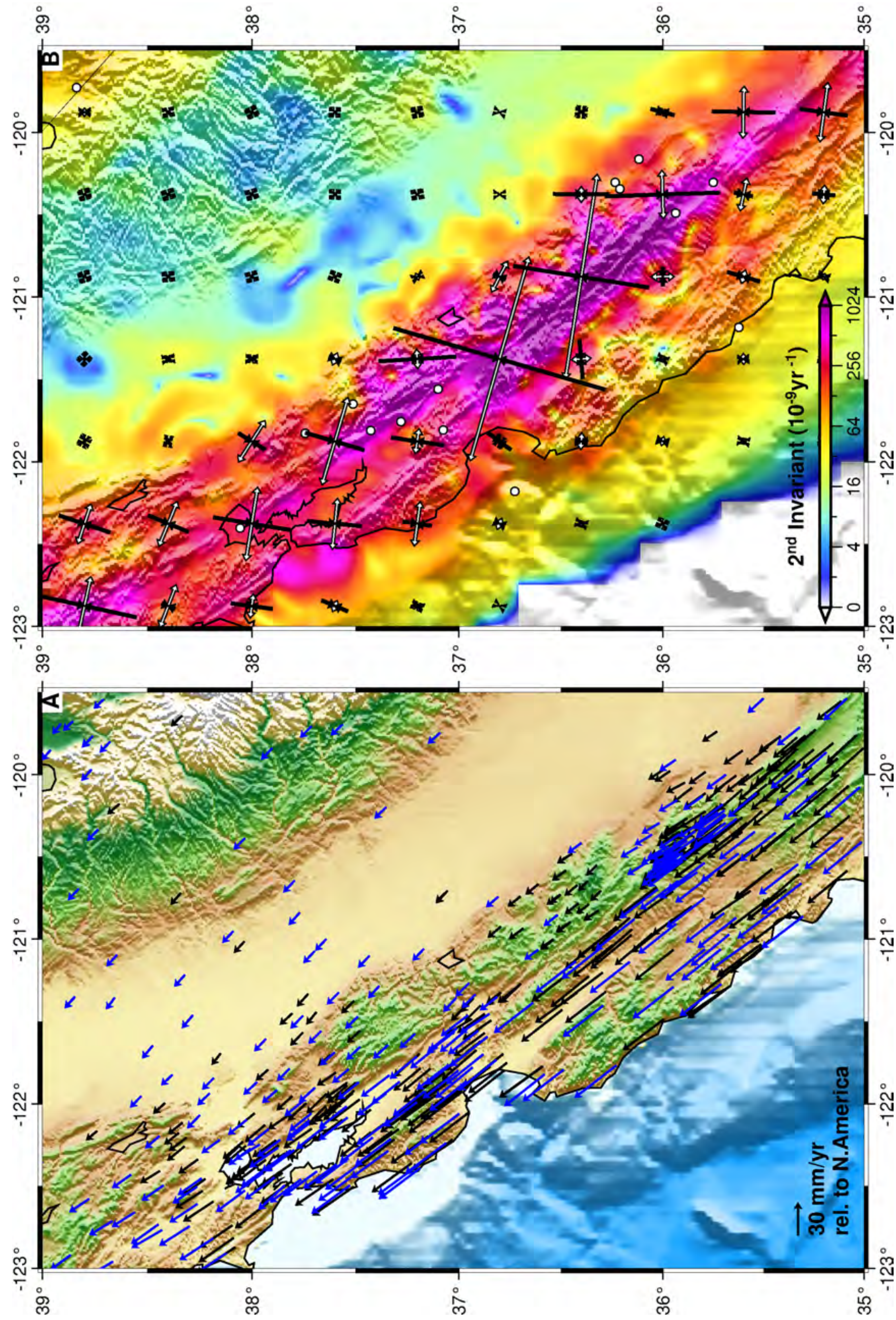
A
B
2nd Invariant (10-9yr-1)
0
4
16
64
256
1024
30 mm/yr
rel. to N.America
39°
38°
37°
36°
35°
-120°
-121°
-122°
-123°

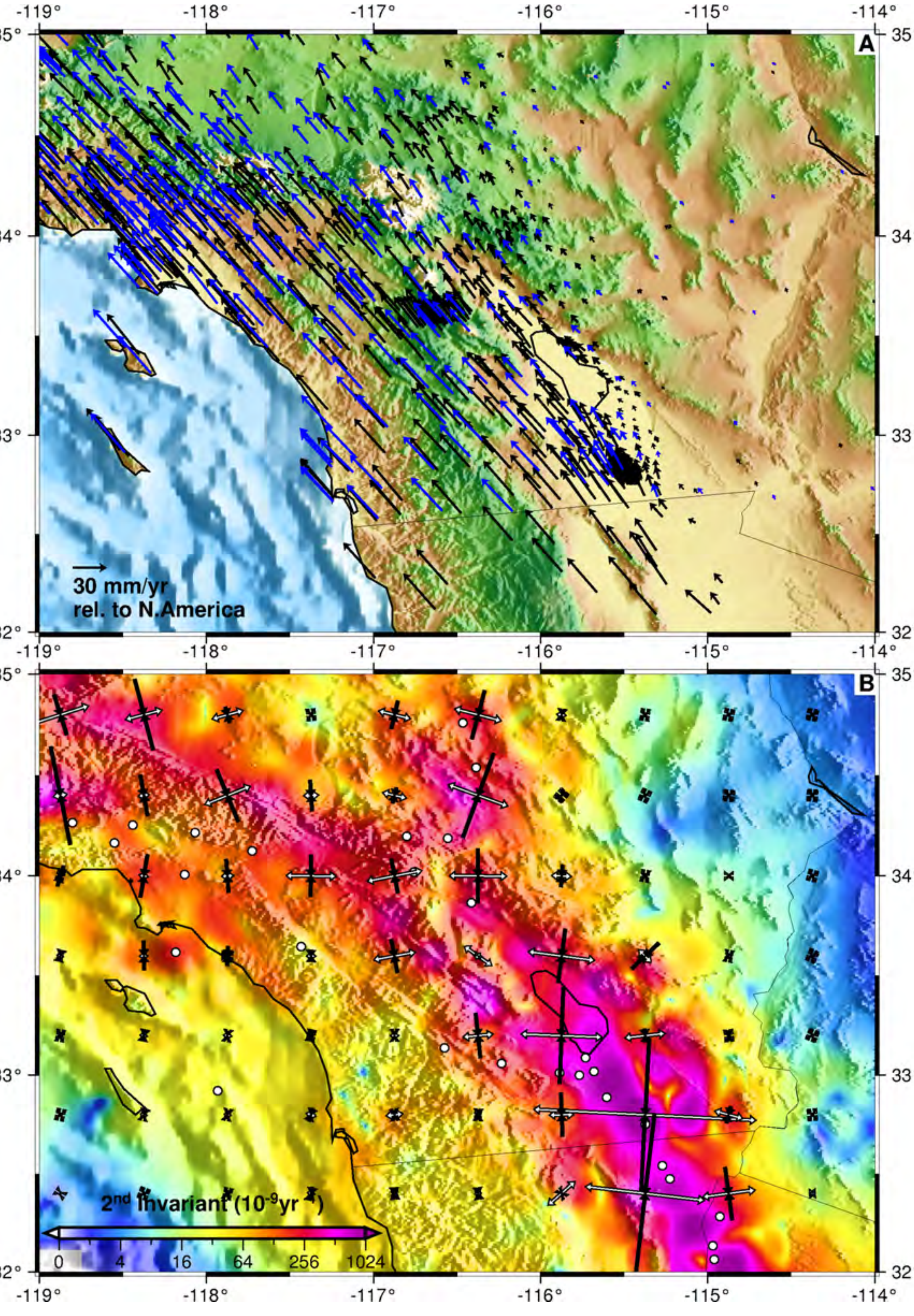
A
B
30 mm/yr
rel. to N.America
2nd invariant (10-9yr-1)
0
4
16
64
256
1024
-119°
-118°
-117°
-116°
-115°
-114°
35°
34°
33°
32°

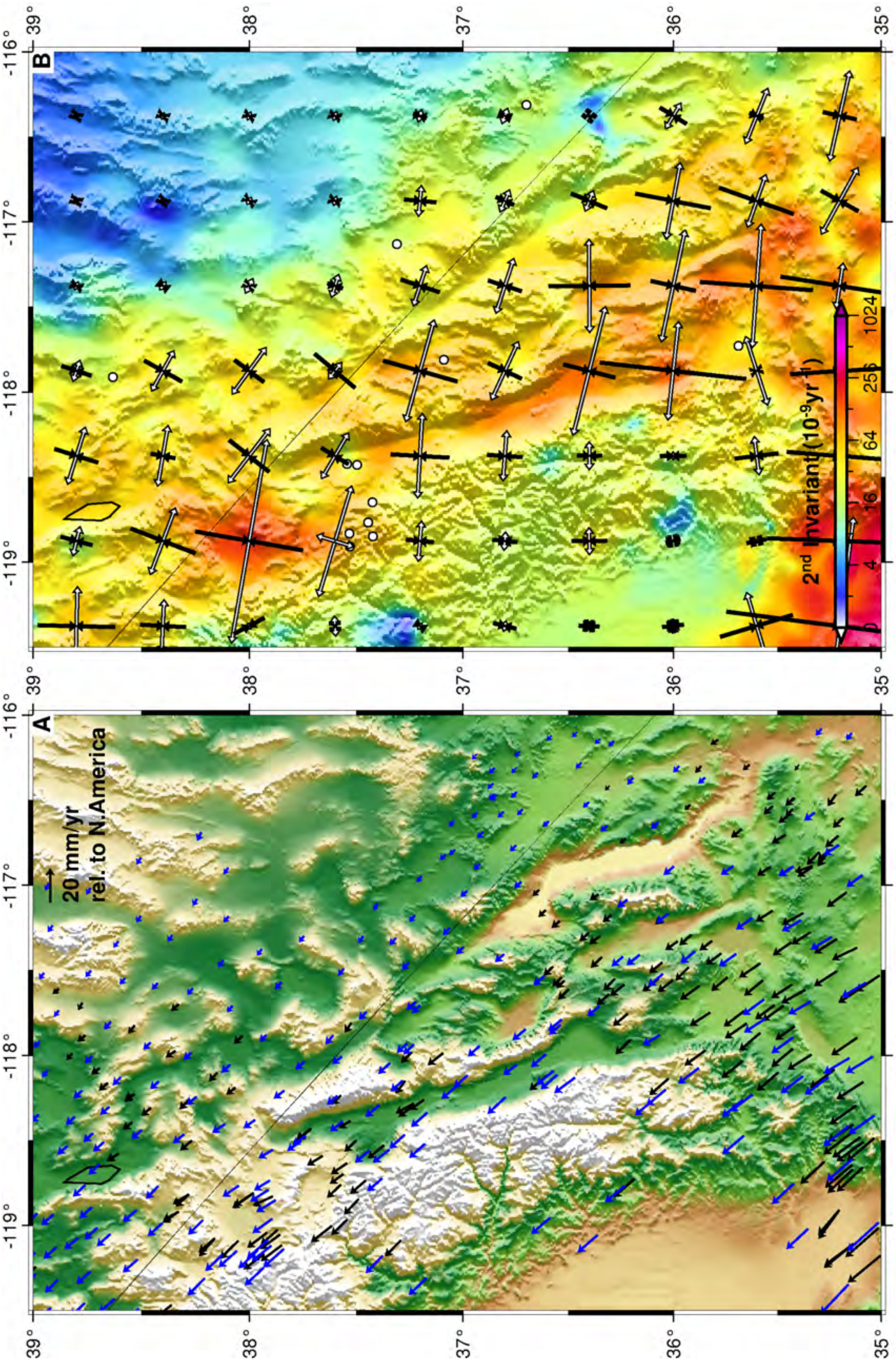
A
20 mm/yr
rel. to N.America
B
2nd Invariant (10^-9 yr^-1)
0
4
16
64
256
1024
-116°
-117°
-118°
-119°
39°
38°
37°
36°
35°

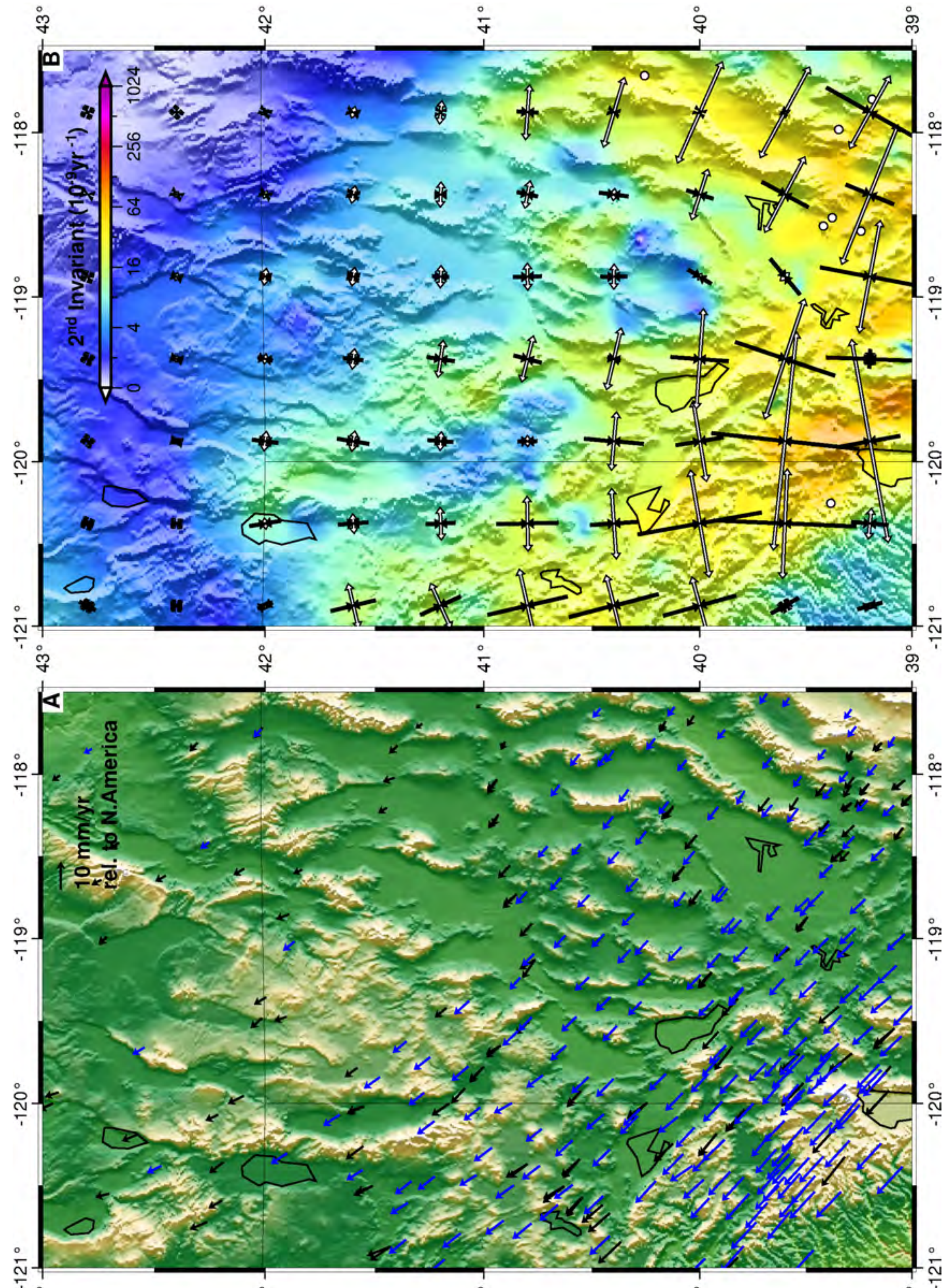
A
10 mm/yr
rel. to N.America
B
2nd Invariant (10^-9 yr^-1)
0
4
16
64
256
1024
43°
42°
41°
40°
39°
-118°
-119°
-120°
-121°

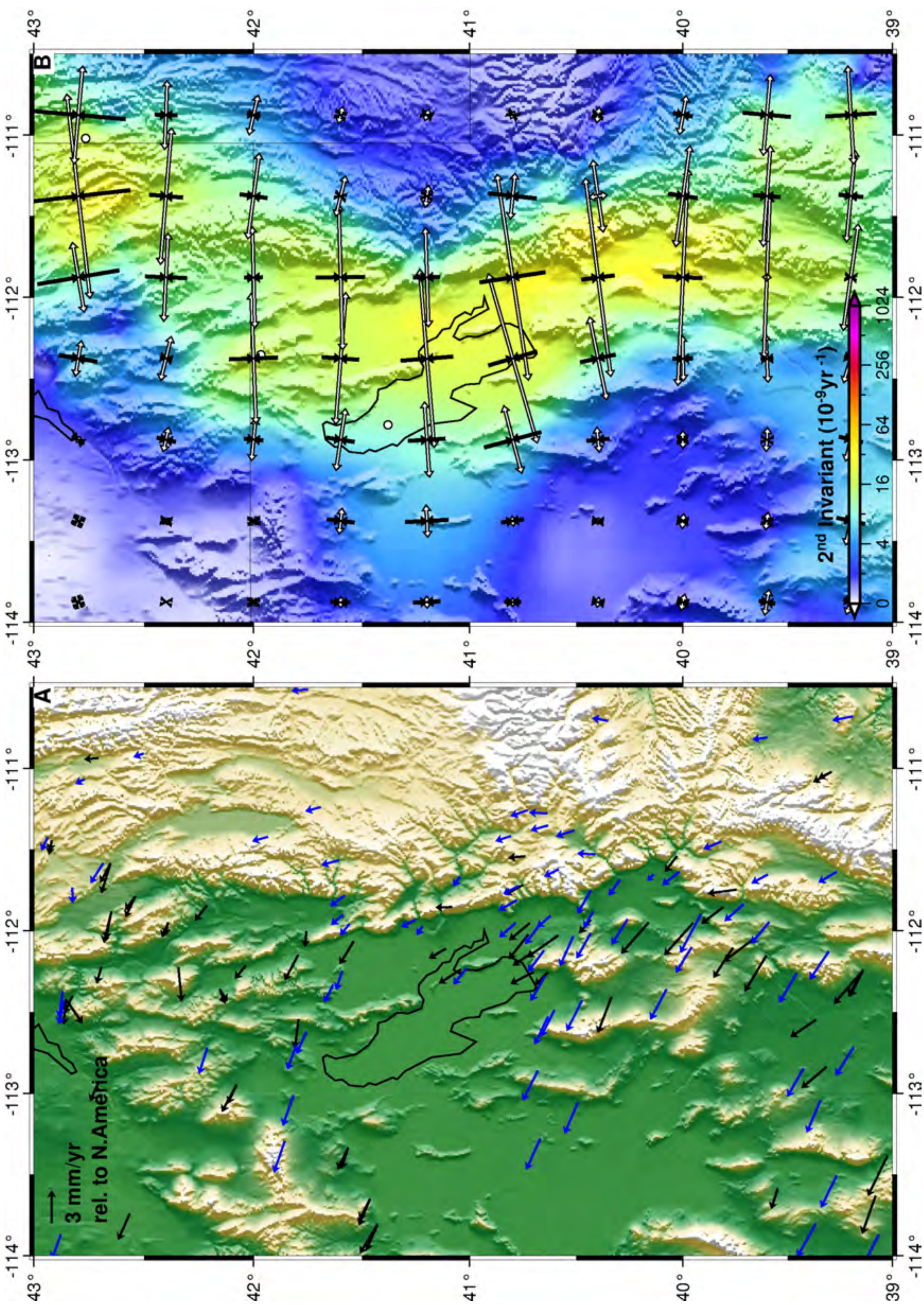
A
B
3 mm/yr
rel. to N.America
2nd Invariant (10-9yr-1)
0
4
16
64
256
1024
43°
42°
41°
40°
39°
-111°
-112°
-113°
-114°

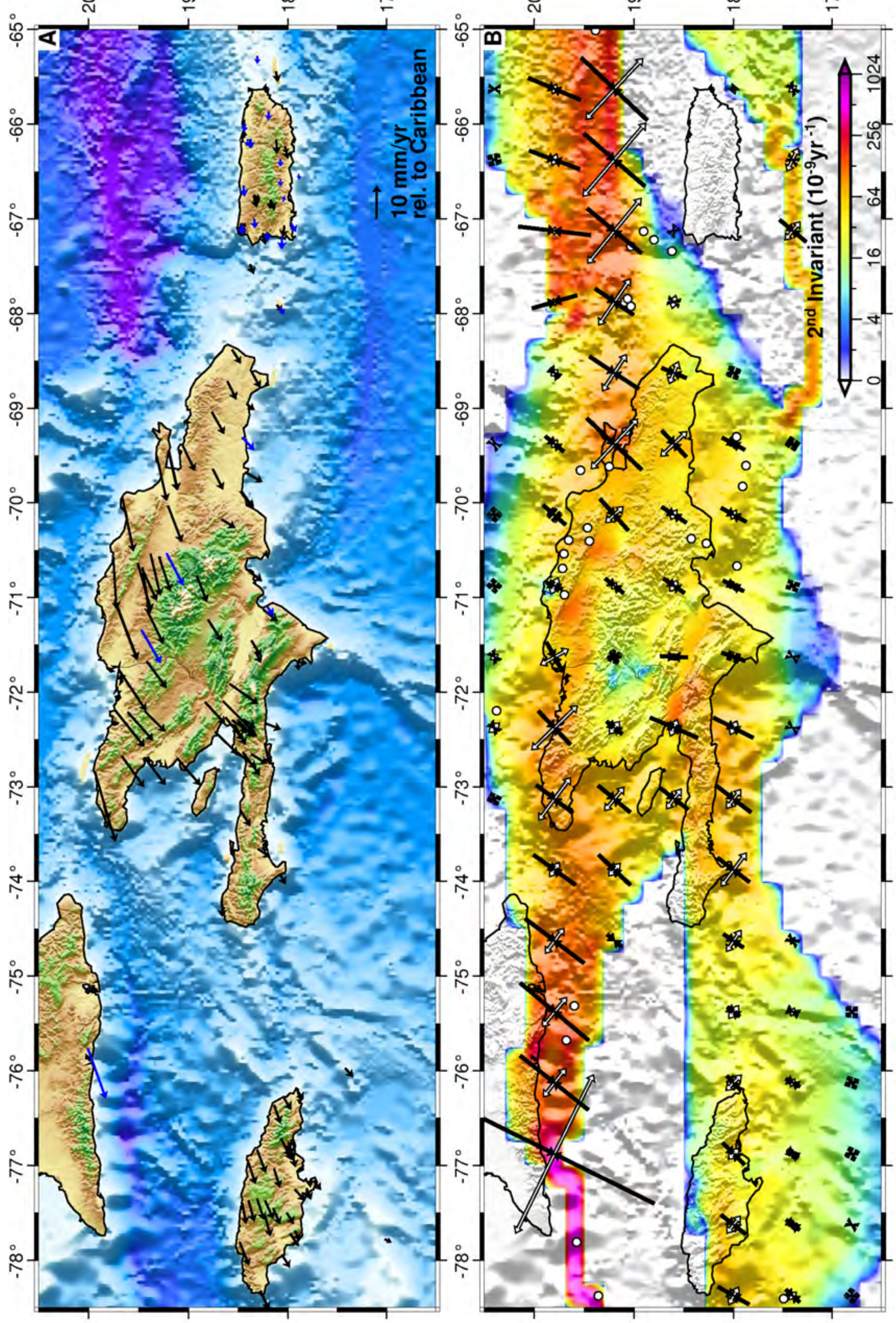
A
10 mm/yr
rel. to Caribbean
B
2nd Invariant (10-9yr-1)
0
4
16
64
256
1024
-65°
-66°
-67°
-68°
-69°
-70°
-71°
-72°
-73°
-74°
-75°
-76°
-77°
-78°
20°
19°
18°
17°

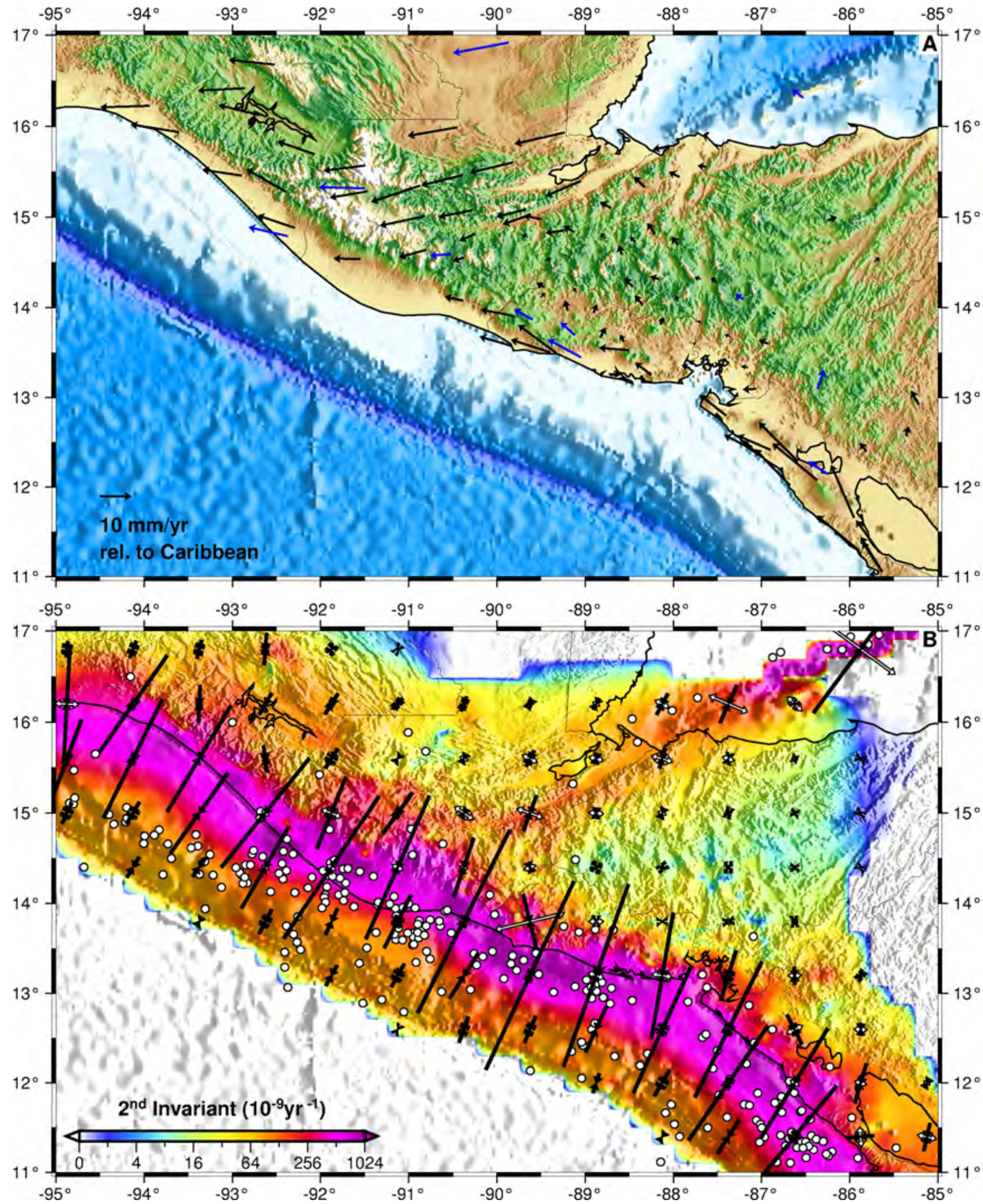
A
10 mm/yr
rel. to Caribbean
B
2nd Invariant (10-9yr -1)
0 4 16 64 256 1024
-95° -94° -93° -92° -91° -90° -89° -88° -87° -86° -85°
17° 16° 15° 14° 13° 12° 11°

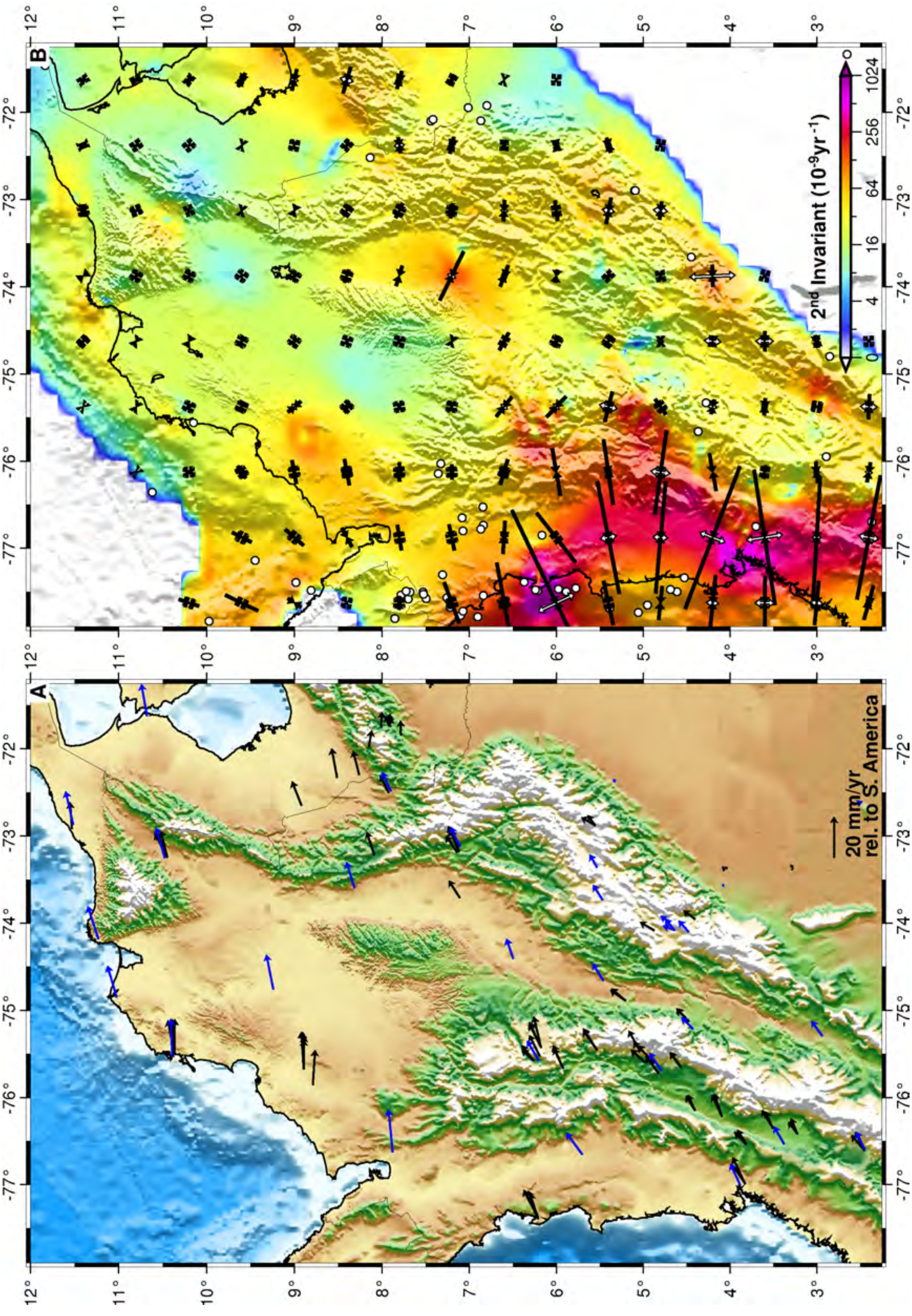
A
B
2nd Invariant (10-9yr-1)
0
4
16
64
256
1024
20 mm/yr
rel. to S. America

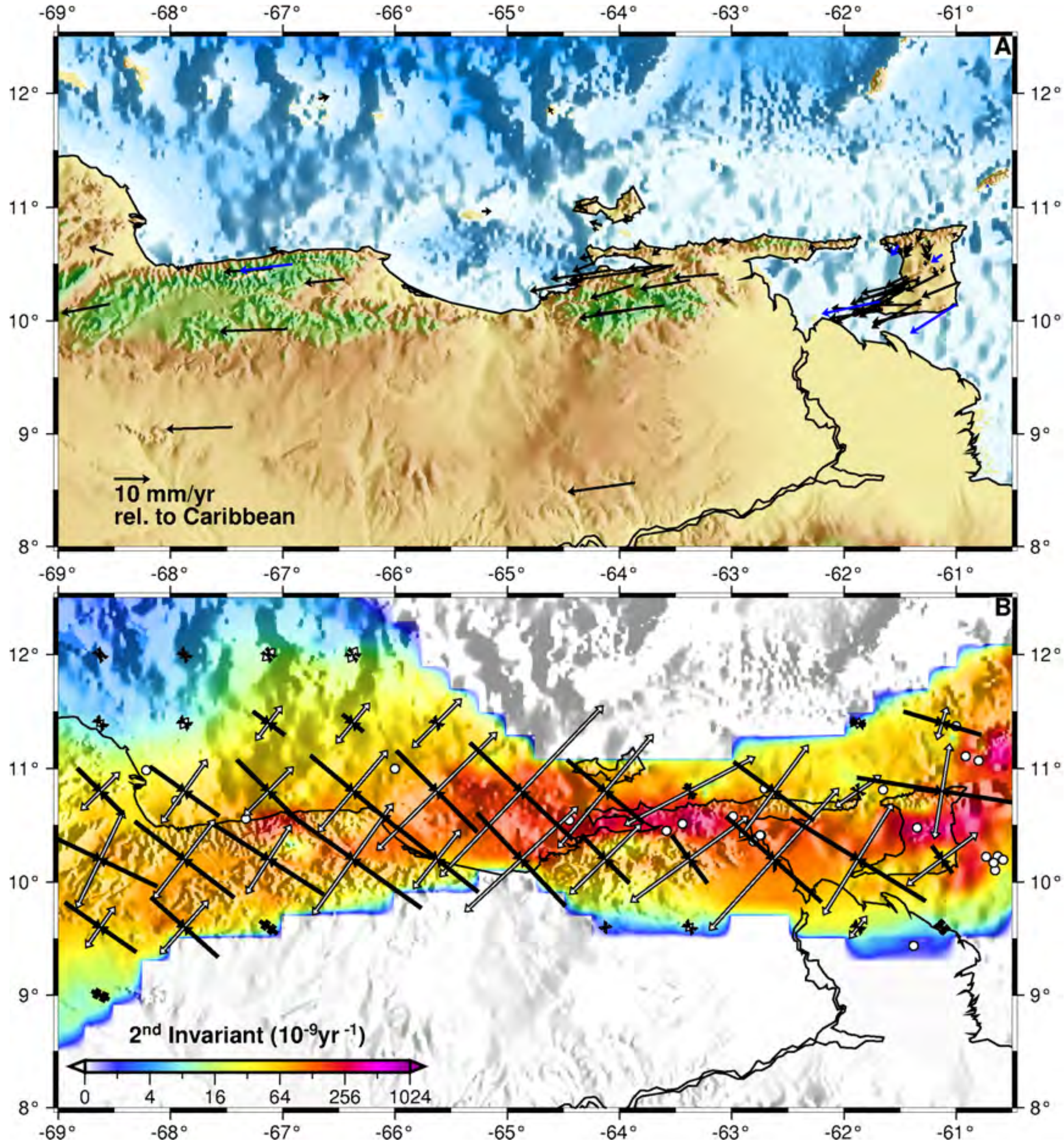
A
10 mm/yr
rel. to Caribbean
B
2nd Invariant (10-9yr -1)
0
4
16
64
256
1024

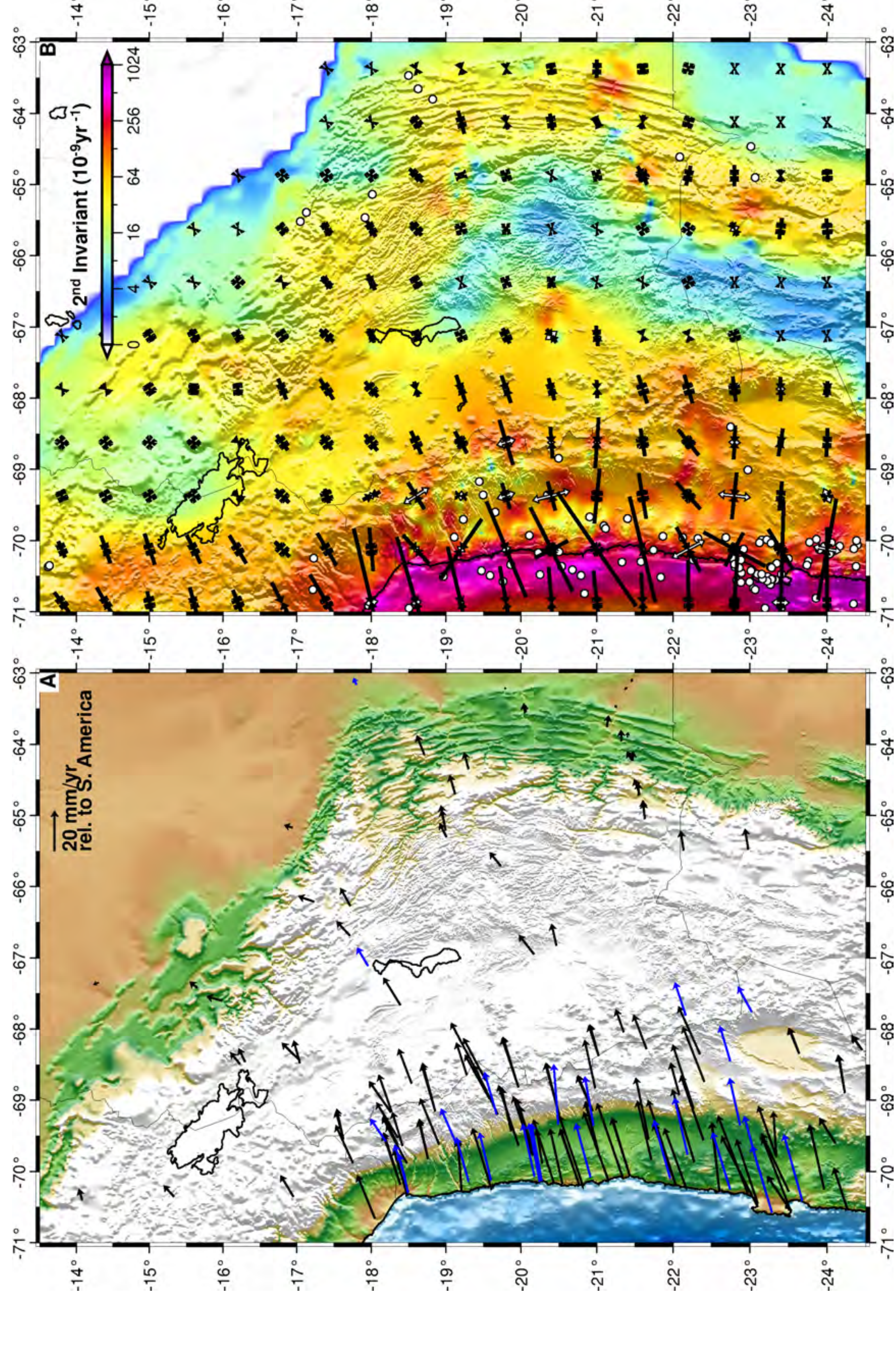
A
20 mm/yr
rel. to S. America
B
2nd Invariant (10-9yr-1)
0
4
16
64
256
1024

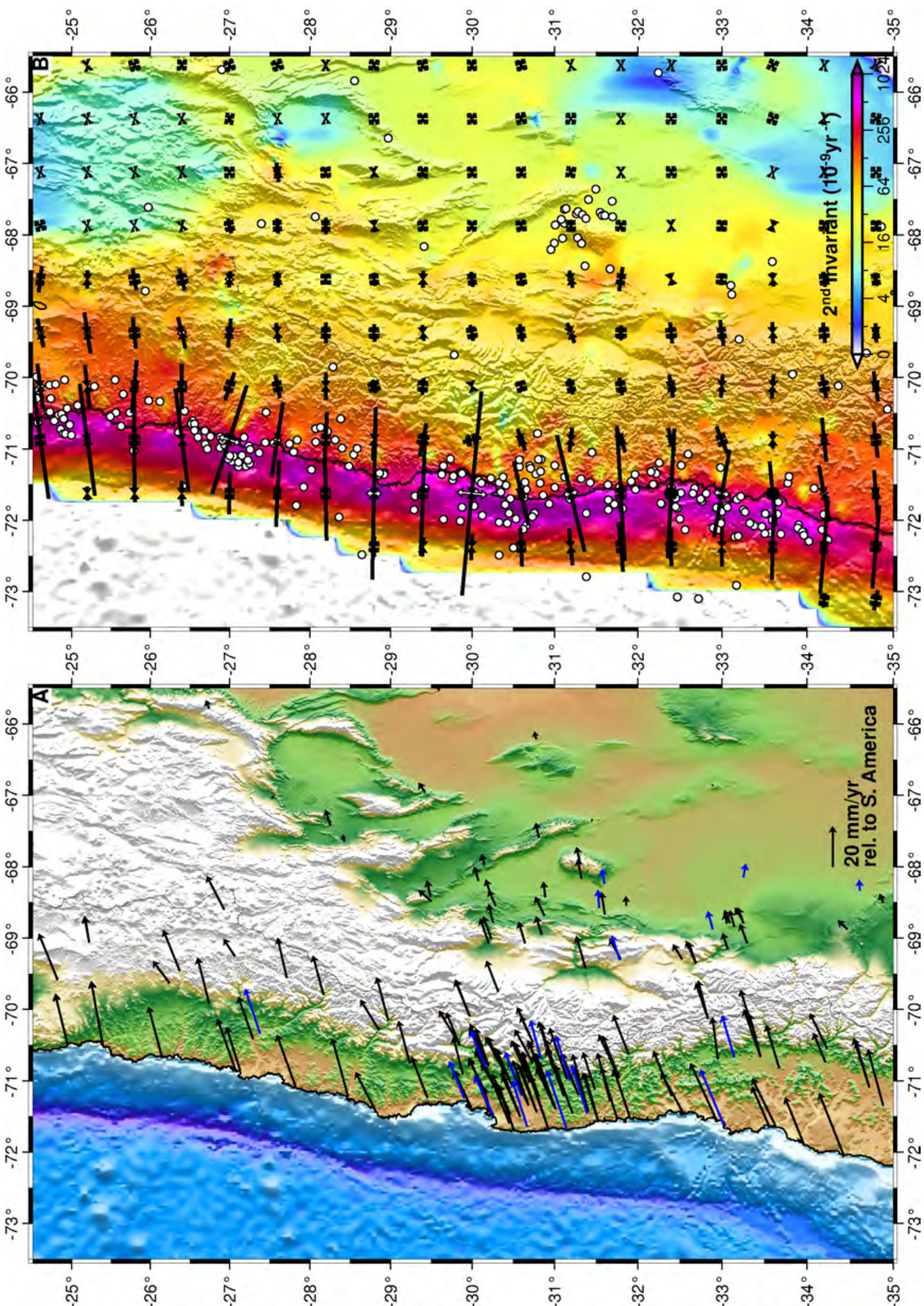

A
B
2nd invariant (10-9yr-1)
0 4 16 64 256 1024
20 mm/yr
rel. to S. America
-25° -26° -27° -28° -29° -30° -31° -32° -33° -34° -35°
-66° -67° -68° -69° -70° -71° -72° -73°

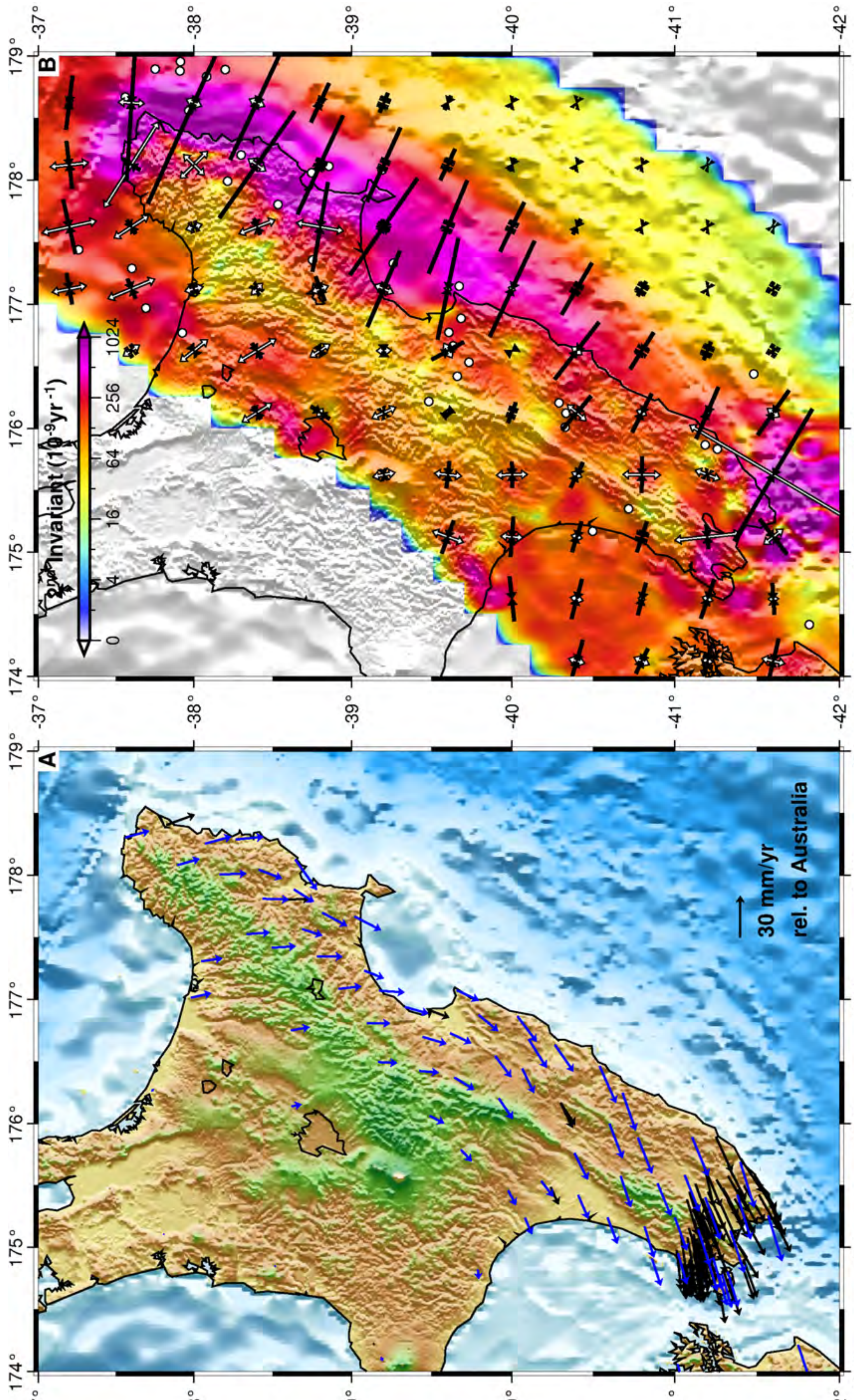
A
B
30 mm/yr
rel. to Australia
2nd Invariant (10-9yr-1)
0
4
16
64
256
1024
174°
175°
176°
177°
178°
179°
-37°
-38°
-39°
-40°
-41°
-42°

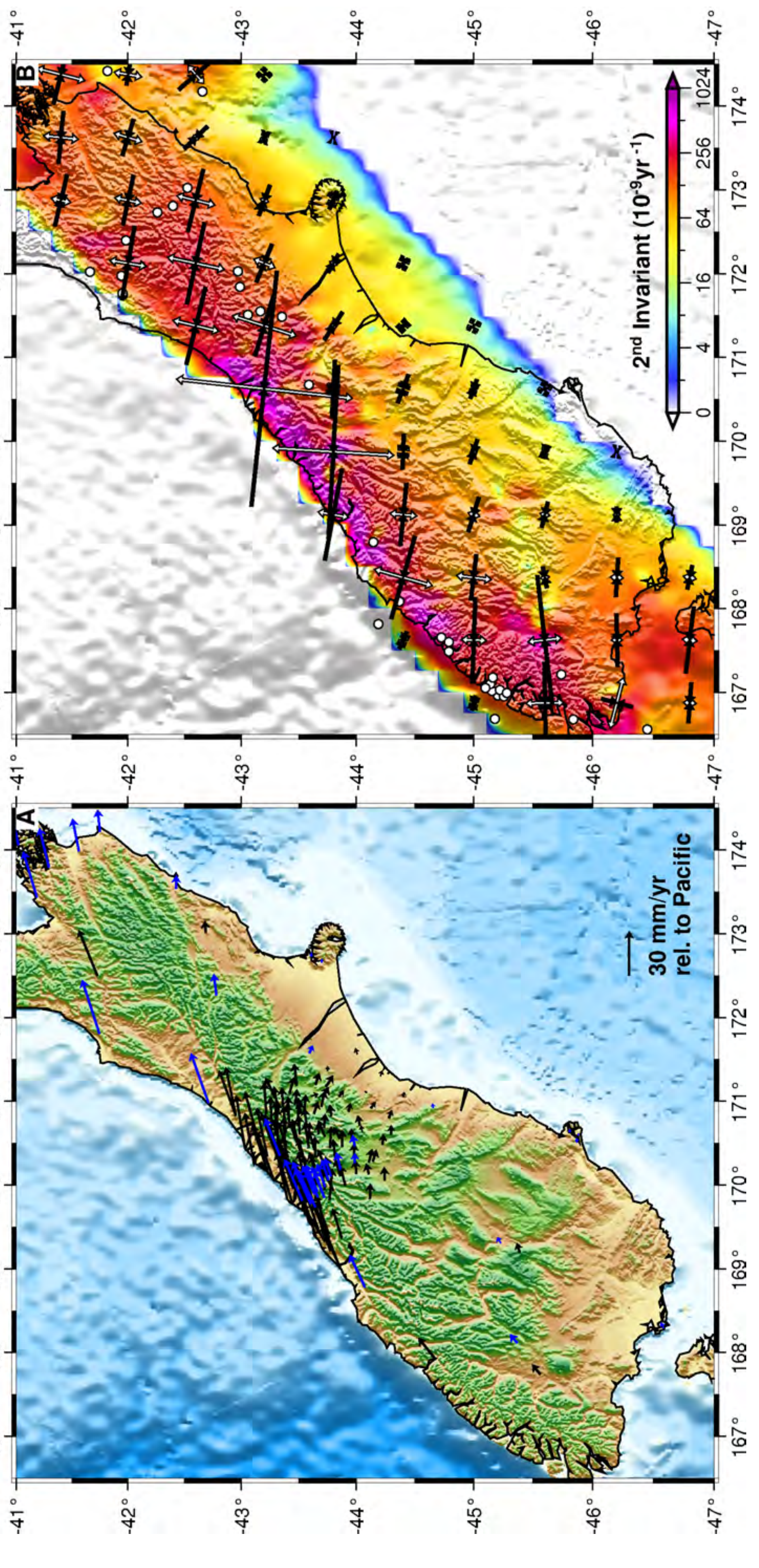
A
B
30 mm/yr
rel. to Pacific
2nd Invariant (10-9yr-1)
0
4
16
64
256
1024
167°
168°
169°
170°
171°
172°
173°
174°
-41°
-42°
-43°
-44°
-45°
-46°
-47°

APPENDIX B Published Studies in GPS Compilation

Aktuğ, B., and A. Kılıçoğlu (2006), Recent crustal deformation of İzmir, Western Anatolia and surrounding regions as deduced from repeated GPS measurements and strain field, J. Geodyn., 41(5), 471–484, doi:10.1016/j.jog.2006.01.004.

Aktuğ, B., E. Parmaksız, M. Kurt, O. Lenk, A. Kılıçoğlu, M. A. Gürdal, and S. Özdemir (2013a), Deformation of Central Anatolia: GPS implications, J. Geodyn., 67, 78–96, doi:10.1016/j.jog.2012.05.008.

Aktuğ, B., E. Meherremov, M. Kurt, S. Özdemir, N. Esedov, and O. Lenk (2013b), GPS constraints on the deformation of Azerbaijan and surrounding regions, J. Geodyn., 67, 40–45, doi:10.1016/j.jog.2012.05.007.

Aktuğ, B., U. Dikmen, A. Dogru, and H. Ozener (2013c), Seismicity and strain accumulation around Karliova Triple Junction (Turkey), J. Geodyn., 67, 21–29, doi:10.1016/j.jog.2012.04.008.

Aktuğ, B. et al. (2009), Deformation of western Turkey from a combination of permanent and campaign GPS data: Limits to block-like behavior, J. Geophys. Res., 114(B10), B10404, doi:10.1029/2008JB006000.

Almuselmani, B., F. . Teferle, R. M. Bingley, and T. Moore (2008), New estimates of present-day Arabia plate motion and deformation from a dense GPS network in Saudi Arabia, EOS Trans. AGU, 89, abstract G34A–02.

Alvarado, D., C. DeMets, B. Tikoff, D. Hernández, T. F. Wawrzyniec, C. Pullinger, G. Mattioli, H. L. Turner, M. Rodriguez, and F. Correa-Mora (2011), Forearc motion and deformation between El Salvador and Nicaragua: GPS, seismic, structural, and paleomagnetic observations, Lithosphere, 3(1), 3–21, doi:10.1130/L108.1.

Antonelis, K., D. J. Johnson, M. M. Miller, and R. Palmer (1999), GPS determination of current Pacific–North American plate motion, Geology, 27(4), 299–302, doi:10.1130/0091-7613(1999)027<0299:GDOCPN>2.3.CO;2.

Apel, E. V., R. Bürgmann, G. Steblov, N. Vasilenko, R. King, and A. Prytkov (2006), Independent active microplate tectonics of northeast Asia from GPS velocities and block modeling, Geophys. Res. Lett., 33(11), L11303, doi:10.1029/2006GL026077.

Árnadóttir, T., W. Jiang, K. L. Feigl, H. Geirsson, and E. Sturkell (2006), Kinematic models of plate boundary deformation in southwest Iceland derived from GPS observations, J. Geophys. Res., 111(B7), B07402, doi:10.1029/2005JB003907.

Árnadóttir, T., B. Lund, W. Jiang, H. Geirsson, H. Björnsson, P. Einarsson, and T. Sigurdsson (2009), Glacial rebound and plate spreading: results from the first countrywide GPS observations in Iceland, Geophys. J. Int., 177(2), 691–716, doi:10.1111/j.1365-246X.2008.04059.x.

Ashurkov, S. V., V. A. San'kov, A. I. Miroshnichenko, A. V. Lukhnev, A. P. Sorokin, M. A. Serov, and L. M. Byzov (2011), GPS geodetic constraints on the kinematics of the Amurian Plate, Russian Geology and Geophysics, 52(2), 239–249, doi:10.1016/j.rgg.2010.12.017.

Aurelio, M. A. (2001), GPS velocities in Mindanao Island, J. Geol. Soc. Phil., 56, 214–224.

Avallone, A., P. Briole, A. M. Agatza-Balodimou, H. Billiris, O. Charade, C. Mitsakaki, A. Nercessian, K. Papazissi, D. Paradissis, and G. Veis (2004), Analysis of eleven years of deformation measured by GPS in the Corinth Rift Laboratory area, Comptes Rendus Geoscience, 336(4–5), 301–311, doi:10.1016/j.crte.2003.12.007.

Avé Lallemant, H. G., and J. S. Oldow (2000), Active displacement partitioning and arc-parallel extension of the Aleutian volcanic arc based on Global Positioning System geodesy and kinematic analysis, Geology, 28(8), 739–742, doi:10.1130/0091-7613(2000)28<739:ADPAAE>2.0.CO;2.

Ayhan, M. E., C. Demir, O. Lenk, A. Kiliçoglu, Y. Altiner, A. A. Barka, S. Ergintav, and H. Özener (2002), Interseismic strain accumulation in the Marmara Sea region, Bull. Seismol. Soc. Am., 92(1), 216–229, doi:10.1785/0120000818.

Bacolcol, T., E. Barrier, T. Duquesnoy, A. Aguilar, R. Jorgio, R. de la Cruz, and M. Lasala (2005), GPS constraints on Philippine Fault slip rate in Masbate Island, central Philippines, J. Geol. Soc. Phil., 1–7.

Banerjee, P., R. Bürgmann, B. Nagarajan, and E. Apel (2008), Intraplate deformation of the Indian subcontinent, Geophys. Res. Lett., 35(18), L18301, doi:10.1029/2008GL035468.

Beavan, J., and J. Haines (2001), Contemporary horizontal velocity and strain rate fields of the Pacific-Australian plate boundary zone through New Zealand, J. Geophys. Res., 106(B1), 741–770, doi:10.1029/2000JB900302.

Beavan, J. et al. (1999), Crustal deformation during 1994–1998 due to oblique continental collision in the central Southern Alps, New Zealand, and implications for seismic potential of the Alpine fault, J. Geophys. Res., 104(B11), 25233–25255, doi:10.1029/1999JB900198.

Béjar-Pizarro, M., A. Socquet, R. Armijo, D. Carrizo, J. Genrich, and M. Simons (2013), Andean structural control on interseismic coupling in the North Chile subduction zone, Nature Geosci, 6, 462-467, doi:10.1038/ngeo1802.

Benford, B., C. DeMets, B. Tikoff, P. Williams, L. Brown, and M. Wiggins-Grandison (2012), Seismic hazard along the southern boundary of the Gônave microplate: block modelling of GPS velocities from Jamaica and nearby islands, northern Caribbean, Geophys. J. Int., 190(1), 59–74, doi:10.1111/j.1365-246X.2012.05493.x.

Bennett, R. A., S. Hreinsdóttir, G. Buble, T. Bašić, Ž. Bačić, M. Marjanović, G. Casale, A. Gendaszek, and D. Cowan (2008), Eocene to present subduction of southern Adria mantle lithosphere beneath the Dinarides, Geology, 36(1), 3–6, doi:10.1130/G24136A.1.

Bennett, R. A. et al. (2012), Syn-convergent extension observed using the RETREAT GPS network, northern Apennines, Italy, J. Geophys. Res., 117(B4), B04408, doi:10.1029/2011JB008744.

Le Beon, M. L., Y. Klinger, A. Q. Amrat, A. Agnon, L. Dorbath, G. Baer, J.-C. Ruegg, O. Charade, and O. Mayyas (2008), Slip rate and locking depth from GPS profiles across the southern Dead Sea Transform, J. Geophys. Res., 113(B11), B11403, doi:10.1029/2007JB005280.

Bergeot, N., M. N. Bouin, M. Diament, B. Pelletier, M. Régnier, S. Calmant, and V. Ballu (2009), Horizontal and vertical interseismic velocity fields in the Vanuatu subduction zone from GPS measurements: Evidence for a central Vanuatu locked zone, J. Geophys. Res., 114(B6), B06405, doi:10.1029/2007JB005249.

Bettinelli, P., J.-P. Avouac, M. Flouzat, F. Jouanne, L. Bollinger, P. Willis, and G. Chitrakar (2006), Plate Motion of India and Interseismic Strain in the Nepal Himalaya from GPS and DORIS Measurements, J. Geodesy, 80(8), 567–589, doi:10.1007/s00190-006-0030-3.

Bock, Y., L. Prawirodirdjo, J. F. Genrich, C. W. Stevens, R. McCaffrey, C. Subarya, S. S. O. Puntodewo, and E. Calais (2003), Crustal motion in Indonesia from Global Positioning System measurements, J. Geophys. Res., 108(B8), 2367, doi:10.1029/2001JB000324.

Brooks, B. A., M. Bevis, R. S. Jr, E. Kendrick, R. Manceda, E. Lauría, R. Maturana, and M. Araujo (2003), Crustal motion in the Southern Andes (26°–36°S): Do the Andes behave like a microplate?, Geochem. Geophys. Geosyst., 4(10), 1085, doi:10.1029/2003GC000505.

Calais, E., L. Dong, M. Wang, Z. Shen, and M. Vergnolle (2006), Continental deformation in Asia from a combined GPS solution, Geophys. Res. Lett., 33(24), L24319, doi:10.1029/2006GL028433.

Calais, E., A. Freed, G. Mattioli, F. Amelung, S. Jónsson, P. Jansma, S.-H. Hong, T. Dixon, C. Prépetit, and R. Momplaisir (2010), Transpressional rupture of an unmapped fault during the 2010 Haiti earthquake, Nature Geoscience, 3(11), 794–799, doi:10.1038/ngeo992.

Calmant, S., B. Pelletier, P. Lebellegard, M. Bevis, F. W. Taylor, and D. A. Phillips (2003), New insights on the tectonics along the New Hebrides subduction zone based on GPS results, J. Geophys. Res., 108(B6), 2319, doi:10.1029/2001JB000644.

Caporali, A. et al. (2009), Surface kinematics in the Alpine–Carpathian–Dinaric and Balkan region inferred from a new multi-network GPS combination solution, Tectonophysics, 474(1–2), 295–321, doi:10.1016/j.tecto.2009.04.035.

Cenni, N., E. Mantovani, P. Baldi, and M. Viti (2012), Present kinematics of Central and Northern Italy from continuous GPS measurements, J. Geodyn., 58, 62–72, doi:10.1016/j.jog.2012.02.004.

Chang, W.-L., R. B. Smith, C. M. Meertens, and R. A. Harris (2006), Contemporary deformation of the Wasatch Fault, Utah, from GPS measurements with implications for interseismic fault behavior and earthquake hazard: Observations and kinematic analysis, J. Geophys. Res., 111(B11), B11405, doi:10.1029/2006JB004326.

Ching, K.-E., R.-J. Rau, J.-C. Lee, and J.-C. Hu (2007), Contemporary deformation of tectonic escape in SW Taiwan from GPS observations, 1995–2005, Earth Planet. Sci. Lett., 262(3-4), 601–619, doi:10.1016/j.epsl.2007.08.017.

Ching, K.-E., R.-J. Rau, K. M. Johnson, J.-C. Lee, and J.-C. Hu (2011), Present-day kinematics of active mountain building in Taiwan from GPS observations during 1995–2005, J. Geophys. Res., 116(B9), B09405, doi:10.1029/2010JB008058.

Chlieh, M., H. Perfettini, H. Tavera, J.-P. Avouac, D. Remy, J.-M. Nocquet, F. Rolandone, F. Bondoux, G. Gabalda, and S. Bonvalot (2011), Interseismic coupling and seismic potential along the Central Andes subduction zone, J. Geophys. Res., 116(B12), B12405, doi:10.1029/2010JB008166.

Chousianitis, K., A. Ganas, and M. Gianniou (2013), Kinematic interpretation of present-day crustal deformation in central Greece from continuous GPS measurements, J. Geodyn., 71, 1–13, doi:10.1016/j.jog.2013.06.004.

Clarke, P. J. et al. (1998), Crustal strain in central Greece from repeated GPS measurements in the interval 1989–1997, Geophys. J. Int., 135(1), 195–214, doi:10.1046/j.1365-246X.1998.00633.x.

Cocard, M., H.-G. Kahle, Y. Peter, A. Geiger, G. Veis, S. Felekis, D. Paradissis, and H. Billiris (1999), New constraints on the rapid crustal motion of the Aegean region: recent results inferred from GPS measurements (1993–1998) across the West Hellenic Arc, Greece, Earth Planet. Sci. Lett., 172(1–2), 39–47, doi:10.1016/S0012-821X(99)00185-5.

Correa-Mora, F., C. DeMets, D. Alvarado, H. L. Turner, G. Mattioli, D. Hernandez, C. Pullinger, M. Rodriguez, and C. Tenorio (2009), GPS-derived coupling estimates for the Central America subduction zone and volcanic arc faults: El Salvador, Honduras and Nicaragua, Geophys. J. Int., 179(3), 1279–1291, doi:10.1111/j.1365-246X.2009.04371.x.

Crowell, B. W., Y. Bock, D. T. Sandwell, and Y. Fialko (2013), Geodetic investigation into the deformation of the salton trough, J. Geophys. Res., in press, doi:10.1002/jgrb.50347.

D'Agostino, N., A. Avallone, D. Cheloni, E. D'Anastasio, S. Mantenuto, and G. Selvaggi (2008), Active tectonics of the Adriatic region from GPS and earthquake slip vectors, J. Geophys. Res., 113(B12), B12413, doi:10.1029/2008JB005860.

D'Agostino, N., S. Mantenuto, E. D'Anastasio, R. Giuliani, M. Mattone, S. Calcaterra, P. Gambino, and L. Bonci (2011a), Evidence for localized active extension in the central Apennines (Italy) from global positioning system observations, Geology, 39(4), 291–294, doi:10.1130/G31796.1.

D'Agostino, N., E. D'Anastasio, A. Gervasi, I. Guerra, M. R. Nedimović, L. Seeber, and M. Steckler (2011b), Forearc extension and slow rollback of the Calabrian Arc from GPS measurements, Geophys. Res. Lett., 38(17), L17304, doi:10.1029/2011GL048270.

Darby, D., and J. Beavan (2001), Evidence from GPS measurements for contemporary interplate coupling on the southern Hikurangi subduction thrust and for partitioning of strain in the upper plate, J. Geophys. Res., 106(B12), 30881–30891, doi:10.1029/2000JB000023.

Devoti, R., A. Esposito, G. Pietrantonio, A. R. Pisani, and F. Riguzzi (2011), Evidence of large scale deformation patterns from GPS data in the Italian subduction boundary, Earth and Planetary Science Letters, 311(3–4), 230–241, doi:10.1016/j.epsl.2011.09.034.

Dietrich, R., A. Rülke, J. Ihde, K. Lindner, H. Miller, W. Niemeier, H.-W. Schenke, and G. Seeber (2004), Plate kinematics and deformation status of the Antarctic Peninsula based on GPS, Global and Planetary Change, 42(1–4), 313–321, doi:10.1016/j.gloplacha.2003.12.003.

Djamour, Y. et al. (2010), GPS and gravity constraints on continental deformation in the Alborz mountain range, Iran, Geophys. J. Int., 183(3), 1287–1301, doi:10.1111/j.1365-246X.2010.04811.x.

Djamour, Y., P. Vernant, H. R. Nankali, and F. Tavakoli (2011), NW Iran-eastern Turkey present-day kinematics: Results from the Iranian permanent GPS network, Earth Planet. Sci. Lett., 307(1–2), 27–34, doi:10.1016/j.epsl.2011.04.029.

Drewes, H., and O. Heidbach (2012), The 2009 horizontal velocity field for South America and the Caribbean, in Geodesy for Planet Earth, vol. 136, edited by S. Kenyon, M. C. Pacino, and U. Marti, pp. 657–664, Springer Berlin Heidelberg.

Duquesnoy, T., M. Kasser, M. Aurelio, R. Gaulon, R. S. Punongbayan, and C. Rangin (1994), Detection of creep along the Philippine Fault: First results of geodetic measurements on Leyte Island, central Philippine, Geophys. Res. Lett., 21(11), 975–978, doi:10.1029/94GL00640.

Echeverria, A., G. Khazaradze, E. Asensio, J. Gárate, J. M. Dávila, and E. Suriñach (2013), Crustal deformation in eastern Betics from CuaTeNeo GPS network, Tectonophysics, in press, doi:10.1016/j.tecto.2013.08.020.

Elliott, J. L., C. F. Larsen, J. T. Freymueller, and R. J. Motyka (2010), Tectonic block motion and glacial isostatic adjustment in southeast Alaska and adjacent Canada constrained by GPS measurements, J. Geophys. Res., 115(B9), B09407, doi:10.1029/2009JB007139.

Elliott, J., J. T. Freymueller, and C. F. Larsen (2013), Active tectonics of the St. Elias Orogen, Alaska, observed with GPS measurements, J. Geophys. Res., in press, doi:10.1002/jgrb.50341.

Feng, L., A. V. Newman, M. Protti, V. González, Y. Jiang, and T. H. Dixon (2012), Active deformation near the Nicoya Peninsula, northwestern Costa Rica, between 1996 and 2010: Interseismic megathrust coupling, J. Geophys. Res., 117(B6), B06407, doi:10.1029/2012JB009230.

Fernandes, R. M. S., L. Bastos, B. A. C. Ambrosius, R. Noomen, S. Matheussen, and P. Baptista (2004), Recent geodetic results in the Azores triple junction region, Pure Appl. Geoph., 161(3), 683–699, doi:10.1007/s00024-003-2469-y.

Fernandes, R. M. S., J. M. Miranda, D. Delvaux, D. S. Stamps, and E. Saria (2013), Re-evaluation of the kinematics of Victoria Block using continuous GNSS data, Geophys. J. Int., 193(1), 1–10, doi:10.1093/gji/ggs071.

Floyd, M. A. et al. (2010), A new velocity field for Greece: Implications for the kinematics and dynamics of the Aegean, J. Geophys. Res., 115(B10), B10403, doi:10.1029/2009JB007040.

Franco, A. et al. (2012), Fault kinematics in northern Central America and coupling along the subduction interface of the Cocos Plate, from GPS data in Chiapas (Mexico), Guatemala and El Salvador, Geophys. J. Int., 189(3), 1223–1236, doi:10.1111/j.1365-246X.2012.05390.x.

Freymueller, J. T., M. H. Murray, P. Segall, and D. Castillo (1999), Kinematics of the Pacific-North America plate boundary zone, northern California, J. Geophys. Res., 104(B4), 7419–7441, doi:10.1029/1998JB900118.

Freymueller, J. T., H. Woodard, S. C. Cohen, R. Cross, J. Elliott, C. F. Larsen, S. Hreinsdóttir, and C. Zweck (2008), Active deformation processes in Alaska, based on 15 years of GPS measurements, in Geophysical Monograph Series, vol. 179, edited by J. T. Freymueller, P. J. Haeussler, R. L. Wesson, and G. Ekström, pp. 1–42, American Geophysical Union, Washington, D. C.

Gahalaut, V. K. et al. (2013), Aseismic plate boundary in the Indo-Burmese wedge, northwest Sunda Arc, Geology, 41(2), 235–238, doi:10.1130/G33771.1.

Galgana, G., M. Hamburger, R. McCaffrey, E. Corpuz, and Q. Chen (2007), Analysis of crustal deformation in Luzon, Philippines using geodetic observations and earthquake focal mechanisms, Tectonophysics, 432(1–4), 63–87, doi:10.1016/j.tecto.2006.12.001.

Genrich, J. F., Y. Bock, R. McCaffrey, L. Prawirodirdjo, C. W. Stevens, S. S. O. Puntodewo, C. Subarya, and S. Wdowinski (2000), Distribution of slip at the northern Sumatran fault system, J. Geophys. Res., 105(B12), 28327–28341, doi:10.1029/2000JB900158.

Giuliani, R. ; D. P. C., N. ; I. N. D. G. E. V. D'Agostino, E. ; I. N. D. G. E. V. D'Anastasio, M. ; D. P. C. Mattone, L. ; I. Bonci, S. ; I. Calcaterra, P. ; I. Gambino, and K. ; I. Merli (2009), Active crustal extension and strain accumulation from GPS data in the Molise region (central-southern Apennines, Italy), Bollettino di Geofisica Teorica ed Applicata, 50, 145–156.

Gomez, F., G. Karam, M. Khawlie, S. McClusky, P. Vernant, R. Reilinger, R. Jaafar, C. Tabet, K. Khair, and M. Barazangi (2007), Global Positioning System measurements of strain accumulation and slip transfer through the restraining bend along the Dead Sea fault system in Lebanon, Geophys. J. Int., 168(3), 1021–1028, doi:10.1111/j.1365-246X.2006.03328.x.

Hammond, W. C., and W. Thatcher (2004), Contemporary tectonic deformation of the Basin and Range province, western United States: 10 years of observation with the Global Positioning System, J. Geophys. Res., 109(B8), B08403, doi:B08403, 10.1029/2003JB002746.

Hammond, W. C., and W. Thatcher (2005), Northwest Basin and Range tectonic deformation observed with the Global Positioning System, 1999–2003, J. Geophys. Res., 110(B10), B10405, doi:B10405, 10.1029/2005JB003678.

Hammond, W. C., and W. Thatcher (2007), Crustal deformation across the Sierra Nevada, northern Walker Lane, Basin and Range transition, western United States measured with GPS, 2000–2004, J. Geophys. Res., 112(B5), B05411, doi:B05411, 10.1029/2006JB004625.

Hashimoto, C., A. Noda, T. Sagiya, and M. Matsu'ura (2009), Interplate seismogenic zones along the Kuril–Japan trench inferred from GPS data inversion, Nature Geoscience, 2(2), 141–144, doi:10.1038/ngeo421.

Hessami, K., F. Nilforoushan, and C. J. Talbot (2006), Active deformation within the Zagros Mountains deduced from GPS measurements, J. Geol. Soc., 163(1), 143–148, doi:10.1144/0016-764905-031.

Hilley, G. E., K. M. Johnson, M. Wang, Z.-K. Shen, and R. Bürgmann (2009), Earthquake-cycle deformation and fault slip rates in northern Tibet, Geology, 37(1), 31–34, doi:10.1130/G25157A.1.

Van der Hoeven, A. G. A., V. Mocanu, W. Spakman, M. Nutto, A. Nuckelt, L. Matenco, L. Munteanu, C. Marcu, and B. A. C. Ambrosius (2005), Observation of present-day tectonic motions in the Southeastern Carpathians: Results of the ISES/CRC-461 GPS measurements, Earth Planet. Sci. Lett., 239(3–4), 177–184, doi:10.1016/j.epsl.2005.09.018.

Hollenstein, C., H.-G. Kahle, A. Geiger, S. Jenny, S. Goes, and D. Giardini (2003), New GPS constraints on the Africa-Eurasia plate boundary zone in southern Italy, Geophys. Res. Lett., 30(18), 1935, doi:10.1029/2003GL017554.

Hreinsdóttir, S., P. Einarsson, and F. Sigmundsson (2001), Crustal deformation at the oblique spreading Reykjanes Peninsula, SW Iceland: GPS measurements from 1993 to 1998, J. Geophys. Res., 106(B7), 13803–13,816, doi:10.1029/2001JB000428.

Hsu, Y.-J., S.-B. Yu, M. Simons, L.-C. Kuo, and H.-Y. Chen (2009), Interseismic crustal deformation in the Taiwan plate boundary zone revealed by GPS observations, seismicity, and earthquake focal mechanisms, Tectonophysics, 479(1–2), 4–18, doi:10.1016/j.tecto.2008.11.016.

Hsu, Y.-J., M. Ando, S.-B. Yu, and M. Simons (2012), The potential for a great earthquake along the southernmost Ryukyu subduction zone, Geophys. Res. Lett., 39(14), L14302, doi:10.1029/2012GL052764.

Hu, J.-C. et al. (2007), Fault activity and lateral extrusion inferred from velocity field revealed by GPS measurements in the Pingtung area of southwestern Taiwan, J. Asian Earth Sci., 31(3), 287–302, doi:10.1016/j.jseaes.2006.07.020.

Ihemedu, D. K. (2012), An updated GPS velocity field for Puerto Rico and Virgin Islands: Constraints on tectonic setting and internal deformation, M.S. Thesis, University of Texas, Arlington.

Iinuma, T., M. Protti, K. Obana, V. González, R. Van der Laat, T. Kato, S. Miyazaki, Y. Kaneda, and E. Hernández (2004), Inter-plate coupling in the Nicoya Peninsula, Costa Rica, as deduced from a trans-peninsula GPS experiment, Earth Planet. Sci. Lett., 223(1–2), 203–212, doi:10.1016/j.epsl.2004.04.016.

Ischuk, A. et al. (2013), Kinematics of the Pamir and Hindu Kush regions from GPS geodesy, J. Geophys. Res., in press, doi:10.1002/jgrb.50185.

Jade, S. et al. (2007), Estimates of interseismic deformation in Northeast India from GPS measurements, Earth and Planetary Science Letters, 263(3–4), 221–234, doi:10.1016/j.epsl.2007.08.031.

Jansma, P. E., and G. S. Mattioli (2005), GPS results from Puerto Rico and the Virgin Islands: Constraints on tectonic setting and rates of active faulting, edited by P. Mann, Geol. Soc. Am. Special Papers, 385, 13–30, doi:10.1130/0-8137-2385-X.13.

Jiang, W.-P., D.-C. E, B.-W. Zhan, and Y.-W. Liu (2009), New model of Antarctic plate motion and its analysis, Chin. j. Geophys., 52(1), 23–32.

Jin, S., Z. Li, and P.-H. Park (2006), Seismicity and GPS constraints on crustal deformation in the southern part of the Korean Peninsula, Geosciences Journal, 10(4), 491–497, doi:10.1007/BF02910442.

Jouanne, F., F. A. Audemard, C. Beck, A. Van Welden, R. Ollarves, and C. Reinoza (2011), Present-day deformation along the El Pilar Fault in eastern Venezuela: Evidence of creep along a major transform boundary, J. Geodyn., 51(5), 398–410, doi:10.1016/j.jog.2010.11.003.

Jouanne, F., J. L. Mugnier, R. Koci, S. Bushati, K. Matev, N. Kuka, I. Shinko, S. Kociu, and L. Duni (2012), GPS constraints on current tectonics of Albania, Tectonophysics, 554–557, 50–62, doi:10.1016/j.tecto.2012.06.008.

Kadirov, F., M. Floyd, A. Alizadeh, I. Guliev, R. Reilinger, S. Kuleli, R. King, and M.N. Toksoz (2012), Kinematics of the eastern Caucasus near Baku, Azerbaijan, Natural Hazards, 63(2), 997–1006, doi:10.1007/s11069-012-0199-0.

Karakhanyan, A. et al. (2013), GPS constraints on continental deformation in the Armenian region and Lesser Caucasus, Tectonophysics, 592, 39–45, doi:10.1016/j.tecto.2013.02.002.

Kato, T., J. Beavan, T. Matsushima, Y. Kotake, J. T. Camacho, and S. Nakao (2003), Geodetic evidence of back-arc spreading in the Mariana Trough, Geophys. Res. Lett., 30(12), 1625, doi:10.1029/2002GL016757.

Keiding, M., T. Árnadóttir, E. Sturkell, H. Geirsson, and B. Lund (2008), Strain accumulation along an oblique plate boundary: the Reykjanes Peninsula, southwest Iceland, Geophys. J. Int., 172(2), 861–872, doi:10.1111/j.1365-246X.2007.03655.x.

Kendrick, E., M. Bevis, R. Smalley Jr., B. Brooks, R. B. Vargas, E. Lauría, and L. P. S. Fortes (2003), The Nazca–South America Euler vector and its rate of change, J. South Am. Earth Sci., 16(2), 125–131, doi:10.1016/S0895-9811(03)00028-2.

Khazaradze, G., and J. Klotz (2003), Short- and long-term effects of GPS measured crustal deformation rates along the south central Andes, J. Geophys. Res., 108(B6), 2289, doi:10.1029/2002JB001879.

Kierulf, H. P., M. Ouassou, M. J. R. Simpson, and O. Vestøl (2013), A continuous velocity field for Norway, J Geod, 87(4), 337–349, doi:10.1007/s00190-012-0603-2.

Klotz, J., G. Khazaradze, D. Angermann, C. Reigber, R. Perdomo, and O. Cifuentes (2001), Earthquake cycle dominates contemporary crustal deformation in Central and Southern Andes, Earth Planet. Sci. Lett., 193(3–4), 437–446, doi:10.1016/S0012-821X(01)00532-5.

Kogan, L., S. Fisseha, R. Bendick, R. Reilinger, S. McClusky, R. King, and T. Solomon (2012), Lithospheric strength and strain localization in continental extension from observations of the East African Rift, J. Geophys. Res., 117(B3), B03402, doi:10.1029/2011JB008516.

Kotzev, V., R. Nakov, T. Georgiev, B. C. Burchfiel, and R. W. King (2006), Crustal motion and strain accumulation in western Bulgaria, Tectonophysics, 413(3–4), 127–145, doi:10.1016/j.tecto.2005.10.040.

Koulali, A., D. Ouazar, A. Tahayt, R. W. King, P. Vernant, R. E. Reilinger, S. McClusky, T. Mourabit, J. M. Davila, and N. Amraoui (2011), New GPS constraints on active deformation along the Africa–Iberia plate boundary, Earth Planet. Sci. Lett., 308(1–2), 211–217, doi:10.1016/j.epsl.2011.05.048.

LaFemina, P., T. H. Dixon, R. Govers, E. Norabuena, H. Turner, A. Saballos, G. Mattioli, M. Protti, and W. Strauch (2009), Fore-arc motion and Cocos Ridge collision in Central America, Geochem. Geophys. Geosyst., 10(5), Q05S14, doi:10.1029/2008GC002181.

LaFemina, P. C., T. H. Dixon, R. Malservisi, T. Árnadóttir, E. Sturkell, F. Sigmundsson, and P. Einarsson (2005), Geodetic GPS measurements in south Iceland: Strain accumulation and partitioning in a propagating ridge system, J. Geophys. Res., 110(B11), B11405, doi:10.1029/2005JB003675.

Lidberg, M., J. M. Johansson, H.-G. Scherneck, and G. A. Milne (2010), Recent results based on continuous GPS observations of the GIA process in Fennoscandia from BIFROST, J. Geodyn., 50(1), 8–18, doi:10.1016/j.jog.2009.11.010.

Liu, Z., S. Owen, D. Dong, P. Lundgren, F. Webb, E. Hetland, and M. Simons (2010), Estimation of interplate coupling in the Nankai trough, Japan using GPS data from 1996 to 2006, Geophys. J. Int., 181(3), 1313–1328, doi:10.1111/j.1365-246X.2010.04600.x.

López, A. M., S. Stein, T. Dixon, G. Sella, E. Calais, P. Jansma, J. Weber, and P. LaFemina (2006), Is there a northern Lesser Antilles forearc block?, Geophys. Res. Lett., 33(7), L07313, doi:10.1029/2005GL025293.

Lukhnev, A. V., V. A. San'kov, A. I. Miroshnichenko, S. V. Ashurkov, and E. Calais (2010), GPS rotation and strain rates in the Baikal–Mongolia region, Russian Geology and Geophysics, 51(7), 785–793, doi:10.1016/j.rgg.2010.06.006.

Mahanta, K., J. D. Chowdhury, A. Kumar, I. Laskar, S. L. Singh, and P. Barman (2012), Earthquakes and crustal deformation studies of the seismically active Kopili Fault as well as North East India: A scientific field study using Global Positioning System (GPS), The Clarion, 1(1), 51–58.

Mahesh, P. et al. (2012), Rigid Indian plate: Constraints from GPS measurements, Gondwana Research, 22(3–4), 1068–1072, doi:10.1016/j.gr.2012.01.011.

Mahmoud, Y., F. Masson, M. Meghraoui, Z. Cakir, A. Alchalbi, H. Yavasoglu, O. Yönlü, M. Daoud, S. Ergintav, and S. Inan (2013), Kinematic study at the junction of the East Anatolian fault and the Dead Sea fault from GPS measurements, J. Geodyn., 67, 30–39, doi:10.1016/j.jog.2012.05.006.

Manaker, D. M., E. Calais, A. M. Freed, S. T. Ali, P. Przybylski, G. Mattioli, P. Jansma, C. Prépetit, and J. B. De Chabalier (2008), Interseismic Plate coupling and strain partitioning in the Northeastern Caribbean, Geophys. J. Int., 174(3), 889–903, doi:10.1111/j.1365-246X.2008.03819.x.

Marjanović, M., Ž. Bačić, and T. Bašić (2012), Determination of horizontal and vertical movements of the Adriatic microplate on the basis of GPS measurements, in Geodesy for Planet Earth, vol. 136, edited by S. Kenyon, M. C. Pacino, and U. Marti, pp. 683–688, Springer Berlin Heidelberg.

Márquez-Azúa, B., and C. DeMets (2003), Crustal velocity field of Mexico from continuous GPS measurements, 1993 to June 2001: Implications for the neotectonics of Mexico, J. Geophys. Res., 108(B9), 2450, doi:10.1029/2002JB002241.

Márquez-Azúa, B., and C. DeMets (2009), Deformation of Mexico from continuous GPS from 1993 to 2008, Geochemistry, Geophysics, Geosystems, 10(2), Q02003, doi:10.1029/2008GC002278.

Matev, K. (2011), GPS constraints on current tectonics of southwest Bulgaria, northern Greece, and Albania, Ph.D. Thesis, Université de Grenoble.

Matson, S. E. (2007), Arc kinematics of the Northern Lesser Antilles from GPS geodesy, M.S., University of Arkansas.

Mattia, M., M. Palano, V. Bruno, and F. Cannavò (2009), Crustal motion along the Calabro-Peloritano Arc as imaged by twelve years of measurements on a dense GPS network, Tectonophysics, 476(3–4), 528–537, doi:10.1016/j.tecto.2009.06.006.

Mattia, M., V. Bruno, F. Cannavò, and M. Palano (2012), Evidences of a contractional pattern along the northern rim of the Hyblean Plateau (Sicily, Italy) from GPS data, Geologica Acta, 10(1), 63–70.

Maurin, T., F. Masson, C. Rangin, U. T. Min, and P. Collard (2010), First global positioning system results in northern Myanmar: Constant and localized slip rate along the Sagaing fault, Geology, 38(7), 591–594, doi:10.1130/G30872.1.

Mazzotti, S., T. S. James, J. Henton, and J. Adams (2005), GPS crustal strain, postglacial rebound, and seismic hazard in eastern North America: The Saint Lawrence valley example, J. Geophys. Res., 110(B11), B11301, doi:10.1029/2004JB003590.

Mazzotti, S., L. J. Leonard, J. F. Cassidy, G. C. Rogers, and S. Halchuk (2011), Seismic hazard in western Canada from GPS strain rates versus earthquake catalog, J. Geophys. Res., 116(B12), B12310, doi:10.1029/2011JB008213.

McCaffrey, R., R. W. King, S. J. Payne, and M. Lancaster (2013), Active tectonics of northwestern U.S. inferred from GPS-derived surface velocities, J. Geophys. Res., 118, doi:10.1029/2012JB009473.

McClusky, S. et al. (2010), Kinematics of the southern Red Sea–Afar Triple Junction and implications for plate dynamics, Geophys. Res. Lett., 37(5), L05301, doi:10.1029/2009GL041127.

Medak, D., and B. Pribicevic (2006), Processing of geodynamic GPS neworks in Croatia with GAMIT software, in The Adriatic Microplate: GPS Geodesy, Tectonics and Hazards, vol. 61, edited by N. Pinter et al., pp. 247–256, Springer.

Meilano, I. et al. (2012), Slip rate estimation of the Lembang Fault West Java from geodetic observation, Journal of Disaster Research, 7(1), 12–18.

Mendes, V. B., J. Madeira, A. Brum da Silveira, A. Trota, P. Elosegui, and J. Pagarete (2013), Present-day deformation in São Jorge Island, Azores, from episodic GPS measurements (2001–2011), Adv. Space Res., 51(8), 1581–1592, doi:10.1016/j.asr.2012.10.019.

Mendoza, L., R. Perdomo, J. L. Hormaechea, D. D. Cogliano, M. Fritsche, A. Richter, and R. Dietrich (2011), Present-day crustal deformation along the Magallanes–Fagnano Fault System in Tierra del Fuego from repeated GPS observations, Geophys. J. Int., 184(3), 1009–1022, doi:10.1111/j.1365-246X.2010.04912.x.

Meng, G. J., X. H. Shen, S. Vladimir, A. R. Eugene, and J. C. Wu (2009), Research on characteristics of present-day crustal motion and deformation in Kamchatka area, Chin. J. Geophys., 52(3), 720–731.

Métois, M., A. Socquet, and C. Vigny (2012), Interseismic coupling, segmentation and mechanical behavior of the central Chile subduction zone, J. Geophys. Res., 117(B3), B03406, doi:10.1029/2011JB008736.

Metzger, S., S. Jónsson, G. Danielsen, S. Hreinsdóttir, F. Jouanne, D. Giardini, and T. Villemin (2013), Present kinematics of the Tjörnes Fracture Zone, North Iceland, from campaign and continuous GPS measurements, Geophys. J. Int., 192(2), 441–455, doi:10.1093/gji/ggs032.

Miranda, J. M., A. Navarro, J. Catalão, and R. M. S. Fernandes (2012), Surface displacement field at Terceira island deduced from repeated GPS measurements, J. Volc. Geoth. Res., 217–218, 1–7, doi:10.1016/j.jvolgeores.2011.10.009.

Moreno, M. et al. (2011), Heterogeneous plate locking in the South–Central Chile subduction zone: Building up the next great earthquake, Earth Planet. Sci. Lett., 305(3–4), 413–424, doi:10.1016/j.epsl.2011.03.025.

Mousavi, Z., A. Walpersdorf, R. T. Walker, F. Tavakoli, E. Pathier, H. Nankali, F. Nilfouroushan, and Y. Djamour (2013), Global Positioning System constraints on the active tectonics of NE Iran and the South Caspian region, Earth Planet. Sci. Lett., 377–378, 287–298, doi:10.1016/j.epsl.2013.07.007.

Mukul, M., S. Jade, A. Bhattacharyya, and K. Bhusan (2010), Crustal shortening in convergent orogens: Insights from global positioning system (GPS) measurements in northeast India, J. Geol. Soc. India, 75(1), 302–312, doi:10.1007/s12594-010-0017-9.

Müller, M. D., A. Geiger, H.-G. Kahle, G. Veis, H. Billiris, D. Paradissis, and S. Felekis (2013), Velocity and deformation fields in the North Aegean domain, Greece, and implications for fault kinematics, derived from GPS data 1993–2009, Tectonophysics, 597-598, 34-49, doi:10.1016/j.tecto.2012.08.003.

Mullick, M., F. Riguzzi, and D. Mukhopadhyay (2009), Estimates of motion and strain rates across active faults in the frontal part of eastern Himalayas in North Bengal from GPS measurements, Terra Nova, 21(5), 410–415, doi:10.1111/j.1365-3121.2009.00898.x.

Nishimura, T. (2011), Back-arc spreading of the northern Izu–Ogasawara (Bonin) Islands arc clarified by GPS data, Tectonophysics, 512(1–4), 60–67, doi:10.1016/j.tecto.2011.09.022.

Nugroho, H., R. Harris, A. W. Lestariya, and B. Maruf (2009), Plate boundary reorganization in the active Banda Arc–continent collision: Insights from new GPS measurements, Tectonophysics, 479(1–2), 52–65, doi:10.1016/j.tecto.2009.01.026.

Ohzono, M., T. Sagiya, K. Hirahara, M. Hashimoto, A. Takeuchi, Y. Hoso, Y. Wada, K. Onoue, F. Ohya, and R. Doke (2011), Strain accumulation process around the Atotsugawa fault system in the Niigata-Kobe Tectonic Zone, central Japan, Geophys. J. Int., 184(3), 977–990, doi:10.1111/j.1365-246X.2010.04876.x.

Ozener, H., O. Yilmaz, A. Dogru, B. Turgut, and O. Gurkan (2013a), GPS-derived velocity field of the Iznik-Mekece segment of the North Anatolian Fault Zone, J. Geodyn., 67, 46–52, doi:10.1016/j.jog.2012.07.001.

Ozener, H., A. Dogru, and B. Turgut (2013b), Quantifying aseismic creep on the Ismetpasa segment of the North Anatolian Fault Zone (Turkey) by 6 years of GPS observations, J. Geodyn., 67, 72–77, doi:10.1016/j.jog.2012.08.002.

Palano, M., L. Ferranti, C. Monaco, M. Mattia, M. Aloisi, V. Bruno, F. Cannavò, and G. Siligato (2012), GPS velocity and strain fields in Sicily and southern Calabria, Italy: Updated geodetic constraints on tectonic block interaction in the central Mediterranean, J. Geophys. Res., 117(B7), B07401, doi:10.1029/2012JB009254.

Pérez, O. J., R. Bilham, R. Bendick, J. R. Velandia, N. Hernández, C. Moncayo, M. Hoyer, and M. Kozuch (2001), Velocity field across the southern Caribbean plate boundary and estimates of Caribbean/South-American plate motion using GPS geodesy 1994–2000, Geophys. Res. Lett., 28(15), 2987–2990, doi:10.1029/2001GL013183.

Pérez, O. J. et al. (2011), GPS derived velocity field in western Venezuela: dextral shear component associated to the Bocono fault and convergent component normal to the Andes, Interciencia, 36(1), 39(6).

Pérez-Peña, A., J. Martín-Davila, J. Gárate, M. Berrocoso, and E. Buforn (2010), Velocity field and tectonic strain in Southern Spain and surrounding areas derived from GPS episodic measurements, J. Geodyn., 49(3–4), 232–240, doi:10.1016/j.jog.2010.01.015.

Pesci, A., G. Teza, G. Casula, N. Cenni, and F. Loddo (2010), Non-permanent GPS data for regional-scale kinematics: reliable deformation rate before the 6 April, 2009, earthquake in the L'Aquila area, Annals of Geophysics, 53(2), 55–68, doi:10.4401/ag-4740.

Peyret, M. et al. (2009), Present-day strain distribution across the Minab-Zendan-Palami fault system from dense GPS transects, Geophys. J. Int., 179(2), 751–762, doi:10.1111/j.1365-246X.2009.04321.x.

Phillips, D. A. (2003), Crustal motion studies in the Southwest Pacific: Geodetic measurements of plate convergence in Tonga, Vanuatu and the Solomon Islands, Ph.D. Thesis, University of Hawaii at Manoa.

Plattner, C., R. Malservisi, T. H. Dixon, P. LaFemina, G. F. Sella, J. Fletcher, and F. Suarez-Vidal (2007), New constraints on relative motion between the Pacific Plate and Baja California microplate (Mexico) from GPS measurements, Geophys. J. Int., 170(3), 1373–1380, doi:10.1111/j.1365-246X.2007.03494.x.

Poland, M., R. Bürgmann, D. Dzurisin, M. Lisowski, T. Masterlark, S. Owen, and J. Fink (2006), Constraints on the mechanism of long-term, steady subsidence at Medicine Lake volcano, northern California, from GPS, leveling, and InSAR, J. Volc. Geoth. Res., 150, 55–78, doi:10.1016/j.jvolgeores.2005.07.007.

Ponraj, M., S. Miura, C. D. Reddy, S. K. Prajapati, S. Amirtharaj, and S. H. Mahajan (2010), Estimation of strain distribution using GPS measurements in the Kumaun region of Lesser Himalaya, J. Asian Earth Sci., 39(6), 658–667, doi:10.1016/j.jseaes.2010.04.037.

Prawirodirdjo, L., R. McCaffrey, C. D. Chadwell, Y. Bock, and C. Subarya (2010), Geodetic observations of an earthquake cycle at the Sumatra subduction zone: Role of interseismic strain segmentation, J. Geophys. Res., 115(B3), B03414, doi:10.1029/2008JB006139.

Protti, M., V. González, J. Freymueller, and S. Doelger (2012), Isla del Coco, on Cocos Plate, converges with Isla de San Andrés, on the Caribbean Plate, at 78mm/yr, Revista de Biología Tropical, 60, 33–41.

Reilinger, R., and S. McClusky (2011), Nubia–Arabia–Eurasia plate motions and the dynamics of Mediterranean and Middle East tectonics, Geophys. J. Int., 186(3), 971–979, doi:10.1111/j.1365-246X.2011.05133.x.

Reilinger, R. et al. (2006), GPS constraints on continental deformation in the Africa-Arabia-Eurasia continental collision zone and implications for the dynamics of plate interactions, J. Geophys. Res., 111(B5), B05411, doi:10.1029/2005JB004051.

Rodriguez, A. (2007), Global Positioning System (GPS) determination of motions, neotectonics, and seismic hazard in Trinidad and Tobago, M.S. Thesis, Grand Valley State University.

Rodriguez, M., C. DeMets, R. Rogers, C. Tenorio, and D. Hernandez (2009), A GPS and modelling study of deformation in northern Central America, Geophys. J. Int., 178(3), 1733–1754, doi:10.1111/j.1365-246X.2009.04251.x.

Rontogianni, S. (2010), Comparison of geodetic and seismic strain rates in Greece by using a uniform processing approach to campaign GPS measurements over the interval 1994–2000, J. Geodyn., 50(5), 381–399, doi:10.1016/j.jog.2010.04.008.

Ruegg, J. C., A. Rudloff, C. Vigny, R. Madariaga, J. B. de Chabalier, J. Campos, E. Kausel, S. Barrientos, and D. Dimitrov (2009), Interseismic strain accumulation measured by GPS in the seismic gap between Constitución and Concepción in Chile, Phys. Earth. Planet. Int., 175(1–2), 78–85, doi:10.1016/j.pepi.2008.02.015.

Sadeh, M., Y. Hamiel, A. Ziv, Y. Bock, P. Fang, and S. Wdowinski (2012), Crustal deformation along the Dead Sea Transform and the Carmel Fault inferred from 12 years of GPS measurements, J. Geophys. Res., 117(B8), B08410, doi:10.1029/2012JB009241.

Sagiya, T., S. Miyazaki, and T. Tada (2000), Continuous GPS array and present-day crustal deformation of Japan, Pure Appl. Geophys., 157(11-12), 2303–2322, doi:10.1007/PL00022507.

Saria, E., E. Calais, Z. Altamimi, P. Willis, and H. Farah (2013), A new velocity field for Africa from combined GPS and DORIS space geodetic solutions: contribution to the definition of the African Reference Frame (AFREF), J. Geophys. Res., in press, doi:10.1002/jgrb.50137.

Sato, M., M. Fujita, Y. Matsumoto, T. Ishikawa, H. Saito, M. Mochizuki, and A. Asada (2013), Interplate coupling off northeastern Japan before the 2011 Tohoku-oki earthquake, inferred from seafloor geodetic data, J. Geophys. Res., in press, doi:10.1002/jgrb.50275.

Scheiber-Enslin, S. E., P. C. LaFemina, E. Sturkell, A. J. Hooper, and S. J. Webb (2011), Geodetic investigation of plate spreading along a propagating ridge: the Eastern Volcanic Zone, Iceland, Geophys. J. Int., 187(3), 1175–1194, doi:10.1111/j.1365-246X.2011.05243.x.

Serpelloni, E., G. Vannucci, S. Pondrelli, A. Argnani, G. Casula, M. Anzidei, P. Baldi, and P. Gasperini (2007), Kinematics of the Western Africa-Eurasia plate boundary from focal mechanisms and GPS data, Geophys. J. Int., 169(3), 1180–1200, doi:10.1111/j.1365-246X.2007.03367.x.

Serpelloni, E., R. Bürgmann, M. Anzidei, P. Baldi, B. Mastrolembo Ventura, and E. Boschi (2010), Strain accumulation across the Messina Straits and kinematics of Sicily and Calabria from GPS data and dislocation modeling, Earth Planet. Sci. Lett., 298(3–4), 347–360, doi:10.1016/j.epsl.2010.08.005.

Shen, Z.-K., R. W. King, D. C. Agnew, M. Wang, T. A. Herring, D. Dong, and P. Fang (2011), A unified analysis of crustal motion in Southern California, 1970–2004: The SCEC crustal motion map, J. Geophys. Res., 116(B11), B11402, doi:10.1029/2011JB008549.

Shestakov, N. V. et al. (2011), Present tectonics of the southeast of Russia as seen from GPS observations, Geophys. J. Int., 184(2), 529–540, doi:10.1111/j.1365-246X.2010.04871.x.

Shin, T.-C., K.-W. Kuo, P.-L. Leu, C.-H. Tsai, and J.-S. Jiang (2011), Continuous CWB GPS array in Taiwan and applications to monitoring seismic activity, Terr. Atmos. Ocean. Sci., 22(5), 521, doi:10.3319/TAO.2011.05.18.01(T).

Simons, W. J. F. et al. (2007), A decade of GPS in Southeast Asia: Resolving Sundaland motion and boundaries, J. Geophys. Res., 112(B6), B06420, doi:10.1029/2005JB003868.

Smalley, R., E. Kendrick, M. G. Bevis, I. W. D. Dalziel, F. Taylor, E. Lauría, R. Barriga, G. Casassa, E. Olivero, and E. Piana (2003), Geodetic determination of relative plate motion and crustal deformation across the Scotia-South America plate boundary in eastern Tierra del Fuego, Geochem. Geophys. Geosyst., 4(9), 1070, doi:10.1029/2002GC000446.

Smalley, R., I. W. D. Dalziel, M. G. Bevis, E. Kendrick, D. S. Stamps, E. C. King, F. W. Taylor, E. Lauría, A. Zakrajsek, and H. Parra (2007), Scotia arc kinematics from GPS geodesy, Geophys. Res. Lett., 34(21), L21308, doi:10.1029/2007GL031699.

Socquet, A., W. Simons, C. Vigny, R. McCaffrey, C. Subarya, D. Sarsito, B. Ambrosius, and W. Spakman (2006), Microblock rotations and fault coupling in SE Asia triple junction (Sulawesi, Indonesia) from GPS and earthquake slip vector data, J. Geophys. Res., 111(B8), B08409, doi:10.1029/2005JB003963.

Sol, S. et al. (2007), Geodynamics of the southeastern Tibetan Plateau from seismic anisotropy and geodesy, Geology, 35(6), 563–566, doi:10.1130/G23408A.1.

Spinler, J. C., R. A. Bennett, M. L. Anderson, S. F. McGill, S. Hreinsdóttir, and A. McCallister (2010), Present-day strain accumulation and slip rates associated with southern San Andreas and eastern California shear zone faults, J. Geophys. Res., 115(B11), B11407, doi:10.1029/2010JB007424.

Stamps, D. S., E. Calais, E. Saria, C. Hartnady, J.-M. Nocquet, C. J. Ebinger, and R. M. Fernandes (2008), A kinematic model for the East African Rift, Geophys. Res. Lett., 35(5), L05304, doi:10.1029/2007GL032781.

Stevens, C. W., R. McCaffrey, Y. Bock, J. F. Genrich, M. Pubellier, and C. Subarya (2002), Evidence for block rotations and basal shear in the world's fastest slipping continental shear zone in NW New Guinea, Geodyn. Ser., 30, 87–99, doi:10.1029/GD030p0087.

Svarc, J. L., J. C. Savage, W. H. Prescott, and A. R. Ramelli (2002), Strain accumulation and rotation in western Nevada, 1993–2000, J. Geophys. Res., 107(B5), 2090, doi:2090, 10.1029/2001JB000579.

Szeliga, W., R. Bilham, D. M. Kakar, and S. H. Lodi (2012), Interseismic strain accumulation along the western boundary of the Indian subcontinent, J. Geophys. Res., 117(B8), B08404, doi:10.1029/2011JB008822.

Tadokoro, K., R. Ikuta, T. Watanabe, M. Ando, T. Okuda, S. Nagai, K. Yasuda, and T. Sakata (2012), Interseismic seafloor crustal deformation immediately above the source region of anticipated megathrust earthquake along the Nankai Trough, Japan, Geophys. Res. Lett., 39(10), L10306, doi:10.1029/2012GL051696.

Al Tarazi, E. al, J. A. Rajab, F. Gomez, W. Cochran, R. Jaafar, and M. Ferry (2011), GPS measurements of near-field deformation along the southern Dead Sea Fault System, Geochem. Geophys. Geosyst., 12(12), Q12021, doi:10.1029/2011GC003736.

Tatar, O. et al. (2012), Crustal deformation and kinematics of the Eastern Part of the North Anatolian Fault Zone (Turkey) from GPS measurements, Tectonophysics, 518–521, 55–62, doi:10.1016/j.tecto.2011.11.010.

Tavakoli, F., A. Walpersdorf, C. Authemayou, H. R. Nankali, D. Hatzfeld, M. Tatar, Y. Djamour, F. Nilforoushan, and N. Cotte (2008), Distribution of the right-lateral strike–slip motion from the Main Recent Fault to the Kazerun Fault System (Zagros, Iran): Evidence from present-day GPS velocities, Earth Planet. Sci. Lett., 275(3–4), 342–347, doi:10.1016/j.epsl.2008.08.030.

Taylor, F. W., M. G. Bevis, I. W. D. Dalziel, R. S. Jr, C. Frohlich, E. Kendrick, J. Foster, D. Phillips, and K. Gudipati (2008), Kinematics and segmentation of the South Shetland Islands-Bransfield basin system, northern Antarctic Peninsula, Geochem. Geophys. Geosyst., 9(4), Q04035, doi:10.1029/2007GC001873.

Tesauro, M., C. Hollenstein, R. Egli, A. Geiger, and H.-G. Kahle (2006), Analysis of central western Europe deformation using GPS and seismic data, J. Geodyn., 42(4–5), 194–209, doi:10.1016/j.jog.2006.08.001.

Tiryakioğlu, İ., M. Floyd, S. Erdoğan, E. Gülal, S. Ergintav, S. McClusky, and R. Reilinger (2013), GPS constraints on active deformation in the Isparta Angle region of SW Turkey, Geophys. J. Int., in press, doi:10.1093/gji/ggt323.

Titus, S. J., M. Dyson, C. DeMets, B. Tikoff, F. Rolandone, and R. Bürgmann (2011), Geologic versus geodetic deformation adjacent to the San Andreas fault, central California, Geol. Soc. Am. Bull., 123, 794–820, doi:10.1130/B30150.1.

Tran, D. T., T. Y. Nguyen, C. C. Duong, Q. H. Vy, W. Zuchiewicz, N. Q. Cuong, and N. V. Nghia (2013), Recent crustal movements of northern Vietnam from GPS data, J. Geodyn., 69, 5-10, doi:10.1016/j.jog.2012.02.009.

Tregoning, P. (2002), Plate kinematics in the western Pacific derived from geodetic observations, J. Geophys. Res., 107(B1), 2020, doi:10.1029/2001JB000406.

Tregoning, P. et al. (1998a), Estimation of current plate motions in Papua New Guinea from Global Positioning System observations, J. Geophys. Res., 103(B6), 12,181–12,203, doi:10.1029/97JB03676.

Tregoning, P., F. Tan, J. Gilliland, H. McQueen, and K. Lambeck (1998b), Present-day crustal motion in the Solomon Islands from GPS observations, Geophys. Res. Lett., 25(19), 3627–3630, doi:10.1029/98GL52761.

Trenkamp, R., J. N. Kellogg, J. T. Freymueller, and H. P. Mora (2002), Wide plate margin deformation, southern Central America and northwestern South America, CASA GPS observations, J. South Am. Earth Sci., 15(2), 157–171, doi:10.1016/S0895-9811(02)00018-4.

Trenkamp, R., H. Mora, E. Salcedo, and J. N. Kellog (2004), Possible rapid strain accumulation rates near Cali, Colombia, determined from GPS measurements (1996-2003), Earth Sci. Res. J., 8(1), 25–33.

Tsai, M.-C., S.-B. Yu, Y.-J. Hsu, H.-Y. Chen, and H.-W. Chen (2012), Interseismic crustal deformation of frontal thrust fault system in the Chiayi–Tainan area, Taiwan, Tectonophysics, 554–557, 169–184, doi:10.1016/j.tecto.2012.05.014.

Tserolas, V., S. P. Mertikas, and X. Frantzis (2013), The Western Crete geodetic infrastructure: Long-range power-law correlations in GPS time series using Detrended Fluctuation Analysis, Adv. Space Res., 51(8), 1448–1467, doi:10.1016/j.asr.2012.08.002.

U.S. Geological Survey (2012), Velocities Equador, [online] Available from: http://earthquake.usgs.gov/monitoring/gps/data/networks/Ecuador/itrf2005_velocity_file (Accessed 23 November 2012)

Vigny, C., J.-B. de Chabalier, J.-C. Ruegg, P. Huchon, K. L. Feigl, R. Cattin, L. Asfaw, and K. Kanbari (2007), Twenty-five years of geodetic measurements along the Tadjoura-Asal rift system, Djibouti, East Africa, J. Geophys. Res., 112(B6), B06410, doi:10.1029/2004JB003230.

Wallace, L. M., C. Stevens, E. Silver, R. McCaffrey, W. Loratung, S. Hasiata, R. Stanaway, R. Curley, R. Rosa, and J. Taugaloidi (2004), GPS and seismological constraints on active tectonics and arc-continent collision in Papua New Guinea: Implications for mechanics of microplate rotations in a plate boundary zone, J. Geophys. Res., 109(B5), B05404, doi:10.1029/2003JB002481.

Walpersdorf, A., D. Hatzfeld, H. Nankali, F. Tavakoli, F. Nilforoushan, M. Tatar, P. Vernant, J. Chéry, and F. Masson (2006), Difference in the GPS deformation pattern of North and Central Zagros (Iran), Geophys. J. Int., 167(3), 1077–1088, doi:10.1111/j.1365-246X.2006.03147.x.

Wang, K., Y. Hu, M. Bevis, E. Kendrick, R. Smalley, R. B. Vargas, and E. Lauría (2007), Crustal motion in the zone of the 1960 Chile earthquake: Detangling earthquake-cycle deformation and forearc-sliver translation, Geochemistry, Geophysics, Geosystems, 8(10), Q10010, doi:10.1029/2007GC001721.

Weber, J., M. Vrabec, P. Pavlovčič-Prešeren, T. Dixon, Y. Jiang, and B. Stopar (2010), GPS-derived motion of the Adriatic microplate from Istria Peninsula and Po Plain sites, and geodynamic implications, Tectonophysics, 483(3–4), 214–222, doi:10.1016/j.tecto.2009.09.001.

Weber, J. C., T. H. Dixon, C. DeMets, W. B. Ambeh, P. Jansma, G. Mattioli, J. Saleh, G. Sella, R. Bilham, and O. Pérez (2001), GPS estimate of relative motion between the Caribbean and South American plates, and geologic implications for Trinidad and Venezuela, Geology, 29(1), 75–78, doi:10.1130/0091-7613(2001)029<0075:GEORMB>2.0.CO;2.

Weber, J. C., J. Saleh, S. Balkaransingh, T. Dixon, W. Ambeh, T. Leong, A. Rodriguez, and K. Miller (2011), Triangulation-to-GPS and GPS-to-GPS geodesy in Trinidad, West Indies: Neotectonics, seismic risk, and geologic implications, Marine and Petroleum Geology, 28(1), 200–211.

Williams, T. B., H. M. Kelsey, and J. T. Freymueller (2006), GPS-derived strain in northwestern California: Termination of the San Andreas fault system and convergence of the Sierra Nevada–Great Valley block contribute to southern Cascadia forearc contraction, Tectonophysics, 413(3–4), 171–184, doi:10.1016/j.tecto.2005.10.047.

Yang, S., J. Li, and Q. Wang (2008), The deformation pattern and fault rate in the Tianshan Mountains inferred from GPS observations, Science in China Series D: Earth Sciences, 51(8), 1064–1080, doi:10.1007/s11430-008-0090-8.

Yavaşoğlu, H., E. Tarı, O. Tüysüz, Z. Çakır, and S. Ergintav (2011), Determining and modeling tectonic movements along the central part of the North Anatolian Fault (Turkey) using geodetic measurements, J. Geodyn., 51(5), 339–343, doi:10.1016/j.jog.2010.07.003.

Yoshioka, S., T. Mikumo, V. Kostoglodov, K. M. Larson, A. R. Lowry, and S. K. Singh (2004), Interplate coupling and a recent aseismic slow slip event in the Guerrero seismic gap of the Mexican subduction zone, as deduced from GPS data inversion using a Bayesian information criterion, Phys. Earth. Planet. Int., 146(3–4), 513–530, doi:10.1016/j.pepi.2004.05.006.

Yoshioka, S., and Y. Matsuoka (2013), Interplate coupling along the Nankai Trough, southwest Japan, inferred from inversion analyses of GPS data: Effects of subducting plate geometry and spacing of hypothetical ocean-bottom GPS stations, Tectonophysics, in press, doi:10.1016/j.tecto.2013.01.023.

Yu, S.-B., and L.-C. Kuo (2001), Present-day crustal motion along the Longitudinal Valley Fault, eastern Taiwan, Tectonophysics, 333(1–2), 199–217, doi:10.1016/S0040-1951(00)00275-4.

Yu, S.-B., Y.-J. Hsu, T. Bacolcol, C.-C. Yang, Y.-C. Tsai, and R. Solidum (2013), Present-day crustal deformation along the Philippine Fault in Luzon, Philippines, J. Asian Earth Sci., 65, 64–74, doi:10.1016/j.jseaes.2010.12.007.

Zubovich, A. V. et al. (2010), GPS velocity field for the Tien Shan and surrounding regions, Tectonics, 29(6), TC6014, doi:10.1029/2010TC002772.

APPENDIX C Velocities used to Constrain Plate Motions

IGS08 velocities and residuals for sites used to constrain the rigid body plate rotations

station	**Lon. (ºE)**	Lat. (ºN)	Vel. E (mm/yr)	Vel. N (mm/yr)	SdVel E. (mm/yr)	SdVel N. (mm/yr)	Resid. E. (mm/yr)	Resid. N. (mm/yr)	Plate	Study
GMAS	**344.366**	27.765	16.67	17.62	0.36	0.29	0.31	0.34	AF	1
HARO[a]	**27.707**	-25.887	17.72	18.51	0.36	0.32	-0.13	0.40	AF	1
HRAO	**27.687**	-25.890	17.71	18.43	0.28	0.27	-0.14	0.32	AF	1
LPAL	**342.106**	28.764	16.03	16.55	0.34	0.38	0.30	-0.40	AF	1
MAS1	**344.367**	27.764	16.69	17.00	0.22	0.20	0.33	-0.28	AF	1
NKLG	**9.672**	0.354	22.28	18.91	0.26	0.22	-0.47	-0.16	AF	1
SUTH	**20.810**	-32.380	16.89	19.02	0.31	0.27	-0.30	0.32	AF	1
TGCV	**337.017**	16.755	19.05	15.86	0.26	0.21	0.22	-0.24	AF	1
WIND	**17.089**	-22.575	19.66	19.38	0.62	0.48	-0.37	0.47	AF	1
YKRO	**354.760**	6.871	21.85	18.59	0.37	0.36	-0.16	0.14	AF	1
E001	**134.290**	48.280	22.67	-12.24	0.80	0.80	-0.43	0.25	AM	1
E018	**122.340**	53.490	23.77	-10.49	0.70	0.70	0.16	0.21	AM	1
E056	**116.780**	48.660	25.87	-9.78	0.70	0.70	0.29	-0.07	AM	1
JB10	**131.170**	46.650	23.98	-12.00	0.80	0.80	-0.03	0.07	AM	1
CHA0[b]	**125.444**	43.791	25.33	-11.58	0.95	0.76	-0.14	-0.37	AM	1
DAV1	**77.973**	-68.577	-2.62	-5.13	0.17	0.25	0.23	0.26	AN	1
DUM1	**140.002**	-66.665	7.96	-11.90	0.40	0.43	0.13	0.62	AN	1
KERG	**70.256**	-49.351	4.94	-3.27	0.28	0.35	0.29	0.55	AN	1
MAW1	**62.871**	-67.605	-3.77	-2.13	0.19	0.25	-0.39	0.13	AN	1
MCM4	**166.669**	-77.838	9.63	-11.67	0.25	0.29	0.18	-0.23	AN	1
SYOG	**39.584**	-69.007	-3.90	2.77	0.19	0.22	-0.03	-0.03	AN	1

VESL	**357.158**	-71.674	-0.38	10.25	0.20	0.23	-0.23	-0.06	AN	1
BAHR	**50.608**	26.209	30.87	30.04	0.26	0.27	-0.29	-0.12	AR	1
BHR1	**50.608**	26.209	31.40	29.98	0.24	0.27	0.24	-0.18	AR	1
KUWT	**47.971**	29.325	29.38	29.64	0.41	0.36	0.39	0.02	AR	1
SOLA	**46.401**	24.911	31.57	29.24	0.31	0.26	0.69	0.03	AR	1
YIBL	**56.112**	22.186	33.37	31.47	0.35	0.28	-0.83	0.31	AR	1
MYKN	**25.333**	37.487	6.78	-13.13	0.60	0.60	0.43	-0.82	AS	2
AKIT	**23.296**	35.873	7.03	-12.88	0.30	0.30	-0.22	-0.07	AS	3
MKN2	**25.379**	37.449	6.23	-12.40	0.20	0.20	-0.13	-0.10	AS	3
TUC2	**24.071**	35.533	7.79	-12.05	0.34	0.33	0.51	0.58	AS	1
ALIC	**133.886**	-23.670	32.34	59.07	0.16	0.14	0.38	0.15	AU	1
CEDU	**133.810**	-31.867	29.01	58.64	0.16	0.17	0.29	-0.28	AU	1
DARW	**131.133**	-12.844	35.80	59.21	0.32	0.33	-0.11	0.06	AU	1
HOB2	**147.439**	-42.805	14.12	55.96	0.27	0.38	-0.03	0.12	AU	1
KARR	**117.097**	-20.981	38.84	58.34	0.16	0.15	-0.25	0.16	AU	1
TIDB	**148.980**	-35.399	18.17	55.28	0.31	0.26	-0.15	-0.01	AU	1
TOW2	**147.056**	-19.269	28.94	55.89	0.23	0.23	-0.14	-0.08	AU	1
YAR2	**115.347**	-29.047	38.73	57.72	0.19	0.18	-0.40	-0.09	AU	1
AGUA	**248.700**	25.590	-47.18	20.74	0.30	0.60	-0.34	0.56	BC	4
CARD	**249.220**	24.150	-48.08	20.84	1.30	0.50	-0.03	0.89	BC	4
MELR	**244.261**	30.980	-41.80	21.28	0.44	0.43	0.78	-0.92	BC	5
AB04	**189.433**	63.657	-0.94	-23.48	0.76	1.05	0.00	0.21	BG	1
AC58	**189.782**	57.156	-4.15	-23.96	1.41	1.04	0.01	-0.20	BG	1
AVES	**296.382**	15.667	12.09	13.99	2.10	0.90	-0.19	-0.41	CA	1
GRE0	**298.360**	12.222	13.66	15.19	0.52	0.48	-0.17	0.11	CA	1
SAN0	**278.284**	12.580	13.04	7.46	0.58	0.49	0.23	0.02	CA	1
EDI1	**41.677**	13.845	38.74	25.18	0.93	0.85	0.81	1.54	DA	6
EDTI	**41.353**	14.359	35.95	22.04	1.23	1.13	0.66	-0.06	DA	6

TIO1	**40.961**	14.615	34.12	20.57	0.63	0.60	0.17	0.35	DA	6
TIGE	**40.477**	14.891	31.43	17.57	1.37	1.23	-1.07	-0.34	DA	6
GELA	**40.088**	15.114	31.71	15.18	0.64	0.61	0.38	-0.88	DA	6
ASAB	**42.654**	13.063	40.78	28.09	0.76	0.68	-1.22	-0.22	DA	1
ARTU	**58.560**	56.430	25.16	6.17	0.23	0.22	-0.15	0.29	EU	1
GLSV	**30.497**	50.364	22.28	12.76	0.28	0.28	-0.58	0.55	EU	1
KOSG	**5.810**	52.178	18.09	15.97	0.24	0.23	0.38	0.54	EU	1
NRIL	**88.360**	69.362	22.13	-2.10	0.21	0.22	-0.93	0.20	EU	1
NVSK	**83.235**	54.841	26.90	-1.14	0.38	0.47	0.40	-0.26	EU	1
NYAL	**11.865**	78.930	10.44	14.12	0.17	0.17	0.12	-0.77	EU	1
VILL	**356.048**	40.444	18.87	16.28	0.22	0.21	0.06	0.34	EU	1
WTZR	**12.879**	49.144	20.32	15.47	0.21	0.20	0.38	0.69	EU	1
BOSC	**283.030**	18.400	3.91	7.30	0.40	0.40	-0.35	-0.18	GV	7
DISC	**282.600**	18.460	4.11	8.10	0.40	0.40	-0.08	0.97	GV	7
NGLF	**281.680**	18.280	4.71	6.30	0.30	0.30	0.40	-0.08	GV	7
NUTF	**283.170**	18.310	3.41	6.80	1.00	0.50	-0.93	-0.79	GV	7
PYRA	**282.190**	18.490	3.21	6.20	1.00	0.80	-0.93	-0.60	GV	7
JERE	**285.828**	18.663	4.59	10.44	2.52	2.19	0.43	0.71	GV	8
HYDE	**78.551**	17.417	41.11	34.33	0.34	0.33	0.21	-0.58	IN	1
IISC	**77.570**	13.021	41.07	35.77	0.50	0.36	-0.68	0.89	IN	1
MALD	**73.526**	4.189	43.88	33.92	1.06	0.73	1.00	-0.73	IN	1
PAGA	**145.757**	18.126	-30.05	9.91	3.17	3.07	0.81	-2.54	MA	9
GUGU	**145.832**	17.309	-29.10	9.79	2.62	2.57	-1.68	-2.97	MA	9
ANAT	**145.633**	16.364	-21.51	8.18	2.75	2.57	1.95	-3.75	MA	9
CNM0[c]	**145.743**	15.230	-18.70	12.74	0.66	0.52	-0.04	0.35	MA	1
ALGO	**281.929**	45.956	-16.39	2.50	0.29	0.28	0.39	-0.76	NA	1
FLIN	**258.022**	54.726	-17.67	-7.15	0.21	0.31	0.75	-0.90	NA	1
GODE	**283.173**	39.022	-14.64	4.14	0.13	0.13	0.10	0.38	NA	1

MSS0[d]	**270.386**	30.375	-12.31	-0.34	0.38	0.20	-0.20	1.03	NA	1
NLI0[e]	**268.425**	41.772	-15.56	-1.20	0.18	0.18	0.14	0.95	NA	1
PLTC	**255.274**	40.182	-14.62	-5.95	0.19	0.19	-0.10	1.36	NA	1
RCM0[f]	**279.616**	25.614	-10.83	3.06	0.23	0.24	-0.42	0.72	NA	1
STJO	**307.322**	47.595	-14.75	12.80	0.21	0.22	-0.20	0.08	NA	1
THU2	**291.175**	76.537	-22.39	4.71	0.12	0.17	-0.89	-2.17	NA	1
YELL	**245.519**	62.481	-17.22	-11.32	0.28	0.28	1.03	-0.42	NA	1
KAVI	**150.807**	-2.582	-63.97	32.67	2.70	1.60	-0.77	1.23	NB	10
KAVI	**150.807**	-2.582	-64.71	30.98	1.70	1.10	-1.51	-0.46	NB	11
PNGM	**147.366**	-2.043	-64.08	24.85	0.42	0.36	0.11	-0.01	NB	1
FLIX	**279.912**	-26.297	62.68	17.57	1.00	1.00	0.24	-0.06	NZ	12
RBSN	**281.163**	-33.629	63.56	17.82	1.00	1.00	0.08	-0.68	NZ	12
GLP0[g]	**269.696**	-0.743	50.37	10.28	0.21	0.24	-0.01	0.04	NZ	1
OKRG	**143.804**	50.292	15.25	-15.76	2.73	2.75	1.23	0.87	OK	13
PILG	**143.646**	50.049	14.26	-15.08	2.55	2.56	0.21	1.51	OK	13
TAL1	**152.392**	61.130	13.01	-20.43	2.30	2.23	1.09	-2.16	OK	13
MAG0	**150.770**	59.576	12.47	-20.14	0.73	1.00	0.07	-2.15	OK	1
MAGJ	**150.810**	59.578	12.22	-17.01	0.55	0.66	-0.17	0.99	OK	1
J734	**128.894**	27.817	31.19	-33.95	1.22	0.80	0.89	1.09	ON	1
J735	**128.651**	27.401	33.20	-34.75	0.82	0.94	1.90	0.71	ON	1
J736	**127.945**	26.944	32.86	-37.27	0.87	0.78	0.34	-0.58	ON	1
J739	**127.232**	26.583	32.80	-37.91	0.73	0.73	-0.73	-0.01	ON	1
J742	**127.144**	26.373	33.58	-37.98	0.80	0.67	-0.43	0.07	ON	1
J743	**126.739**	26.348	32.69	-40.44	0.91	0.98	-1.49	-1.70	ON	1
GAMB	**225.035**	-23.130	-67.51	31.96	0.37	0.28	-0.03	0.16	PA	1
ASPA	**189.278**	-14.326	-63.48	34.12	0.59	0.62	-0.06	-0.11	PA	1
THT0[h]	**210.394**	-17.577	-65.81	34.40	0.36	0.28	0.06	-0.01	PA	1
KOKB	**200.335**	22.126	-62.15	34.67	0.37	0.28	0.19	-0.25	PA	1

KRTM	**202.552**	2.047	-67.16	34.77	0.27	0.21	-0.02	-0.13	PA	1
MCI0[i]	**153.979**	24.290	-71.73	23.79	0.34	0.37	-0.01	-0.17	PA	1
MKEA	**204.544**	19.801	-62.45	34.94	0.23	0.19	-0.01	0.10	PA	1
KIRI	**172.923**	1.355	-67.75	31.28	0.45	0.34	-0.17	0.37	PA	1
ALBR	**280.442**	8.988	17.52	10.36	1.00	1.00	-1.80	-2.98	PM	14
CHEP	**281.965**	8.252	24.45	13.77	1.00	1.00	3.38	-2.94	PM	14
CHIT	**279.594**	7.989	25.83	11.64	1.00	1.00	4.24	0.18	PM	14
FLAM	**280.480**	8.910	19.63	11.86	1.00	1.00	0.13	-1.56	PM	14
CHEP	**281.965**	8.252	24.74	18.32	4.88	1.58	3.67	1.61	PM	15
CHIT	**279.594**	7.989	22.67	11.64	2.70	0.93	1.08	0.19	PM	15
ACP1	**280.050**	9.371	17.02	11.28	0.54	0.77	-1.41	-1.19	PM	1
ACP6	**280.592**	9.238	17.07	12.32	0.77	1.26	-1.68	-1.34	PM	1
AZUE	**279.567**	7.956	22.69	13.85	0.63	0.48	1.03	2.45	PM	1
PMPA	**280.439**	8.955	18.10	12.47	1.04	0.87	-1.29	-0.86	PM	1
BYSP	**293.839**	18.408	8.94	13.76	0.47	0.39	0.20	0.10	PR	1
CUPR	**294.717**	18.307	8.89	13.90	0.68	0.49	-0.02	-0.52	PR	1
MIPR	**293.473**	17.886	9.56	13.37	0.47	0.41	0.35	0.02	PR	1
MOPR	**292.069**	18.077	8.69	11.85	1.19	0.75	-0.25	-0.29	PR	1
P780	**293.421**	18.075	8.94	13.34	0.59	0.56	-0.09	0.04	PR	1
ZSU1	**294.007**	18.431	8.54	14.03	0.30	0.35	-0.19	0.22	PR	1
J746	**131.291**	25.954	-39.17	24.17	0.51	0.44	-0.10	0.47	PS	1
PAL0[j]	**134.450**	7.328	-65.09	20.11	0.27	0.22	0.03	-0.12	PS	1
NMPL	**39.258**	-15.123	19.63	15.91	0.23	0.19	-0.01	-0.01	RO	16
PMBA	**40.484**	-12.964	20.31	15.91	1.41	0.72	0.30	0.14	RO	1
BELE	**311.537**	-1.409	-4.79	12.55	0.28	0.38	-0.03	0.10	SA	1
BRAZ	**312.122**	-15.947	-3.82	12.45	0.32	0.31	0.04	-0.03	SA	1
BRF0[k]	**321.574**	-3.877	-4.58	12.83	0.47	0.30	0.19	0.05	SA	1
CHPI	**315.015**	-22.687	-3.64	12.49	0.37	0.33	-0.04	-0.11	SA	1

KOUR	**307.194**	5.252	-5.33	12.87	0.38	0.35	-0.15	0.68	SA	1
LPGS	**302.068**	-34.907	-0.72	11.82	0.36	0.39	0.38	0.04	SA	1
MPL0[l]	**302.429**	-38.006	-0.73	12.02	0.70	0.61	0.04	0.20	SA	1
RIOD	**316.694**	-22.818	-3.73	12.33	0.30	0.34	0.01	-0.34	SA	1
UFP0[m]	**310.769**	-25.448	-3.18	12.25	0.26	0.27	-0.17	-0.16	SA	1
VICO	**317.130**	-20.761	-3.86	12.43	0.36	0.43	0.04	-0.25	SA	1
JACQ	**151.505**	-5.645	15.54	-49.63	4.10	2.20	0.33	-0.04	SB	10
WITU	**149.435**	-4.688	26.14	-22.93	8.10	4.20	-1.28	0.16	SB	10
ABOZ	**33.102**	29.141	24.25	18.79	0.54	0.49	-0.04	-0.05	SI	6
ALON	**34.607**	31.708	22.46	19.20	0.39	0.34	-0.23	-0.26	SI	1
CSAR	**34.890**	32.488	22.12	19.57	0.29	0.22	-0.06	-0.01	SI	1
TELA	**34.781**	32.068	22.64	19.68	0.27	0.24	0.18	0.15	SI	1
J500	**123.792**	24.426	38.50	-61.22	1.22	1.92	-0.59	-0.93	SK	1
J748	**124.692**	24.642	35.51	-49.97	1.65	1.46	-0.31	-0.50	SK	1
J749	**124.301**	24.537	37.90	-53.92	1.00	0.72	0.52	0.25	SK	1
DAL1	**301.322**	-62.241	8.12	14.07	1.49	2.36	-4.00	-3.15	SL	17
PRA1	**300.350**	-62.478	7.12	15.20	1.87	3.16	-4.46	-3.36	SL	17
FERR	**301.607**	-62.086	14.54	17.50	0.26	0.24	1.97	0.67	SL	18
PRTT	**300.334**	-62.484	8.93	18.91	0.37	0.35	-2.64	0.33	SL	19
JUAN	**299.604**	-62.662	10.84	17.82	0.32	0.38	-0.35	-1.77	SL	19
FREI	**301.019**	-62.194	9.26	17.24	0.86	0.97	-3.10	-0.40	SL	1
MAL0[n]	**40.194**	-2.996	17.60	10.84	0.54	0.48	0.31	-0.43	SO	1
REUN	**55.572**	-21.208	24.92	11.33	1.06	0.66	0.31	0.03	SO	1
SEY1	**55.479**	-4.674	16.98	11.02	0.68	0.48	-0.62	0.42	SO	1
VACS	**57.497**	-20.297	31.31	-23.68	1.06	0.79	0.46	-1.37	SO	1
J723	**130.275**	30.785	26.55	-21.39	1.45	0.84	-0.86	1.53	ST	1
J777	**130.136**	31.416	26.28	-9.47	3.90	1.80	-1.41	0.75	ST	1
PANG	**111.670**	-2.686	33.04	-8.89	1.17	0.79	-0.58	0.04	SU	20

NONN	**108.263**	16.004	34.06	-5.92	0.43	0.32	0.30	-0.21	SU	21
UTHA	**100.013**	15.384	33.23	-8.11	0.87	0.64	-0.34	-0.48	SU	21
UBRT	**104.871**	15.245	33.15	-7.82	0.45	0.32	-0.35	-0.37	SU	21
SRIS	**104.416**	14.901	32.64	-5.57	0.42	0.28	-0.50	0.56	SU	21
CHON	**101.045**	13.121	32.17	-6.26	4.56	2.96	-0.87	-0.14	SU	21
RYNG	**101.033**	12.764	32.43	-12.65	1.00	0.71	0.68	0.13	SU	21
PUER	**118.851**	10.086	30.17	-8.25	1.26	0.95	1.12	0.92	SU	21
TABA	**108.891**	0.863	29.07	-8.25	1.11	0.72	1.09	-0.12	SU	21
TANJ	**106.176**	-1.881	33.34	-13.63	1.00	0.70	1.60	-0.85	SU	21
PUER	**118.851**	10.086	89.61	-6.33	1.66	1.60	0.90	0.44	SU	22
TNGA	**184.818**	-21.149	89.25	-5.63	1.14	0.94	0.47	1.19	TO	1
TONG	**184.821**	-21.145	131.15	-26.00	0.73	0.70	-0.37	-0.75	TO	1
VAVS	**186.017**	-18.651	22.65	16.17	0.89	0.68	0.43	-0.14	TO	1
KIOM	**33.912**	-6.134	24.56	16.32	1.70	1.37	1.61	-0.24	VI	16
NZG2	**33.183**	-4.257	24.96	16.34	0.43	0.50	0.49	-0.47	VI	16
EBBE	**32.445**	0.038	23.74	17.55	0.35	0.23	-0.52	0.17	VI	1
MBAR	**30.738**	-0.601	24.14	17.09	0.82	0.76	0.33	-0.50	VI	1
NURK	**30.090**	-1.945	19.76	84.68	4.60	2.00	-5.16	1.43	VI	1
GUA1	**152.943**	-9.225	20.66	76.07	2.50	1.40	-2.22	-0.70	WL	10
LOUS	**151.125**	-8.535	25.66	63.97	2.90	1.80	5.02	-0.01	WL	10
MORO	**147.590**	-7.742	31.94	-11.70	0.80	0.80	-0.46	-0.21	WL	10
C053	**113.860**	34.030	32.63	-11.95	0.90	0.90	-1.00	-0.15	YA	1
F027	**115.800**	23.430	31.91	-12.51	0.33	0.30	-0.18	0.08	YA	1
SHAO	**121.200**	31.100	33.34	-11.61	0.33	0.37	0.41	-0.04	YA	1
WUHN	**114.357**	30.532	16.67	17.62	0.36	0.29	0.31	0.34	YA	1

Studies: 1) This Study, 2) [*Floyd et al.*, 2010], 3) [*Müller et al.*, 2013], 4) [*Plattner et al.*, 2007], 5) [*Shen et al.*, 2011], 6) [*Reilinger and McClusky*, 2011], 7) [*Benford et al.*, 2012], 8) [*Manaker et al.*, 2008], 9) [*Kato et al.*, 2003], 10) [*Tregoning et al.*, 1998], 11) [*Tregoning*, 2002], 12) [*Wang et al.*, 2007], 13) [*Apel et al.*, 2006], 14) [*Drewes and Heidbach*, 2012], 15) [*Trenkamp et al.*, 2002], 16) [*Saria et al.*, 2013], 17) [*Dietrich et al.*, 2004], 18) [*Jiang et al.*, 2009], 19) [*Taylor et al.*, 2008], 20) [*Bock et al.*, 2003], 21) [*Simons et al.*, 2007], 22) [*Yu et al.*, 2013]. Velocities were derived for concatenated time-series for: a) HART, HARK & HARB, b) CC06 & CHAN, c) CNMI & CNMR, d) NDBC & MSSC, e) NLIB & IACI, f) RCM5, RCM6 & RMND, g) GALA & GLPS, h) PAMA & THTI, i) MARC & MCIL, j) PAL1 & PALA, k) FORT & BRFT, l) MPLA & MPL2, m) PARA & UFPR, and n) MALI & MAL2

APPENDIX D GPS Data Analysis Details (IGS Format)

```
|===========================================================================
|                                                                          |
|                                                                          |
|               NGL/UNR GPS Data Analysis Strategy Summary                 |
|                                                                          |
|                                                                          |
|                                                                          |
|==========================================================================|
|ANALYSIS CENTER     | Nevada Geodetic Laboratory                          |
|                    | University of Nevada, Reno                          |
|                    | 1664. N. Virginia St.                               |
|                    | MS 178                                              |
|                    | Reno                                                |
|                    | NV 89557                                            |
|                    | USA                                                 |
|                    | Data Archives:                                      |
|                    |    http://geodesy.unr.edu/                          |
|--------------------------------------------------------------------------|
|CONTACT PERSON      | Dr. Geoffrey Blewitt                                |
|                    |   E-mail: gblewitt (at) unr.edu                     |
|--------------------------------------------------------------------------|
|SOFTWARE USED       | GIPSY/OASIS-II Version 6.1.1 developed at JPL       |
|--------------------------------------------------------------------------|
|PRODUCTS USED       | Final, non-fiducial daily products from JPL archive: |
|                    |ftp://sideshow.jpl.nasa.gov/pub/JPL_GPS_Products/Final|
|                    | Including:                                          |
|                    |   GPS satellite orbit estimates                     |
|                    |   GPS satellite clock estimates                     |
|                    |   WLPB estimates (widelane & phase biases)          |
|                    |   Name of TRF (terrestrial reference frame)         |
|                    |   Transformation parameter estimates to named TRF   |
|                    |   Time-pole parameter estimates                     |
|                    |   GPS satellite eclipse times                       |
|                    |   Name of IGS ANTEX antenna calibration file        |
|                    | Auxiliary data updated periodically from JPL:       |
|                    |   IGS ANTEX antenna calibration file                |
|                    |   JPL planetary ephemeris                           |
|                    |   CODE CA-P DCB (differential code biases)          |
```

```
|                        |   GPS receiver type codes                          |
|                        |   GPS constellation configuration history          |
|                        |   IERS/BIH leap seconds history                    |
|                        |   IERS earth orientation parameters                |
|                        | Auxiliary data updated from IGS Central Bureau:    |
|                        |   http://igscb.jpl.nasa.gov/                       |
|                        |   IGS station receiver/antenna configuration history |
|                        | Auxiliary data from Chalmers University, Sweden:   |
|                        |   http://holt.oso.chalmers.se/loading/             |
|                        |   Ocean tidal loading coefficients for all stations |
|                        | Custom daily data (from NGL/UNR)                   |
|                        |   ftp://gneiss.nbmg.unr.edu/xfiles                 |
|                        |   Transformation parameter estimates to frame NA12 |
|                        |   Ref: http://dx.doi.org/10.1016/j.jog.2013.08.004 |
|-----------------------------------------------------------------------------|
|GPS DATA USED:          | RINEX files from various archives, including:      |
|                        |  UNAVCO     ftp://data-out.unavco.org              |
|                        |  CDDIS      ftp://cddis.gsfc.nasa.gov              |
|                        |  CORS       ftp://cors.ngs.noaa.gov/cors           |
|                        |  SIO        ftp://garner.ucsd.edu                  |
|                        |  EUREF      ftp://igs.bkg.bund.de/EUREF            |
|                        |  GEONET     ftp://ftp.geonet.org.nz                |
|                        |  GREF       ftp://igs.bkg.bund.de/GREF             |
|                        |  IGN        ftp://rgpdata.ign.fr                   |
|                        |  AUSTRALIA  ftp://ftp.ga.gov.au                    |
|                        |  GSI        ftp://terras.gsi.go.jp                 |
|                        |  SONEL      ftp://ftp.sonel.org                    |
|-----------------------------------------------------------------------------|
|PREPARATION DATE        | October 15, 2013                                   |
|-----------------------------------------------------------------------------|
|MODIFICATION DATES      | October 15, 2013  Creation                         |
|-----------------------------------------------------------------------------|
|EFFECTIVE DATE  FOR     | 2011-12-17 onward using JPL version 2 reprocessing |
|DATA ANALYSIS           | with IERS2010/IGS08 conventions                    |
===============================================================================


===============================================================================
|                         MEASUREMENT MODELS                                  |
|-----------------------------------------------------------------------------|
| Preprocessing        | RINEX header must be interpretable                   |
|                      |   - approximate XYZ replaced with NGL database values |
|                      |   - alias table replaces antenna type with IGS standard|
|                      |   - fix obvious formatting errors                    |
|                      |   - require antenna type has IGS ANTEX calibrations  |
|                      |   - non-calibrated radome set to "NONE" (IGS standard) |
|                      | Require minimum file size, typically ~18 hr/day      |
|                      | Apply CA-P1 biases                                   |
```

	Fix non-compliant time-tags for older receiver types Remove non-GPS GNSS data (e.g., GLONASS) Remove L2C and C2 data Cycle slip detection Delete phase connected arcs < 20 minutes Carrier Phase: Decimated to 5 minutes Pseudorange: Carrier aided smoothing to 5 minutes
Basic Observable	Undifferenced ionosphere-free carrier phase, LC Undifferenced ionosphere-free pseudorange, PC
	Elevation angle cutoff: 7 degrees Sampling rate: 5 minutes Data weight, LC: 1 cm Data weight, PC: 1 m
Modeled observable	Undifferenced LC and PC combinations CA-P1 biases from CODE applied
RHC phase rotation corr.	Applied
Marker -> antenna ARP eccentricity	dN, dE, dU eccentricities from RINEX header applied to compute station marker coordinates
Ground antenna phase center cal.	PCV model from igs08_wwww.atx applied Receiver antenna and radome types from RINEX header
Troposphere	A priori model: Pressure from GPT model (Boehm et al, 2007) Hydrostatic delay from Davis (1985) Wet delay 10 cm Mapping Function: Global Mapping Function (GMF) Estimation: Zenith delay and horizontal gradients
Ionosphere	1st order effect: Removed by LC and PC combinations 2nd order effect: Not modeled
Plate motions	Not applied to apriori positions
Tidal	Solid earth tide: IERS 2010 Conventions
	Permanent tide: NOT removed from model, so NOT in estimated site coordinates
	Pole tide: IERS 2010 Conventions
	Ocean Tide Loading: Diurnal, Semidiurnal, MF, and MM Model: FES04

	Semiannual: Self-consistent equilibrium model hardisp.f from IERS2010 Surface deformations computed with respect to instantaneous center of mass
	Ocean Pole Tide Loading: Not applied
Non-tidal loading	Atmospheric Pressure: Not applied
	Ocean Bottom Pressure: Not applied
	Surface Hydrology: Not applied
	Other Effects: None applied
Earth Orientation Parameter (EOP) Model	IERS 2010 Conventions for diurnal, semidiurnal, and long period tidal effects on polar motion and UT1
Satellite center of mass correction	Phase centers offsets from igs08_wwww.atx applied
Satellite antenna phase variations	PCV model w.r.t. phase center from igs08_www.atx applied
Relativistic corrections	Periodic Clock Corrections, (-2*R*V/c): Applied Gravitational Bending (Shapiro Delay): Applied
GPS Attitude model	GYM95 nominal yaw rate model from Bar-Sever (1996) and yaw rates estimated for Block II satellites

ORBIT MODELS (JPL ORBIT PRODUCTS)	
Geopotential	EGM2008 12x12 C20, C30, C40, C21, S21 from IERS2010 standards
	GM = 398600.4415 km**3/sec**2
	AE = 6378.1363 km
Third-body	Sun, Moon, and All Planets
	Ephemeris: JPL DE421

Solar radiation pressure	Block II/IIA/IIR: JPL empirical SRP model, GSPM-10, Bar-Sever and Kuang, (2004) Sibthorpe et al, 2010
	Estimate GPS "Y-Bias" and solar radiation pressure(SRP) coefficient as constant with no a-priori constraint. Make small time-varying (stochastic) adjustments to SRP coefficients in spacecraft body-fixed X and Z directions (1% process noise sigma with 1 hr 11 sec updates and 4-hour correlation time.) Estimate tightly constrained time-varying empirical acceleration in spacecraft Y direction (0.01 nm/s^2 process noise sigma with 1 hr 11 sec updates and 4-hour correlation time.)
	Earth shadow model: conic model with oblate Earth, umbra and penumbra
	Earth albedo: applied
	Attitude Model: GYM95 yaw model from Bar-Sever (1996)
Tidal forces	Solid earth tides: IERS 2010 Conventions
	Ocean tides: FES2004 to degree and order 30 with convolution formalism of Desai and and Yuan (2006)
	Solid Earth Pole tide: IERS 2010 conventions
	Ocean Pole tide: IERS 2010 conventions
Relativity	Applied Acceleration due to point mass of Earth Acceleration due to geodesic precession Acceleration due to Lense-Thirring precession
Numerical Integration	Variable high order Adams predictor-corrector with direct integration of second-order equations
	Integration step: variable
	Starter procedure: RKF
	Arc length: 30 hours centered at 12:00 of each day

ESTIMATED PARAMETERS (APRIORI VALUES & SIGMAS)	
Adjustment	Stochastic Kalman filter/smoother implemented as square root information filter with smoother
Station coordinates	Daily PPP estimates for all sites Apply daily transformation into IGS08 and NA12
Satellite clock	Fixed to JPL clock products, which are given every 5 minutes relative to reference clock (e.g. USN3/AMC2
Receiver clock	Estimate every 5 minutes relative to satellite clocks
Orbital	Fixed to JPL ECEF orbit products interpolated to 5 min
GPS Attitude	Fixed to JPL products: yaw rates when in eclipse
Troposphere	Zenith delay: random walk 5.0d-8 km/sqrt(sec) Horizontal delay gradients: random walk 5.0e-9 km/sqrt(sec)
	Mapping function: GMF
Ionosphere	1st order effects removed by LC and PC combinations and 2nd order effects not modeled
Ambiguity	Resolve ambiguities using WLPB products from JPL
Earth Orientation Parameters	Fix to JPL products: polar motion, polar motion rate, and LOD, where UT1 is integrated from estimated LOD

REFERENCE FRAMES	
Inertial	J2000 Geocentric
Terrestrial	Daily transformed coordinates into IGS08 and NA12
Interconnection	Precession: IAU 2006 Precession Theory
	Nutation: IAU 2006 Nutation Theory
	A priori EOPS: EOPC04 updated daily, with polar motion and length of day estimated daily

REFERENCES

Bar-Sever, Y. E. (1996), "A new model for GPS yaw attitude", Journal of Geodesy, 70:714-723

Bar-Sever, Y. E., and D. Kuang (2004), New empirically-derived solar radiation pressure model for GPS satellites, IPN Progress Reports 42-159, JPL. Available online: http://ipnpr.jpl.nasa.gov/progress_report/42-160/title.htm

Bassiri, S., and G. A. Hajj, (1993), Higher-order ionospheric effects on the global positioning systems observables and means of modeling them, Manuscripta Geodtica, 18, 280-289, 1993

Blewitt, G., (1990), An automatic editing algorithm for GPS data. Geophysical Research Letters, Vol. 17, No. 3, p. 199-202

Blewitt, G., C. Kreemer, W.C. Hammond, and J.M. Goldfarb (2013), "Terrestrial reference frame NA12 for crustal deformation studies in North America", J. Geodyn, http://dx.doi.org/10.1016/j.jog.2013.08.004

Boehm, J., A.E. Niell, P. Tregoning, H. Schuh (2006), "Global Mapping Functions (GMF): A new empirical mapping function based on numerical weather model data", Geophysical Research Letters, Vol. 33, L07304, DOI:10.1029/2005GL025545.

Boehm, J., R. Heinkelmann and H. Schuh (2007), "Short Note: A global model of pressure and temperature for geodetic applications", Journal of Geodesy, DOI: 10.1007/s00190-007-0135-3

IERS Conventions 2003, D.D. McCarthy & G. Petit (editors), IERS Technical Note 32, Frankfurt am Main: Verlag des Bundesamts fuer Kartographie und Geodaesie, 2004.

Kedar, S., G. Hajj, B. Wilson, and M. Heflin (2003), The effect of the second order GPS ionospheric correction on receiver positions, Geophys. Res. Lett., 30(16), 1829, doi:10.1029/2003GL017639

Moyer, T.D., (2000) Formulation of observed and computed values of deep space network data types for navigation, Deep Space Communications and Navigation Series, Jet Propulsion Laboratory, California Institute of Technology, Pasadena, CA, Chapter 4, pp, 19-28.

Sibthorpe, A., J. Weiss, N. Harvey, D. Kuang, and Y. Bar-Sever, Empirical modeling of solar radiation pressure forces affecting GPS satellites, AGU Fall Meeting, San Francisco, CA, 2010.

THE GLOBAL EARTHQUAKE MODEL

The mission of the Global Earthquake Model (GEM) collaborative effort is to increase earthquake resilience worldwide.

To deliver on its mission and increase public understanding and awareness of seismic risk, the GEM Foundation, a non-profit public-private partnership, drives the GEM effort by involving and engaging with a very diverse community to:

- Share data, models, and knowledge through the OpenQuake platform
- Apply GEM tools and software to inform decision-making for risk mitigation and management
- Expand the science and understanding of earthquakes.

GEM Foundation

Via Ferrata 1
27100 Pavia, Italy
Phone: +39 0382 5169865
Fax: +39 0382 529131
info@globalquakemodel.org
www.globalquakemodel.org

MARCH 2014

GLOBAL EARTHQUAKE MODEL
working together to assess risk